Universidade do Minho
Escola de Engenharia

Daniela Maria da Silva Correia

Three dimensional scaffolds based on electroactive polymers for tissue engineering applications

outubro de 2015

Daniela Maria da Silva Correia **Three dimensional scaffolds based on electroactive polymers for tissue engineering applications**

UMinho | 2015

Universidade do Minho
Escola de Engenharia

Daniela Maria da Silva Correia

Three dimensional scaffolds based on electroactive polymers for tissue engineering applications

Tese de Doutoramento em Engenharia de Materiais

Trabalho realizado sob a orientação do
Professor Doutor Senentxu Lanceros-Méndez
da
Professora Doutora Maria Gabriela Botelho
e do
Professor Doutor José Luis Gómez Ribelles

outubro de 2015

STATEMENT OF INTEGRITY

I hereby declare having conducted my thesis with integrity. I confirm that I have not used plagiarism or any form of falsification of results in the process of the thesis elaboration.

I further declare that I have fully acknowledged the Code of Ethical Conduct of the University of Minho.

University of Minho, Braga, 26 de outubro, 2015

Full name:

Signature: Daniela Maria Silva Conneia

Acknowledgments

I would like to express my deep gratitude to all the persons who somehow contributed for the development of this work.

Firstly, to the Foundation for Science and Technology (FCT) (grant SFRH/BD/82411/2011) for the financial support to this project.

The development of this work would not have been accomplished without the accompaniment of my super-visors and co-supervisors. In this sense, I'm grateful for the opportunity to work with Professor Senentxu Lanceros-Mendez, Professor Gabriela Botelho and Professor José Luis Gómez Ribelles. Thank you for the availability and all the scientific knowledge transmitted, as well as for all the support spirit, encouragement, sympathy, patient and collaborative spirit that they always paid to me.

To Professor José Luis Gómez Ribelles and the researchers of Biomaterials Center from the Polytechnic University of Valencia I would also like to thank the kind reception at the Biomaterials Center and all the scientific support and friendship.

To the Electroactive Smart Materials Group (ESM), I would like to thank for all the companionship and encouragement they have always given me. A special acknowledge to Doctor Vitor Sencadas and Doctor Clarisse Ribeiro due to all the help and friendship they devoted to me during the work.

Concerning the personal domain, I would like to thank all my friends for always believing in me and in my capabilities. Finally, I would like to deeply express and recognize the importance of my parents, sister and grandparents for their crucial support, persistence and love paid to me throughout my academic journey.

For everyone my sincere thank you!

To my parents and sister for everything

"Nothing in life is to be feared, it is only to be understood. Now is the time to understand more, so that we may fear less."

Marie Curie

Abstract

Biomaterials play an increasingly prominent important role in the development and success of tissue engineering, particularly in the regeneration or reestablishment of tissue functions and organs. The improvement in the understanding of the role of biomaterials in the formation and regeneration of new tissue has promoted faster and more effective developments in this area.

Biomaterials based on electroactive polymers have gained special interest in the scientific community for applications in tissue engineering, in particular for mechano-sensitive tissues (bone, ligaments/tendons) and electroative tissues (brain cells, heart and muscles). Among them, piezoelectric materials show a strong application potential due to their ability to mimic specific biological environments through electrical stimulation.

The main objective of this study was to produce scaffolds with different morphologies (fibers, particles and three-dimensional scaffolds) based on piezoelectric polymers, poly(vinylidene fluoride) (PVDF), poly(hydroxybutyrate) (PHB) and poly(L- lactic acid) (PLLA) for tissue engineering applications. Plasma treatments were also used to modify the wettability of the materials.

Thus, PVDF samples were processed by electrospinning technique and plasma treatments were performed under oxygen atmosphere for different times and applied power, in order to modify the wettability of the hydrophobic fiber surface. It was observed that plasma treatments didn´t significantly change the average fiber diameter (~ 400 ± 200 nm) or the physicochemical properties of the membranes, in particularly the β-phase content (~ 80-85 %) and the crystallinity degree (42 ± 2 %), showing that this is a suitable method to obtain superhydrophilic membranes.

PVDF microspheres were processed by electrospray technique. Among the different processing parameters, polymer concentration was the one that most influenced the microspheres formation. Microspheres with average diameter ranging between 0.81±0.34 μm and 5.55±2.34 μm with a β-phase content between 63-74 % and a degree of crystallinity between 45 and 55% were obtained from dilute or semi-dilute solutions. Cell viability assays demonstrated the potential of the PVDF microspheres for tissue engineering applications.

Three dimensional scaffolds based on PVDF with different porosities were produced using three different methods: solvent casting with sodium chloride (NaCl), solvent casting and freeze extraction using nylon and poly (vinyl alcohol) (PVA) templates. Regardless of the processing method, the scaffolds showed polymer crystallization in the β-phase and a degree of crystallinity of ~ 45%. Mechanical tests demonstrated the suitability of the materials for tissue engineering applications.

PHB membranes were processed by electrospinning and the influence of processing parameters on the size and distribution of fibers was studied. It was found that the average fiber diameter of the PHB membranes decreased with decreasing internal diameter of the needle and increased with increasing applied electric field and flow rate up to ~ 2.0 μm. The processing parameters didn´t affect the crystalline phase of the PHB membranes yielding a degree of crystallinity of 53%. Further, cell viability studies proved the suitability of the material for tissue engineering applications.

Plasma treatments under argon and oxygen atmospheres were performed with thin films and PLLA membranes obtained by solvent casting and electrospinning, respectively. The average diameter of the fibers didn´t change significantly for argon (866 ± 361 nm) or oxygen (1179 ± 397 nm) treatments. However, it was found an increase of the roughness of the films. Surface wettability studies proved that plasma treatments allowed to obtain superhydrophilic or low contact angles on membranes and films, with no influence on cell viability.

PLLA microspheres with sizes between 0.16 and 3.9 μm and a degree of crystallinity of 40% and composite PLLA microspheres with cobalt ferrite nanoparticles ($CoFe_2O_4$) in the range of 0.8 to 2.2 μm were produced by emulsifying an oil (PVA solution) in water. PLLA spheres proved to be more stable in alkaline environments compared to magnetic composite PLLA microspheres. Moreover, it was found that the introduction of nanoparticles promoted the amorphous state in PLLA. It was shown that PLLA microspheres with and without $CoFe_2O_4$ particles didn´t inhibit cellular viability.

In conclusion, it was demonstrated the possibility of processing different electroactive polymers in the form of microspheres, fibers, membranes and three-dimensional scaffolds, as well as evaluated the possibility to modify their wettability. This work represents thus a relevant contribution for increasing the use of these materials in innovative strategies for tissue engineering.

Resumo

Os biomateriais desempenham um papel cada vez mais proeminente no desenvolvimento e sucesso da engenharia de tecidos, nomeadamente na regeneração ou no restabelecimento da função de tecidos/órgãos do corpo humano. Os avanços registados relativamente à compreensão do papel dos biomateriais na formação de novos tecidos e na sua regeneração têm promovido uma maior rapidez e eficácia nos estudos desenvolvidos nesta área.

Biomateriais à base de polímeros eletroativos têm despertado especial interesse na comunidade científica, para aplicações em engenharia de tecidos, nomeadamente para tecidos mecano-sensitivos (osso, ligamentos/tendões) e tecidos eletroativos (neurónios, coração e músculos). Em particular, materiais eletroativos à base de polímeros piezoelétricos apresentam uma forte potencialidade por serem capazes de mimetizar o ambiente biológico do tecido através de estímulos eletromecânicos.

O principal objetivo do presente trabalho consistiu na produção de *scaffolds* com diferentes morfologias (fibras, partículas e *scaffolds* tridimensionais) baseados em polímeros piezoelétricos, o poli(fluoreto de vinilideno) (PVDF), poli(hidroxibutirato) (PHB) e o poli(L-ácido láctico) (PLLA) para aplicações de engenharia de tecidos. Igualmente, foram utilizados tratamentos de plasma para modificar a hidrofobicidade dos materiais.

Deste modo, foram processadas membranas de PVDF pela técnica de *electrospinning* e realizados tratamentos de plasma sobre atmosfera de oxigénio para diferentes tempos de tratamento e potência aplicada de modo a modificar a molhabilidade da superfície hidrofóbica das fibras. Foi observado que o plasma não altera significativamente o diâmetro médio das fibras (~400±200 nm) nem as suas propriedades físico-químicas nomeadamente o conteúdo de fase β (~80-85%) e o seu grau de cristalinidade (42±2 %) demonstrando ser um método eficaz na obtenção de membranas superhidrofílicas.

Microesferas de PVDF foram processadas pela técnica de *electrospray*. De todos os parâmetros estudados (concentração de polímero e parâmetros de processamento) verificou-se que a concentração de polímero é aquela que mais influência a formação de microesferas. Microesferas com diâmetros médios variando entre os 0,81±0,34 μm e 5,55±2,34 μm com um conteúdo de fase β entre os 63-74% e um grau de cristalinidade entre 45 e 55% foram obtidas através de soluções diluídas ou semi-diluídas. Ensaios de viabilidade celular demonstraram a potencialidade destas microesferas para aplicações

em engenharia de tecidos. *Scaffolds* tridimensionais à base de PVDF com diferentes porosidades foram produzidos recorrendo a três métodos distintos: *solvent casting* – com cloreto de sódio (NaCl), *solvent casting* e extração a frio utilizando telas de nylon e poli(vinil álcool) (PVA). Independentemente do método de processamento utilizado, os *scaffolds* apresentam a fase β e um grau de cristalinidade de ~ 45 %. Ensaios mecânicos demostraram a viabilidade dos materiais para a aplicação em causa.

Membranas de PHB foram produzidas por *electrospinning*, realizando-se igualmente um estudo da influência dos parâmetros de processamento no diâmetro e distribuição de fibras. Assim, verificou-se que o diâmetro médio das fibras de PHB diminui com o do diâmetro interno da agulha e aumenta com o aumento do campo elétrico aplicado e taxa de fluxo até ~2,0 μm. Os parâmetros de processamento não influenciaram a fase cristalina das membranas de PHB tendo sido obtido um grau de cristalinidade de 53%. Estudos de viabilidade celular comprovaram a sua potencialidade para aplicações na área de engenharia de tecidos. Tratamentos de plasma sobre atmosferas de árgon e oxigénio foram efetuados em filmes e membranas de PLLA obtidas por *solvent casting* e por *electrospinning*, respetivamente. O diâmetro médio das fibras não sofreu uma alteração significativa para o árgon (866±361 nm) nem para o oxigénio (1179±397 nm) tendo-se, no entanto, verificado um aumento da rugosidade dos filmes. Estudos de molhabilidade de superfície demonstraram ser possível obter membranas superhidrofílicas e filmes com um menor valor de ângulo de contacto, não influenciando a viabilidade celular.

Microesferas de PLLA com tamanhos compreendidos entre os 0,16 -3,9 μm e um grau de cristalinidade de 40% e microesferas compósitas de PLLA com nanopartículas de ferrita de cobalto ($CoFe_2O_4$) na ordem dos 0,8-2,2 μm foram produzidas pelo método de emulsão de um óleo (solução de PVA) em água. Esferas de PLLA demonstraram ser mais estáveis em ambientes alcalinos comparativamente às esferas de PLLA magnéticas. Verificou-se que a introdução de nanopartículas promove o estado amorfo no PLLA. Foi demonstrado que as microesferas de PLLA com e sem partículas de $CoFe_2O_4$ não inibem a viabilidade celular.

Em conclusão, testou-se a possibilidade de processar diferentes polímeros eletroativos nas formas de microesferas, fibras, membranas e *scaffolds* tridimensionais, sendo igualmente provada a possibilidade de modificar a sua molhabilidade. Este trabalho representa um contributo relevante para a crescente utilização destes materiais em estratégias inovadoras de engenharia de tecidos.

Table of contents

List of figures

List of tables

List of symbols

A	Pre-exponential factor
A	Absorbance
A_α	Absorbance - α–phase
A_β	Absorbance - β-phase
E_{act}	Activation energy
E	Elastic modulus
Ɛ	Porosity
F(β)	β-phase content,
K_α	Absorption coefficient of α-PVDF
K_β	Absorption coefficient of β-PVDF
k(T)	Rate degradation constant
R	Ideal gas constant
T_m	Melting temperature
v/v	Volume ratio
w/v.	Weight/volume ratio
w/w	Weight ratio
x	Amount of the α-phase
X_c	Degree of crystallinity
y	Amount of the β-phase
ΔH	Melting enthalpy
ΔH_α	Enthalpy of pure crystalline α-PVDF
ΔH_β	Enthalpy of pure crystalline β-PVDF
ΔH_0^f	Thermodynamic melting enthalpy of a 100 % crystalline polymer
ΔH^o_m	Melting enthalpy
φ_{Ray}	Rayleigh limit
α	*D*egree of conversion

List of abbreviations

A

AC	Alternating current
ACP	Carbonated apatite
ALP	Alkaline phosphatase
Ar	Argon
ASCs	Human adipose-derived stem cells
ATR	Attenuated total reflection

B

BE	Binding energy
BT	Barium titanate

C

c	Concentration of the solution
CAD	Computer-aided design
c_{ent}	Entanglement concentration
CF	Chloroform
c_{ov}	Chain overlap concentration
CT	Computed tomography

D

DBP	Demineralized bone powders
DBSA	Dodecylbenzene sulfonic acid
DMEM	Dulbecco's modified Eagle's medium
DMF	N,N-Dimethyl Formamide
DMSO	Dimethyl sulfoxide
DNA	Deoxyribonucleic acids
DSC	Differential scanning calorimetry

E

E	Elastic modulus
EAP	Electroactive polymers
ECM	Extracelular matrix

F

FAT	Fixed analyser transmission

FBS	Fetal Bovine Serum
FDM	Fused deposition modelling
FTIR	Infrared spectroscopy
H	
HAP	Hydroxyapatite
hASCs	Human adipose-derived stem cells
He	Helium
HFIP	1, 1, 1, 3, 3, 3-hexafluoro-2-propanol
hFOB	Human fetal osteoblasts
hMSCs	Human mandible–derived mesenchymal stem cells
HOB	Human osteoblasts
HOS	Human osteosarcoma
hPDLF	Human periodontal ligament
M	
MC3T3-E1	Pre-osteoblast cells
MRI	Magnetic resonance imaging
MSCs	Human mesenchymal stem cells
MTS	3-(4,5-dimethylthiazol-2-yl)-5-(3-carboxymethoxyphenyl)-2-(4-sulfophenyl)-2H-tetrazolium
MTT	3-(4, 5-Dimethylthiazol-2-yl)-2,5-diphenyltetrazolium bromide)
N	
Nb2a	Mouse neuroblastoma cells
NGF	Nerve growth factor
NR	Natural rubber
O	
O_2	Oxygen
P	
PCL	Poly(caprolactone)
PEG	Poly(ethylene glycol)
PGA	Poly(glycolic acid)
PHB	Poly(hydroxybutyrate)
PLA	Poly(lactic acid)
PLAs	Polylactides

PLGA	Poly(lactic-co-glycolic)
PLLA	Poly(L-lactic acid)
PU	Polyurethane
PVDF	Poly(vinylidene fluoride)
PVDF-TrFE	Poly(vinylidene fluoride-trifluoroethylene)

R

RP	Rapid prototyping

S

SCC9	Keratinocytes
SEM	Scanning electron microscopy
SFF	Solid free-form
SLA	Stereolithography apparatus
SLS	Selective laser sintering

T

TCP	Tricalcium Phosphate
THF	Tetrahydrofuran

X

XPS	X-ray photoelectron spectroscopy
2D	Two dimensional
3D	Three dimensional
3DP	Three dimensional printing

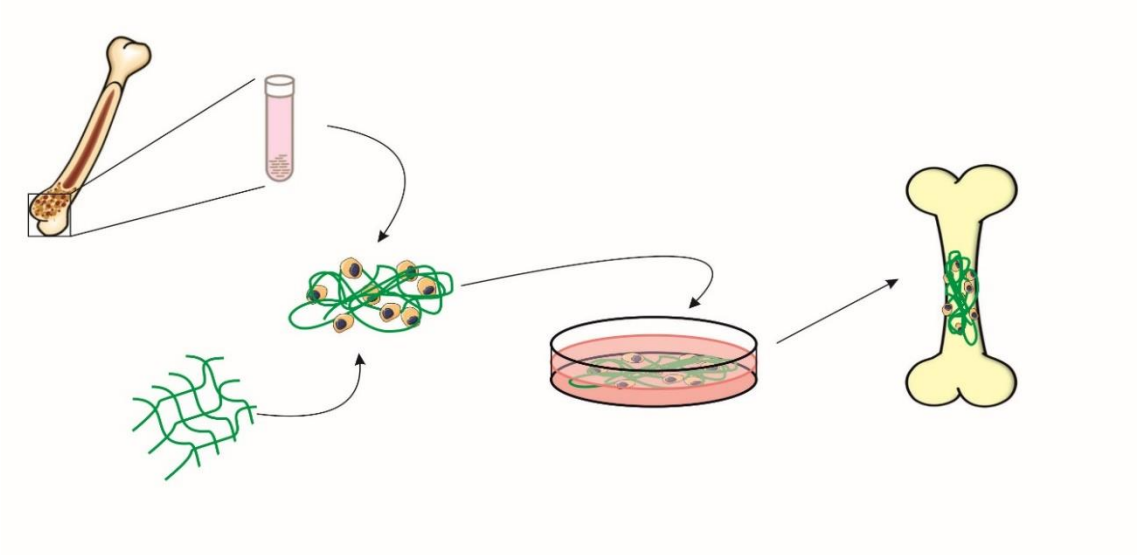

1. Introduction

Tissue engineering often rely on scaffolds for supporting cell differentiation and growth. New paradigms for tissue engineering include the need of active or smart scaffolds, in particular piezoelectric polymers, in order to properly regenerate specific tissues. The present chapter presents a state of art of the main concepts of tissue engineering and piezoelectric materials used for this application, which are essential for the present work. This chapter also indicates the main objectives of the study and the structure of the document.

This chapter is based on the following publication: C. Ribeiro, V. Sencadas, D. M. Correia, and S. Lanceros-Méndez. *Piezoelectric polymers as biomaterials for tissue engineering*. Colloids and Surfaces B: Biointerfaces 136 (2015) 46–55.

1.1. Tissue engineering

The interdisciplinary field of tissue engineering combine principles and innovations from engineering, cells and micro environmental factors [1-3]. The fundamental concept involves the combination of a supporting matrix with living cells and/or biologically active molecules with the aim to regenerate damaged tissues instead of replacing them by developing biological substitutes that restore, maintain or improve tissue function [4, 5]. The supporting matrix that essentially act as a template for tissue formation is often called scaffold and it is needed to provide the appropriate environment for tissue and organs regeneration thought the necessary physico-chemical or mechanical stimuli. In this sense, scaffolds play a key role in the cells accommodation, migration, growth and differentiation [5, 6]. The cells-seeded scaffolds can be either cultured *in vitro* to synthetsze tissues or directly implanted *in vivo* into the injured site.

Different tissue engineering strategies can be applied (Figure 1.1a). Basically, they consist in selecting the appropriate cells, materials and biochemical and physical signals to repair, maintain and/or regenerate the tissue function.

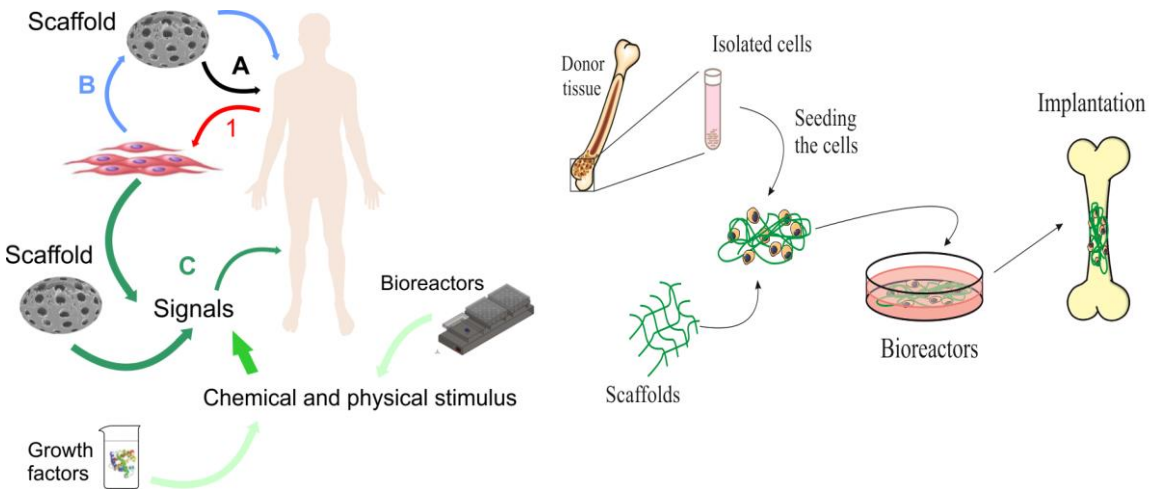

a) b)

Figure 1.1. a) Schematic representation of different strategies for tissue engineering: 1—the cells can be harvested directly from the patient; A—scaffold implanted directly; B—cells cultured in scaffolds and then implanted; C—cells cultured in scaffolds with appropriate signal, namely chemical (such as growth factors) and physical (such as mechanical using a bioreactor) and then implanted. b) Tissue engineering strategies for bone regeneration.

The cells can be harvested directly from the patient or stem cells can be used to be combined with a biomaterial scaffold to grown in vitro without (route B of Figure 1.1a) or with (route C of Figure 1.1a) signals and then implanted. It should be also noted that bioreactors are used for "in vitro" culture in tissue engineering in an attempt to simulate an in vivo physiological environment. The scaffolds can also be implanted directly to facilitate cell regeneration in vivo (route A of Figure 1.1a). Figure 1.1b shows a promising strategy for the repair or regeneration of damaged bone. This tissue engineering therapy involves harvesting healthy cells (adult or stem cells) culturing them in an appropriate scaffold for growth *in vitro* in a bioreactor which will provide the proper biochemical and physical stimulus and then implanted.

1.1.1. General requirements of scaffolds

Metals, alloys, ceramic and polymers are being used for the development of scaffolds for tissue engineering applications. Together with the materials physico-chemical properties, some general requirements are needed for proper scaffold performance [7]. The structure of the scaffolds has influence in the transmission of biochemical, morphological, electrical and mechanical signals. Thus, the architecture of the scaffold defines the ultimate shape of the newly grown soft or hard tissue [5], the surface properties of the scaffolds and resulting cellular response playing an essential role in tissue engineering applications [8, 9].

The suitability and success of the scaffold as a support depends on some key issues that must be addressed before material selection and design for specific tissue engineering applications [5, 6]. Thus, the scaffold must be biocompatible, allowing cell infiltration in order to promote a specific cellular response and stimulate tissue regeneration [5, 6]. After implantation, the scaffold must stimulate a negligible immune reaction in order to prevent severe inflammatory response that might reduce healing or cause rejection by the body [8, 10]. Scaffolds must preferentially be biodegradable in many cases, to allow cells to produce their own ECM. The degradation products should also be non-toxic and eliminated from the body via natural occurring processes without interference with other organs [6]. Additionally, the scaffold should show mechanical properties consistent with the replaced tissue into which is to be implanted [6]. Scaffolds with appropriate mechanical properties are a great challenge in tissue engineering due to the fact that healing rate is age dependent and a match between the mechanical properties

and material degradation must occur [5, 6]. In general, high mechanical properties are obtained in detriment of the high porosity present in the samples and consequently some limitations arise during in vitro experiments due to insufficient capacity of vascularization which is specially important in bone regeneration. A commitment between mechanical properties, porosity and porous architecture sufficient enough to allow cell infiltration and vascularization is a key to success of any scaffold [5]. In particular, bone or cartilage tissue engineering, where the tissue are continuously exposed to mechanical stimulus while walking or exercising, the scaffold must present sufficient mechanical integrity during the time of implantation attending to the fact that the healing rates varying with age [11]. The scaffold architecture characteristics (pore size, degree of porosity, pore interconnectivity and permeability) are also a critical requirement. The interconnection of the pores into the scaffold and a high porosity is necessary to ensure cell penetration, adequate diffusion of nutrients to cells and to allow the diffusion of waste products out of the scaffold [5, 6]. The pore size needs to be large enough to allow cells to migrate into the scaffold and small enough to establish a sufficiently high surface leading to a minimal ligand density promoting the efficient binding of a critical number of cells to the scaffold. The easy processing of the materials into three dimensional complex shapes is thus critically important for the successful translation of tissue engineering strategies to the clinic [5, 6].

1.1.2. Biomaterials for tissue engineering

Metals, alloys and ceramic materials are being replaced by polymers in different application areas including aerospace and automotive industries, electronics, sensors, actuators and tissue and biomedical engineering. Different processing techniques have been developed for the production of polymers with tailored properties, including electrical, mechanical, thermal, chemical and surface properties, among others, addressing specific applications demands [12, 13].

Polymers present attractive properties when compared to inorganic materials. They are light weight, inexpensive, mechanically and electrically tough, they show excellent compatibility with other organic and inorganic materials for the development of multifunctional hybrid systems, and some of them are biodegradable and/or biocompatible [14-16].

The increasing advances in materials science and engineering is allowing the improvement and optimization of the so-called smart materials and, in particular, smart polymer materials, for a larger number of application areas [17-21].

Smart materials are materials with reproducible, significant and stable variations of at least one property when subjected to external stimuli. Smart materials are typically classified according to the output response and include piezoelectric materials, materials that develop a voltage when a mechanical stress is applied or vice-versa; shape memory materials, in which a large deformation can be induced and recovered by temperature or stress variations; temperature responsive polymers, magnetostrictive materials, pH sensitive materials, self-healing materials, thermoelectric materials and conductive polymers, among others [22-24]. These materials are also generally knowns as active materials.

Particularly interesting for sensor and actuator applications, are materials that undergo deformation under a specific stimuli or that provide a specific stimuli under mechanical force and/or deformation. Depending on the transduction mechanism, they can be broadly classified as non-electrically deformable polymers (actuated by non-electric stimulus such as pH, light and temperature, for example) and electroactive polymers (EAP) when the transduction mechanism involves electro-mechanical coupling. The later are further classified as dielectric EAP, which electromechanical response is dominated by electrostatic forces and ionic EAP which actuation mechanism involves the diffusion of ions [25, 26]. Electrically conductive polymers are another class of electrically active materials that is attracting increased attention as they show simultaneously high conductivity and the physico-chemical properties of polymers [27-29].

In the last decades, a variety of natural and synthetic materials with various molecular designs emerged as potential biomaterials for tissue and biomedical engineering [30]. Natural materials are attractive for biomedical and related applications as they are obtained from natural sources, exhibiting similar properties to the tissue they are replacing, many of them containing specific cues for cell adhesion and proliferation and allowing cell infiltration [31]. On the other hand, polymers from natural origin are often difficult to process and show poor mechanical and electrical properties [32]. In this way, a variety of synthetic polymers such as poly(lactic acid) (PLA) [33, 34], poly(glycolic acid) (PGA) [35, 36], poly(lactic-co-glycolic acid) (PLGA) [37, 38], poly(ethylene

glycol) (PEG) [39, 40], and poly(caprolactone) (PCL) [41] have been widely used to produce materials/scaffolds for tissue engineering [42].

Although an extensive list of polymers have been studied regarding tissue engineering applications, most of the developed scaffolds have been used in a passive way, just as support for the cells and tissues [43]. Nevertheless, it was verified that for some specific cells and tissues, the active behavior of the material used for the scaffold development can be taken to advantage, providing even the necessary stimuli for proper tissue regeneration. This fact gave rise to the strong increase of the development of smart materials for tissue engineering applications [44].

Being electrical signals one of the main physical stimuli present in the human body and, in particular, the electromechanical signals, this work is devoted on piezoelectric polymers for tissue engineering applications.

In a piezoelectric material (Figure 1.2), an electrical response due to mechanical excitation or *vice versa* can be observed. In these types of materials a certain anisotropy in its structure is required. In synthetic polymers that are in the noncrystalline or semicrystalline form and are originally isotropic, they are typically subjected to a poling procedure (such as corona) to meet this requirement [45].

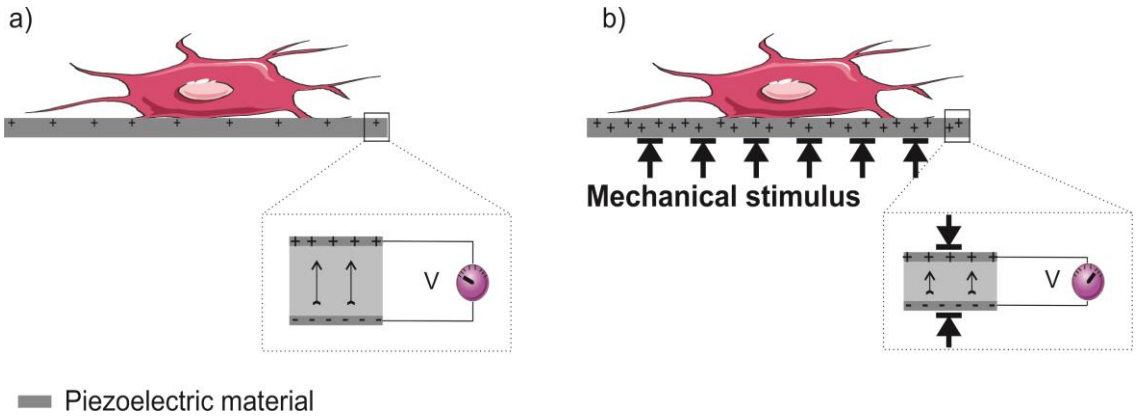

Figure 1.2. Schematic representation of the piezoelectric effect (piezoelectric material representation at the bottom of the image) and corresponding cell culture on piezoelectric supports a) without and b) with mechanical stimulus, the later leading to an electrical potential variation of the materials which, in turn, influences cell response.

The most common way to describe the piezoelectric effect is by the so-called direct effect, where the piezoelectric d_{ij} coefficient is given by (Equation 1.1).

$$d_{ij} = \left(\frac{\partial D_i}{\partial X_j}\right)^E = \left(\frac{\partial x_i}{\partial E_j}\right)^X \quad (1.1)$$

where D is the electric induction; E is the electric field strength; X is the mechanical stress; and x is the strain [46]. In this sense, it is possible to observe that the piezoelectricity is the relation between the electrical variables (D and E) and the mechanical parameters (X and x).

With respect to the so-called inverse piezoelectric effect, the e_{ij} coefficient is obtained by (Equation 1.2).

$$e_{ij} = \left(\frac{\partial D_i}{\partial x_j}\right)^E = -\left(\frac{\partial X_i}{\partial E_j}\right)^x \quad (1.2)$$

The direct piezoelectric effect (d_{ij}) concerns the conversion of the mechanical energy into electrical energy while the inverse piezoelectric effect (e_{ij}) describes the conversion of electrical energy into mechanical energy.

1.2. Electrical cues in human body

Many of the major functions in cells and organs of the human body are controlled by electrical signals. As early as in the 18th century it is described the use of electrostatic charge for skin lesion treatment [47] and in 1983, electrical potentials ranging between 10 and 60 mV, depending on the human body location were measured [48].

Electric fields and potentials induce distinct effects on cells and it has been proven that small applied electric fields can guide a variety of different cell types to move and migrate directionally such as corneal, epidermal and epithelial cells [49-52]; can modulate the phenotypes of vascular endothelial cells [53]; can regenerated nerve fibers [54] and are widely used in orthopedic practices, showing the improvement of ligament healing *in vivo* [55].

1.2.1. Piezoelectricity in human body

Extensive and classic studies of the piezoelectric properties of bone and other biological materials have also been reported. The piezoelectricity can be referred as an extended property of living tissue, playing a significant role in several physiological phenomena [56]. Piezoelectricity can be found in different parts of the human body (Figure 1.3)

such as bone, tendon, ligaments, cartilage, skin, dentin, collagen, deoxyribonucleic acids (DNA) and conceivably, in cell membranes [56-61].

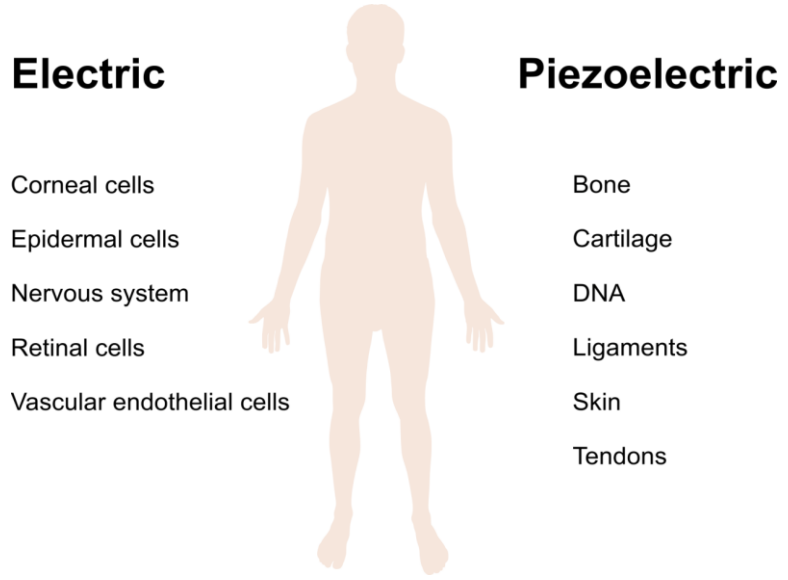

Figure 1.3. Representative human body location in which electrical and piezoelectric signals are relevant.

1.2.1.1. Bone

Bone is a dynamic tissue in constant adaptation and remodeling through complex feedback mechanisms, involving electromechanical processes, due to its piezoelectric characteristics. Due to its piezoelectric nature, bone is the paradigm for piezoelectric electromechanical effect in human tissue [62].

The first study reporting the piezoelectric properties of the bone was in 1955 [63]. Few years later, electric currents in bone and the generation of electric potentials when the bone is mechanically stressed were verified [64, 65]. This phenomenon, recognized as piezoelectricity, is independent of cell viability. The mechanical stress produces electrical signals and these signals represent the stimulus that promotes bone growth and remodeling according to Wolff's law [66]. The biomechanical properties of bone, in particular its piezoelectric activity, have been addressed microscopically [67] and macroscopically, with models using finite element analysis [68]. Further, it has been also hypothesized a mechanism by which the piezoelectric signals can regulate bone growth [69]. At the cellular level, the bone cell type that plays an important role in the

bone structure development and appears to be involved in bone mechanotransduction, the osteocytes, was identified [70]. Consequently, for bone regeneration, these cells communicate with other bone cells, such as osteoblasts and osteoclasts. The influence of electrical stimulation on bone healing has been studied *in vitro* [71-77] and *in vivo* [78-83] and it has been demonstrated that the application of these stimulus can enhance and stimulate osteogenic activities. In this way, the osteoblasts are affected by electromechanical signals to apposite bone tissue [84, 85], the piezoelectric nature of bone, leading to natural conversion of the mechanical stimuli into electrical ones.

1.2.1.2. Collagen and other piezoelectric tissues

Due to their collagenous structure, tendons and ligaments also exhibit piezoelectricity, giving rise, therefore, to an electrical potential variation when a mechanical stress is applied [86, 87]. The piezoelectricity of dry tendons was measured [88], as well as the electrical potentials generated in hydrated tendon [89, 90], the piezoelectric coefficient decreasing with increasing hydration [91].

Piezoelectric effect has been also observed in different soft tissues, such as skin, callus, cartilage and tendons, as well as in hard ones, such as bone, and appears to be associated with the presence of oriented fibrous proteins [56, 92]. All connective tissue contains one or more types of fibrous molecules such as, collagen, keratin, fibrin, elastin, reticulum or cellulose structure, showing also piezoelectric properties [56].

It seems evident from the literature that the piezoelectric effect can be attributed to the main organic constituent of tissue, which is collagen in the case of the bone and tendons [93, 94]. Thus, it has been shown that the crystalline unit of collagen is polar hexagonal (C_6) [67], showing piezoelectric properties. Further, as previously indicated, it has been shown that dry bone is piezoelectric, i.e., a mechanical stress induces a polarization (direct effect) and an application of an electric field produces a change in the material geometry or strain (converse effect). It was reported that for dry fibers, the polarization results from the displacement of the hydrogen bonds formed in the polypeptide chains of the collagen crystals. Thus, in [95] the piezoelectric and pyroelectric behavior of collagen were measured independently from the bone, confirming that the electroactive properties arise from the structure of collagen molecules. It was suggested that the crystalline structure of collagen changed under wet conditions and that bound water promotes a change in its crystal symmetry to the point where no piezoelectric properties

were observed [89, 96]. A certain minimum amount of water concentration, which increases crystal symmetry, is nevertheless required to maintain the overall structural integrity. Further, it was also suggested that, due to the variability of the electroactive behavior of collagen in wet and dry states, wet bone shows different piezoelectric symmetry relation [89, 96]. More recently, studies of the piezoelectric response of human bone using a piezoresponse force microscope, in order to measure this effect at nanometer scale resolution directly in the collagen matrix, resulted in the quantification of the piezoelectric response in 7 – 8 $pC.N^{-1}$ [97].

With respect to other biological tissues, the electrical polarization variations were also verified in hair when subjected to stress [98] as well as in DNA [75]. Finally, investigations in the calcifications commonly found in human pineal gland tissues resulted in the determination that pineal gland contains non centrosymmetric material which, according to crystallographic symmetry considerations, is also piezoelectric [99].

1.3. Piezoelectric soft biomaterials and structures

General for all materials used as scaffolds, the design of these bioactive biomaterials is another important parameter to consider and a suitable morphology, in combination to the piezoelectric characteristics, has to be optimized for proper cell response.

Many manufacturing methods have been developed to process biomaterials into scaffolds with different dimensionalities and morphologies [100, 101]. Different structures of biomaterials including microspheres, fibers, porous membranes, hydrogels and sponges have been designed and used in tissue engineering [30]. However, effects of internal biomaterials structures remain largely unexplored and the comparison of cell response in the different structures types remains elusive

Porous scaffolds have been obtained by solvent casting/salt leaching, phase separation, gas foaming, gel casting, precipitation and emulsion freeze-drying [100, 101]. The main drawbacks of these methods are associated with the microstructural features and inaccurate and limited pore interconnectivity that is disadvantageous for uniform cell seeding and tissue growth [42, 102]. These major drawbacks can be overcome by the used of fibrous scaffolds produced by electrospinning, a method that offers the ability of control the pore interconnectivity and moreover the internal and external morphology of the fibers, which sizes in the order of the extracellular matrix of the cells, by controlling

processing parameters such as applied voltage, solution viscosity and conductivity, among others [102]. Moreover, electrospinning allows the production of scaffolds with small pore size, density and high surface area [101, 102]. The scaffolds pores should be large enough to allow cell migration, where they eventually become bound to the ligands within the scaffold. Therefore, for any scaffold, a critical range of pore sizes exists, which may vary depending on the cell type and tissue being engineered [5]. The fiber diameter of the scaffolds produced by electrospinning can range from 5 nm to a few microns [102]. A similar method to electrospinning is electrospray, which allows the preparation of polymeric micro- and nanoparticles that can also be used as support for cell expansion and differentiation [103]. Other methods can be used for particle formation however this method might overcome some of the drawbacks associated with conventional microparticle-producing methods, such as solvent casting, single and double emulsion, spray-drying, porous glass membrane emulsification and coacervation [104].

More recently, rapid prototyping (RP) technologies also known as solid free-form fabrication (SFF) allows translating computer data files such as computer-aided design (CAD), computed tomography (CT), magnetic resonance imaging (MRI) and convert the digital information through layered manufacturing SFF machines into a 3D scaffold [101, 102, 105]. Three-dimensional printing (3DP), fused deposition modeling (FDM), stereolithography apparatus (SLA) and selective laser sintering (SLS) are widely been applied in the fabrication of materials with unique geometries with controllable pore architecture which could not obtained by conventional methods [102]. Various biomaterials are commonly used in RP technologies such as PEG, PLGA, PCL, collagen, starch, hyaluronic acid (HA) and tricalcium phosphate (TCP) [6, 100, 106]. However, to the best of our knowledge few studies report the production of piezoelectric scaffolds by these methods, being stereolithography the most commonly used method for the fabrication of piezoelectric scaffolds based on poly(L-lactic acid) PLLA [6].

These scaffold structures have to be achieved with the few natural and synthetic materials exhibiting piezoelectric properties, the most relevant ones, with the respective piezoelectric properties being reported in Table 1.1 and 1.2, respectively.

Table 1.1. Biodegradable polymers with natural origin and corresponding main piezoelectric response (adapted from [86]).

Natural Polymers			**Piezoelectric coefficient -d_{14} (pC/N)**
Polysaccharides	Cellulose	Wood	0.10
		Ramie	0.20
	Chitin	Crab shell	0.20
		Lobster apodeme	1.50
	Amylose	Starch	2.00
Proteins	Collagen	Bone	0.20
		Tendon	2.00
		Skin	0.20
	Keratin	Wool	0.10
		Horn	1.80
	Fibrin	Elongated films of fibrinogen-thrombin clot	0.20
		Deoxyribonucleic acids salmon DNA (at -100 ºC)	0.07

However, to demonstrate the suitability and effect of the piezoelectric properties for tissue engineering applications, synthetic polymers have been mostly chosen instead the natural ones for their use as scaffolds. These have known compositions and can be designed to minimize immune response. They can be tailored to produce a wide range of scaffold geometries and hybrid structures by combining polymers with other organic or inorganic hybrid structures.

Table 1.2. Piezoelectric properties of natural and synthetic polymers.

Polymer	**Dielectric constant** (1 kHz; 25ºC)	**Modulus of the Piezoelectric Coefficient (pC/N)**	**Reference**
PLA	3.0 – 4.0	9.82	[107, 108]
Poly(hydroxybutyrate) (PHB)	2.0 – 3.5	1.6 – 2.0	[109, 110]
PVDF	6 - 12	24 - 34	[111, 112]
Poly(vinylidene fluoride-trifluoroethylene) (PVDF-TrFE)	18	38	[112]
Polyamide-11	5	4	[113]

Among all polymers, PVDF [114] and vinylidene fluoride (VDF) [115] copolymers, are the synthetic, semi-crystalline polymers with the highest electroactive properties, including piezoelectric, pyroelectric and ferroelectric properties [115].

As mentioned above, it is possible to find electrical activity and even piezoelectricity in many parts of the human body. For that reason, it seems to be advantageous to employ biomaterials based on piezoelectric properties for active tissue engineering of specific tissues.

1.4. Tissue engineering based on piezoelectric polymers

Studies of the use of piezoelectric polymers for tissue engineering applications are mostly devoted to bone, neural and muscle regeneration. Table 1.3 summarizes the main works using piezoelectric polymers, the intended applications and scaffold morphology, together with the cultivated cells.

Table 1.3. Material type, scaffold design and cells used for different applications. * indicates that dynamic assays have been performed.

Applications	Material type		Scaffold design	Cells type used	Reference
Bone regeneration or Bone tissue engineering	PVDF and copolymer		Films	MC3T3-E1 Goat marrow stromal cells into osteoblast	[116-118] [119]*
			Fibers	Human mesenchymal stem cells (MSCs)	[120]
			Blends membranes (porous)	NIH3T3 mouse fibroblast	[121]
	PLLA			Implementation on male cats	[122]
			Fibers	Human fetal osteoblasts (hFOB) Human mandible–derived mesenchymal stem cells (hMSCs)	[123] [124]
	PHB and copolymers		Films	Bone marrow cells	[125]
			Fibers	Human osteoblasts (HOB) Bone marrow cells	[126] [125]
			3D Blends membranes (porous)	MC3T3-E1	[127]
	Collagen		Fibers - hydrogel D-periodic type I collagen fibrils	Rat tail tendon	[128]
			3D matrices	Human fetal osteoblastic cells (hFOB 1.19) and Bovine osteoblasts Human adipose-derived stem cells (ASCs)	[129] [130]
	Composites	PVDF/starch/natural rubber (NR)	Blends membranes (porous)	NIH3T3 mouse fibroblast	[121]
		PVDF-TrFE/starch/NR	Blends membranes (porous)	NIH3T3 mouse fibroblast	[121]
		PVDF-TrFE/Barium titanate (BT)	Membranes	*in vivo* evaluation of rats Human alveolar bone-derived cells (Osteoblastic cells)	[131] [132]

				Osteoblastic cells from human alveolar bone fragments Fibroblasts from human periodontal ligament (hPDLF) and keratinocytes (SCC9)	[133] [134]
		PLA/demineralized bone powders (DBP)	Fibers	hMSCs	[124]
		PLLA covered with bonelike apatite	3D Porous Scaffold	Saos-2 osteoblast-like cells	[135]
		Apatite/collagen	3D Porous Scaffold	Saos-2 osteoblast-like cells	[135]
Nerve or neural regeneration	PVDF		Films	Mouse neuroblastoma cells (Nb2a) Spinal cord neurons	[54, 136]* [137]
			Blends membranes (porous)	Dense and microporous membranes: neuronal cells	[138]
			Channels/Tubes	Nerve guidance channels: *in vivo* assay: mouse sciatic nerve model. Tube containing nerve growth factor (NGF) and Collagen gel: in vivo assay: Wistar rats.	[139] [140]
	PVDF-TrFE		Films	Poietics Normal Human Neural Progenitors Nb2a	[141] [54]
			Fibers	Dorsal root ganglion Poietics normal human neural progenitors	[142] [141]
			Tubes	In vivo implementation: rat sciatic nerves	[143]
	PLLA		3D Porous scaffold	*In vivo* implementation: Sprague Dawley rats	[144]
	Collagen		Fibers	Schwann cells	[145]
			3D gel matrices	Embryonic rat cerebral cortices	[146]

Muscle regeneration	PVDF		Films	C2C12 myoblast	[147]
			Fibers	C2C12 myoblast	[147]
			Meshes	In vivo study in rabbits	[148]
			Fibers	In vivo study in rabbits	[149]
	Composites	Au–PLLA	Fibers	primary rat muscle cells	[150]
Others applications	Cartilage	PHB	3D scaffolds	Human adipose-derived stem cells (hASCs)	[151]
	Abdominal hernia repair	PVDF	Meshes	Implanted subcutaneously in rats	[152] [153]
	Endothelialization	PVDF	Films	Human cell line, EA.hy 926	[53]
	Vascular surgery	PVDF	Monofilament sutures	In vivo study Adult female chinchilla rabbits	[154] [155]
	Spinal cord injury regeneration	PHB-co-3-hydroxyvalerate (PHB-HV)	3D scaffold by freeze-drying technique	primary culture of neurons and astrocytes from the hippocampus of P4 Wistar rats	[156]
	Wound healing	PPy/PLLA	Membranes	Human Skin Fibroblast	[157]
		PVDF-TrFE	Electrospun fibers	Human skin fibroblasts	[158]
	Tissue sensors	PVDF	Microstructures	Human osteosarcoma (HOS)	[159]

Dynamic assays were performed in the studies marked with * contrary to the others where only static assays were carried out. It is to notice that when no dynamic conditions are used, the suitability of the piezoelectric effect is not proven, but just the suitability of the material and the relevance of the (positive or negative) surface charge, when the material is poled.

It is to notice that the most used polymer is PVDF and its co-polymers as, due to its larger piezoelectric response, they serve as an ideal material platform for proving the concept of mechano-electrical transductions for tissue engineering. Also, several sample morphologies have been used, such as films, fibers, porous membranes and 3D porous scaffolds for different applications in tissue engineering, mainly for bone, muscle and nerve regeneration. With the challenge to mimic the architecture of these tissues, the fibers have proved to be one of the favorite choices and for most of the studies mesenchymal stem cells have been chosen. For bone tissue engineering applications, PVDF fibers were produced and their effect on biological function was studied with hMSCs [120]. It was verified that the cells attach to PVDF fibers and present a larger alkaline phosphatase activity and early mineralization when compared with the control, showing the potential for the use of PVDF scaffolds for bone tissue engineering applications. The same cells were also used with PLLA fibers to study their biocompatibility and suitability for bone differentiation and the same results were obtained [124]. Regarding nerve regeneration, fibers were also used and it was verified that the cells attach and the neurites extend radially on the randomly oriented fibers, whereas the aligned fibers directed the neurite outgrowth, demonstrating their potential for neural tissue engineering [141, 142]

On the other hand, despite the demonstrated potential, there are still just a few conclusive works addressing the effect of the electrical stimulus promoted by the piezoelectric response of the materials, as for these studies, specific dynamical mechanical stimulus should be applied during cell culture, for example, by the use of mechanical bioreactors. The applied mechanical stimulus can be vibration, compression or stretching of the piezoelectric scaffold.

In this scope, piezoelectric materials based on PVDF films, have been used to study the effect of mechanical stimulation of bone cells, by converse piezoelectric effect. On a substrate submitted to dynamic mechanical conditions, the stimulation was achieved with an alternating sinusoidal current (AC) of 5 V at 1 and 3 Hz for 15 min at each frequency. It was verified that mechanical stimulation of bone induces new bone

formation *in vivo* and increases the metabolic activity and gene expression of osteoblasts in culture [116]. The influence of the same piezoelectric substrate, PVDF film, on the bone response cultivated under static and dynamic conditions was also investigated [118]. The dynamic culture was performed on a home-made bioreactor system with mechanical stimulation by placing the culture plate on a vertical vibration module at a frequency of 1 Hz with amplitude of ~1 mm. The results showed that the surface charge under mechanical stimulation improves the osteoblast growth and consequently, that electroactive membranes and scaffolds can provide the necessary electrical stimuli for the growth and proliferation of electrically responsive tissue and in particular of tissues which also show piezoelectric response, such as bone. The same dynamic culture was used to enhance osteogenic differentiation of human adipose stem cells, proving that dynamic mechanical stimulus in combination with suitable osteogenic differentiation media can offer tools to better mimic the conditions found in vivo [160]. Moreover, the use of a piezoelectric (PVDF) actuator in *in vivo* assays for orthopedic application [117] and after one month implantation it was verified that the converse piezoelectric effect can be used to stimulate bone growth at the bone implant interface, eliciting an early response.

Concerning nerve regeneration, neurons were cultured directly on electrically charged PVDF polymer growth substrates to determine if local electrical charges enhance nerve fiber outgrowth in vitro [54, 136]. Piezoelectric PVDF substrates generated 2-3 mV at 1200 Hz when placed on standard incubator shelves and it was concluded that the enhanced outgrowth process was induced effectively by the piezoelectric output of the films.

The study of the piezoelectric effect of polyurethane/PVDF (PU/PVDF) fibers was also investigated for wound healing applications [161]. For this, the scaffolds were subjected to intermittent deformation of 8 % at a frequency of 0.5 Hz for 24 h and the results indicated piezoelectric-excited scaffolds showed enhanced migration, adhesion and secretion, exhibiting faster wound healing than those on the control scaffolds. *In vivo* assays were also performed with the implantation of these scaffolds in rats and a higher fibrosis level was verified due to the piezoelectric stimulation, which was caused by random animal movements followed by mechanical deformation of the scaffolds.

So, it is possible to conclude that piezoelectric materials would be useful in many tissue engineering applications. In *in vitro* assay, the mechanical deformation can be made by the use of bioreactors and in *in vivo* assay, the stimulation would be produced by

movements of the patient which will cause the mechanical deformation of the scaffolds (Figure 1.1). Further, since the piezoelectric effect can be found in several human body tissues, as previously mentioned, it is natural to assume that piezoelectric scaffolds will be needed, at least, for the proper regeneration of those tissues.

Up to now, the most commonly used polymer to study the piezo-electric effect in tissue engineering applications was the PVDF, due to its larger piezoelectric response. This polymer is non-degradable, which can be a limitation for applications including scaffold implantation. On the other hand, it can be successfully used as scaffold for cells stimulation before implantation, due to its large piezoelectric response and physico-chemical stability.

Thus, it is shown the large potential of piezoelectric materials for tissue engineering applications, but in order to further explore their true possibilities, it is needed to obtain materials in different morphologies suitable for tissue engineering. In this way, it is to notice that there are no reports on the processing of PVDF into microspheres and 3D scaffolds and just few studies based on PHB and PLLA with different morphologies exists.

1.5. Objectives

The main objective of this work was to develop piezoelectric biomaterials based on PVDF, PHB and PLLA with different morphologies, including microspheres, fiber membranes and three dimensional scaffolds. Further, the wettability of the materials was evaluated and modified by plasma treatment in specific cases.

In summary, the main specific objectives of this work are:

- Processing of PVDF electrospun membranes and study the influence of plasma treatments on the surface wettability of the hydrophobic PVDF membranes.
- Processing of PVDF microspheres by electrospray.
- Processing of three dimensional macroporous PVDF scaffolds by three distinct methods.
- Processing of PHB electrospun membranes by electrospinning.
- Study the influence of plasma treatments on the surface wettability of PLLA electrospun membranes.

- Processing of neat and magnetic PLLA microspheres by an oil-in-water method.
- Study of the influence of the processing conditions on the physico-chemical properties (chemical structure, phase content and crystallinity) of the materials processed into the different morphologies.
- Evaluation of the applicability of the different morphologies for tissue engineering applications.

1.6. Structure of the work and document

The present thesis is divided in eight chapters, seven of them are based on published or submitted scientific papers. The chapters are presented in a sequential order including first the studies on biocompatible and non-biodegradable (PVDF) piezoelectric structures and then the results on biocompatible and biodegradable piezoelectric structures based on PHB and PLLA. Thus, a comprehensive and logic report of the progress achieved during this investigation is provided.

As reported before, PVDF and copolymers are the polymers with the highest piezoelectric constant and have been processed in films and fibrous membranes by electrospinning, giving rise to highly hydrophobic membranes. Thus, the first work was to modify the wettability of electrospun PVDF membranes by plasma treatments. After proving that it is possible to modify the surface wettability of PVDF membranes, the following step was to develop different morphologies such as spheres and three dimensional scaffolds. After this step was successfully achieved, some of the most interesting morphologies for tissue engineering applications were reproduced for biodegradable polymers (PHB and PLLA), addressing also surface modification for increased wettability.

In the following, a summary of the covered work in each chapter is briefly described.

Chapter 1 presents a literature review with a general overview on tissue engineering and, specifically, on the importance of piezoelectric biomaterials for cell stimulation. It is to notice that the specific state of the art on the different issues related to the present work is provided in the different chapters. Finally, the main objectives and the structure of the document are also reported in this chapter.

The **chapter 2** is dedicated to the processing of electrospun PVDF membranes and on the modification of the surface wettability of the PVDF membranes by oxygen plasma treatment. The influence of the plasma treatment on the fiber average size, morphology, electroactive phase content and degree of crystallinity was evaluated. The wettability was evaluated by contact angle measurements and related to the surface variations of the membranes causes by the plasma treatments.

The **chapter 3** reports on the production of PVDF microspheres by electrospray as a suitable substrate for tissue engineering applications. The influence of the polymer solution concentration and processing parameters, such as electric field, flow rate and inner needle diameter on microsphere size and distribution, are reported. The viability of cells cultured in a 3D environment formed by PVDF microspheres is also assessed in order to evaluate its potential application in tissue engineering.

PVDF can be also fabricated with a three dimensional (3D) porous morphology. **Chapter 4** shows the several strategies implemented in order to develop PVDF 3D scaffolds. Three processing methods, including solvent casting with particulate leaching and 3D nylon, and freeze extraction with poly(vinyl alcohol) (PVA) templates are presented in order to obtain three-dimensional scaffolds with different pore architectures and interconnected porosity. The physico-chemical and mechanical properties of the scaffolds obtained by the distinct methods are shown.

In **chapter 5** the production of PHB electrospun membranes by electrospinning is reported. The influence of several processing parameters on fiber size and distribution is shown, together with a characterization of the physico-chemical properties, including thermal degradation. Cell adhesion on these substrates was also assessed in order to study the potential use of the materials for biomedical applications.

PLLA electrospun membranes were also produced by electrospinning and **Chapter 6** shows the influence of oxygen and argon plasma treatments in the obtained membranes. The influence of plasma treatments on the morphology, fiber average size, roughness and physical–chemical characteristics of PLLA, such as polymer phase or degree of crystallinity are reported. Surface wettability studies are also performed by contact

angle measurements and the potential application of the materials before and after plasma treatment evaluated through viability studies.

Chapter 7 reports on the production of neat PLLA microspheres and magnetic nanoparticles/PLLA composite microspheres by an oil-in-water emulsion method. The average size of the microspheres is presented together with their physico-chemical properties and the influence of the magnetic microspheres in cell viability.

Finally, **chapter 8** presents the overall conclusions and suggestions for future work.

1.7. References

1. Barnes, C.P., et al., *Nanofiber technology: Designing the next generation of tissue engineering scaffolds.* Advanced Drug Delivery Reviews, 2007. **59**(14): p. 1413-1433.
2. Malafaya, P.B., G.A. Silva, and R.L. Reis, *Natural–origin polymers as carriers and scaffolds for biomolecules and cell delivery in tissue engineering applications.* Advanced Drug Delivery Reviews, 2007. **59**(4–5): p. 207-233.
3. Kim, B.-S., et al., *Design of artificial extracellular matrices for tissue engineering.* Progress in Polymer Science, 2011. **36**(2): p. 238-268.
4. Tessmar, J.K. and A.M. Göpferich, *Matrices and scaffolds for protein delivery in tissue engineering.* Advanced Drug Delivery Reviews, 2007. **59**(4–5): p. 274-291.
5. O'Brien, F.J., *Biomaterials & scaffolds for tissue engineering.* Materials Today, 2011. **14**(3): p. 88-95.
6. Rana, D., et al., *Chapter 10 - Considerations on Designing Scaffold for Tissue Engineering*, in *Stem Cell Biology and Tissue Engineering in Dental Sciences*, A.V.S.S. Ramalingam, Editor. 2015, Academic Press: Boston. p. 133-148.
7. Jang, J.-H., O. Castano, and H.-W. Kim, *Electrospun materials as potential platforms for bone tissue engineering.* Advanced Drug Delivery Reviews, 2009. **61**(12): p. 1065-1083.
8. Valence, S.d., et al., *Plasma treatment for improving cell biocompatibility of a biodegradable polymer scaffold for vascular graft applications.* European Journal of Pharmaceutics and Biopharmaceutics, 2013. **85**(1): p. 78-86.
9. Kessler, F., et al., *Wettability and cell spreading enhancement in poly(sulfone) and polyurethane surfaces by UV-assisted treatment for tissue engineering purposes.* Tissue Engineering and Regenerative Medicine, 2014. **11**(1): p. 23-31.
10. Yoshida, S., et al., *Surface modification of polymers by plasma treatments for the enhancement of biocompatibility and controlled drug release.* Surface and Coatings Technology, 2013. **233**: p. 99-107.
11. Kim, H.N., et al., *Nanotopography-guided tissue engineering and regenerative medicine.* Advanced Drug Delivery Reviews, 2013. **65**(4): p. 536-558.
12. Samatham, R., et al., *Active Polymers: An Overview*, in *Electroactive Polymers for Robotics Applications: Artificial Muscles and Sensors*, K.J. Kim and S. Tadokoro, Editors. 2007, Springer-Verlag: London.
13. Mercier, J.P., G. Zambelli, and W. Kurz, *Chapter 1 - Materials*, in *Introduction to Materials Science*, J.P. Mercier, G. Zambelli, and W. Kurz, Editors. 2002, Elsevier: Oxford. p. 1-16.
14. Alexander, H., et al., *Chapter 2 - Classes of Materials Used in Medicine*, in *Biomaterials Science*, B.D. Ratner and A.S.H.J.S.E. Lemons, Editors. 1996, Academic Press: San Diego. p. 37-130.

15. Fattahi, P., et al., *A review of organic and inorganic biomaterials for neural interfaces.* Advanced Materials, 2014. **26**(12): p. 1846-1885.

16. Jordan, J., et al., *Experimental trends in polymer nanocomposites—a review.* Materials Science and Engineering: A, 2005. **393**(1–2): p. 1-11.

17. Mano, J.F., *Smart Polymers: Applications in Biotechnology and Biomedicine.* Macromolecular Bioscience, 2009. **9**(6): p. 622-622.

18. Custódio, C.A., et al., *Smart instructive polymer substrates for tissue engineering*, in *Smart Polymers and their Applications*. 2014. p. 301-326.

19. Kumari, P., et al., *Smart polymeric materials emerging for biological applications*, in *Smart Polymer Materials for Biomedical Applications*. 2011. p. 103-118.

20. Kumar, A., et al., *Smart polymers: Physical forms and bioengineering applications.* Progress in Polymer Science, 2007. **32**(10): p. 1205-1237.

21. Stuart, M.A.C., et al., *Emerging applications of stimuli-responsive polymer materials.* Nature Materials, 2010. **9**(2): p. 101-113.

22. Roy, D., J.N. Cambre, and B.S. Sumerlin, *Future perspectives and recent advances in stimuli-responsive materials.* Progress in Polymer Science, 2010. **35**(1–2): p. 278-301.

23. Alarcon, C.d.l.H., S. Pennadam, and C. Alexander, *Stimuli responsive polymers for biomedical applications.* Chemical Society Reviews, 2005. **34**(3): p. 276-285.

24. Jeong, B. and A. Gutowska, *Lessons from nature: stimuli-responsive polymers and their biomedical applications.* Trends in Biotechnology, 2002. **20**(7): p. 305-311.

25. Kim, K.J. and S. Tadokoro, *Electroactive polymers for robotic applications: Artificial muscles and sensors*. Electroactive Polymers for Robotic Applications: Artificial Muscles and Sensors. 2007. 1-281.

26. Bar-Cohen, Y., *Current and future developments in artificial muscles using electroactive polymers.* Expert Review of Medical Devices, 2005. **2**(6): p. 731-740.

27. Galvin, M.E., *Electrically active polymers and their application.* JOM, 1997. **49**(3): p. 52-55.

28. Gurunathan, K., et al., *Electrochemically synthesised conducting polymeric materials for applications towards technology in electronics, optoelectronics and energy storage devices.* Materials Chemistry and Physics, 1999. **61**(3): p. 173-191.

29. Guimard, N.K., N. Gomez, and C.E. Schmidt, *Conducting polymers in biomedical engineering.* Progress in Polymer Science, 2007. **32**(8–9): p. 876-921.

30. Dhandayuthapani, B., et al., *Polymeric scaffolds in tissue engineering application: A review.* International Journal of Polymer Science, 2011. **2011**: p. 290602.

31. Lu, Q., et al., *Novel porous aortic elastin and collagen scaffolds for tissue engineering.* Biomaterials, 2004. **25**(22): p. 5227-5237.

32. Yoo, H.S., T.G. Kim, and T.G. Park, *Surface-functionalized electrospun nanofibers for tissue engineering and drug delivery.* Advanced Drug Delivery Reviews, 2009. **61**(12): p. 1033-1042.

33. Khang, G., et al., *Preparation and characterization of small intestine submucosa powder impregnated poly(L-lactide) scaffolds: The application for tissue engineered bone and cartilage.* Macromolecular Research, 2002. **10**(3): p. 158-167.

34. Yuan, J., J. Shen, and I.K. Kang, *Fabrication of protein-doped PLA composite nanofibrous scaffolds for tissue engineering.* Polymer International, 2008. **57**(10): p. 1188-1193.

35. Boland, E.D., et al., *Utilizing acid pretreatment and electrospinning to improve biocompatibility of poly(glycolic acid) for tissue engineering.* Journal of Biomedical Materials Research - Part B Applied Biomaterials, 2004. **71**(1): p. 144-152.

36. Boland, E.D., et al., *Tailoring tissue engineering scaffolds using electrostatic processing techniques: A study of poly(glycolic acid) electrospinning.* Journal of Macromolecular Science - Pure and Applied Chemistry, 2001. **38 A**(12): p. 1231-1243.

37. Kang, S.W., W.G. La, and B.S. Kim, *Open macroporous poly(lactic-co-glycolic acid) microspheres as an injectable scaffold for cartilage tissue engineering.* Journal of Biomaterials Science, Polymer Edition, 2009. **20**(3): p. 399-409.

38. Shao, H.J., et al., *Designing a three-dimensional expanded polytetrafluoroethylene-poly(lactic- co-glycolic acid) scaffold for tissue engineering.* Artificial Organs, 2009. **33**(4): p. 309-317.

39. Beamish, J.A., et al., *The effects of monoacrylated poly(ethylene glycol) on the properties of poly(ethylene glycol) diacrylate hydrogels used for tissue engineering.* Journal of Biomedical Materials Research - Part A, 2010. **92**(2): p. 441-450.

40. Zhu, J., *Bioactive modification of poly(ethylene glycol) hydrogels for tissue engineering.* Biomaterials, 2010. **31**(17): p. 4639-4656.

41. Schappacher, M., et al., *Comparative in vitro cytotoxicity toward human osteoprogenitor cells of polycaprolactones synthesized from various metallic initiators.* Macromolecular Bioscience, 2010. **10**(1): p. 60-67.

42. Liu, X. and P. Ma, *Polymeric Scaffolds for Bone Tissue Engineering.* Annals of Biomedical Engineering, 2004. **32**(3): p. 477-486.

43. Hofmann Boss, S. and M. Garcia-Fuentes, *Bioactive scaffolds for the controlled formation of complex skeletal tissues*, in *Regenerative medicine and tissue engineering: cells and biomaterials* D. Eberli, Editor. 2011, InTech: Rijeka. p. 393 - 432.

44. Ravichandran, R., et al., *Advances in Polymeric Systems for Tissue Engineering and Biomedical Applications.* Macromolecular Bioscience, 2012. **12**(3): p. 286-311.

45. Furukawa, T., *Piezoelectricity and pyroelectricity in polymers.* Electrical Insulation, IEEE Transactions on, 1989. **24**(3): p. 375-394.

46. Kochervinskiĭ, V.V., *Piezoelectricity in crystallizing ferroelectric polymers: Poly(vinylidene fluoride) and its copolymers (a review).* Crystallography Reports, 2003. **48**(4): p. 649-675.

47. Moore, A.D., *Electrostatic discharges for treating skin lesions: does it deserve some new research?* Medical Instrumentation, 1975. **9**(6): p. 274-275.

48. Foulds, I.S. and A.T. Barker, *Human-skin battery potentials and their possible role in wound-healing.* British Journal of Dermatology, 1983. **109**(5): p. 515-522.

49. Sulik, G.L., et al., *Effects of steady electric fields on human retinal pigment epithelial cell orientation and migration in culture.* Acta Ophthalmologica, 1992. **70**(1): p. 115-122.

50. Zhao, M., et al., *Orientation and directed migration of cultured corneal epithelial cells in small electric fields are serum dependent.* Journal of Cell Science, 1996. **109**(6): p. 1405-1414.

51. Pu, J., et al., *EGF receptor signalling is essential for electric-field-directed migration of breast cancer cells.* Journal of Cell Science, 2007. **120**(19): p. 3395-3403.

52. Wang, E., et al., *Bi-directional migration of lens epithelial cells in a physiological electrical field.* Experimental Eye Research, 2003. **76**(1): p. 29-37.

53. Bouaziz, A., A. Richert, and A. Caprani, *Vascular endothelial cell responses to different electrically charged poly(vinylidene fluoride) supports under static and oscillating flow conditions.* Biomaterials, 1997. **18**(2): p. 107-112.

54. Valentini, R.F., et al., *Electrically charged polymeric substrates enhance nerve fibre outgrowth In vitro.* Biomaterials, 1992. **13**(3): p. 183-190.

55. Chao, P.H.G., et al., *Effects of applied DC electric field on ligament fibroblast migration and wound healing.* Connective Tissue Research, 2007. **48**(4): p. 188-197.

56. Shamos, M.H. and L.S. Lavine, *Piezoelectricity as a fundamental property of biological tissues.* Nature, 1967. **213**(5073): p. 267-269.

57. Telega, J.J. and R. Wojnar, *Piezoelectric effects in biological tissues*. Vol. 40. 2002.

58. Fukada, E., *Electrical phenomena in biorheology.* Biorheology, 1982. **19**(1-2): p. 15-27.

59. Athenstaedt, H., *Pyroelectric and piezoelectric behaviour of human dental hard tissues.* Archives of Oral Biology, 1971. **16**(5): p. 495-501.

60. De Rossi, D., C. Domenici, and P. Pastacaldi, *Piezoelectric properties od dry human skin. SKIN.* IEEE transactions on electrical insulation, 1985. **EI-21**(3): p. 511-517.

61. Ingber, D.E., *The architecture of life.* Scientific American, 1998. **278**(1): p. 48-57.

62. Guzelsu, N. and H. Demiray, *Electromechanical properties and related models of bone tissues. A review.* International Journal of Engineering Science, 1979. **17**(7): p. 813-851.

63. Yasuda, I., K. Noguchi, and T. Sato, *Dynamic callus and electric callus.* Journal of bone and joint surgery 1955. **37**: p. 1292-1293.

64. Fukada, E. and I. Yasuda, *On the piezoelectric effect of bone.* Journal of the Physical Society of Japan, 1957. **12**(10): p. 1158-1162.

65. Bassett, C.A.L. and R.O. Becker, *Generation of electric potentials by bone in response to mechanical stress.* Science, 1962. **137**(3535): p. 1063-1064.

66. Frost, H.M., *Wolff's Law and bone's structural adaptations to mechanical usage: an overview for clinicians.* The Angle Orthodontist, 1994. **64**(3): p. 175-188.

67. Fukada, E. and I. Yasuda, *On the Piezoelectric Effect of Bone.* Journal of the Physical Society of Japan, 1964. **12**(10): p. 1158-1162.

68. Mahanian, S. and R.L. Piziali, *Finite element evaluation of the AIA shear specimen for bone.* Journal of Biomechanics, 1988. **21**(5): p. 347-356.

69. Marino, A.A. and R.O. Becker, *Piezoelectric effect and growth control in bone.* Nature, 1970. **228**(5270): p. 473-474.

70. Baiotto, S. and M. Zidi, *Theoretical and numerical study of a bone remodeling model: The effect of osteocyte cells distribution.* Biomechanics and Modeling in Mechanobiology, 2004. **3**(1): p. 6-16.

71. Ferrier, J., et al., *Osteoclasts and osteoblasts migrate in opposite directions in response to a constant electrical field.* Journal of Cellular Physiology, 1986. **129**(3): p. 283-288.

72. Hartig, M., U. Joos, and H.P. Wiesmann, *Capacitively coupled electric fields accelerate proliferation of osteoblast-like primary cells and increase bone extracellular matrix formation in vitro.* European Biophysics Journal, 2000. **29**(7): p. 499-506.

73. Brighton, C.T., et al., *In vitro bone-cell response to a capacitively coupled electrical field: The role of field strength, pulse pattern, and duty cycle.* Clinical Orthopaedics and Related Research, 1992(285): p. 255-262.

74. Brighton, C.T., et al., *Signal transduction in electrically stimulated bone cells.* Journal of Bone and Joint Surgery - Series A, 2001. **83**(10): p. 1514-1523.

75. Zhuang, H., et al., *Electrical Stimulation Induces the Level of TGF-β1 mRNA in Osteoblastic Cells by a Mechanism Involving Calcium/Calmodulin Pathway.* Biochemical and Biophysical Research Communications, 1997. **237**(2): p. 225-229.

76. Korenstein, R., et al., *Capacitative pulsed electric stimulation of bone cells. Induction of cyclic-AMP changes and DNA synthesis.* Biochimica et Biophysica Acta (BBA) - Molecular Cell Research, 1984. **803**(4): p. 302-307.

77. McCullen, S.D., et al., *Application of low-frequency alternating current electric fields via interdigitated electrodes: Effects on cellular viability, cytoplasmic calcium, and osteogenic differentiation of human adipose-derived stem cells.* Tissue Engineering - Part C: Methods, 2010. **16**(6): p. 1377-1386.

78. Akai, M., Y. Shirasaki, and T. Tateishi, *Electrical stimulation on joint contracture: An experiment in rat model with direct current.* Archives of Physical Medicine and Rehabilitation, 1997. **78**(4): p. 405-409.

79. Mohr, T., et al., *Increased Bone Mineral Density after Prolonged Electrically Induced Cycle Training of Paralyzed Limbs in Spinal Cord Injured Man.* Calcified Tissue International, 1997. **61**(1): p. 22-25.

80. Bassett, C.A.L., R.J. Pawluk, and R.O. Becker, *Effects of electric currents on bone in vivo.* Nature, 1964. **204**(4959): p. 652-654.

81. Brighton, C.T., et al., *Direct current stimulation of non union and congenital pseudarthrosis. Exploration of its clinical application.* Journal of Bone and Joint Surgery - Series A, 1975. **57**(3): p. 368-377.

82. Rubinacci, A., et al., *Changes in bioelectric potentials on bone associated with direct current stimulation of osteogenesis.* Journal of Orthopaedic Research, 1988. **6**(3): p. 335-345.

83. Yonemori, K., et al., *Early effects of electrical stimulation on osteogenesis.* Bone, 1996. **19**(2): p. 173-180.

84. Anselme, K., *Osteoblast adhesion on biomaterials.* Biomaterials, 2000. **21**(7): p. 667-681.

85. Miara, B., et al., *Piezomaterials for bone regeneration design - homogenization approach.* Journal of the Mechanics and Physics of Solids, 2005. **53**(11): p. 2529-2556.

86. Fukada, E., *History and recent progress in piezoelectric polymers.* Ieee Transactions on Ultrasonics Ferroelectrics and Frequency Control, 2000. **47**(6): p. 1277-1290.

87. West, C.R. and A.E. Bowden, *Using Tendon Inherent Electric Properties to Consistently Track Induced Mechanical Strain.* Annals of Biomedical Engineering, 2012. **40**(7): p. 1568-1574.

88. Fukada, E. and I. Yasuda, *Piezoelectric Effects in Collagen.* Japanese Journal of Applied Physics, 1964. **3**(2): p. 117.

89. Anderson, J.C. and C. Eriksson, *Piezoelectric properties of dry and wet bone.* Nature, 1970. **227**(5257): p. 491-492.

90. Gross, D. and W.S. Williams, *Streaming potential and the electromechanical response of physiologically-moist bone.* Journal of Biomechanics, 1982. **15**(4): p. 277-295.

91. Marino, A.A. and R.O. Becker, *Piezoelectricity in hydrated frozen bone and tendon.* Nature, 1975. **253**(5493): p. 627-628.

92. Lavine, L.S., et al., *Electric Enhancement of Bone Healing.* Science, 1972. **175**(4026): p. 1118-1121.

93. Fukada, E., H. Ueda, and R. Rinaldi, *Piezoelectric and related properties of hydrated collagen.* Biophysical Journal, 1976. **16**(8): p. 911-918.

94. Ahn, A.C. and A.J. Grodzinsky, *Relevance of collagen piezoelectricity to "Wolff's Law": A critical review.* Medical Engineering & Physics, 2009. **31**(7): p. 733-741.

95. Lang, S.B., *Pyroelectric Effect in Bone and Tendon.* Nature, 1966. **212**(5063): p. 704-705.

96. Anderson, J.C. and C. Eriksson, *Electrical Properties of Wet Collagen.* Nature, 1968. **218**(5137): p. 166-168.

97. Halperin, C., et al., *Piezoelectric Effect in Human Bones Studied in Nanometer Scale.* Nano Letters, 2004. **4**(7): p. 1253-1256.

98. Martin, A.J.P., *Tribo-electricity in wool and hair.* Proceedings of the Physical Society, 1941. **53**: p. 186-189.

99. Lang, S.B., et al., *Piezoelectricity in the human pineal gland.* Bioelectrochemistry and Bioenergetics, 1996. **41**(2): p. 191-195.

100. Liu, C., Z. Xia, and J.T. Czernuszka, *Design and Development of Three-Dimensional Scaffolds for Tissue Engineering.* Chemical Engineering Research and Design, 2007. **85**(7): p. 1051-1064.

101. Fallahiarezoudar, E., et al., *A review of: Application of synthetic scaffold in tissue engineering heart valves.* Materials Science and Engineering: C, 2015. **48**: p. 556-565.

102. Zhang, L., et al., *Review scaffold design and stem cells for tooth regeneration.* Japanese Dental Science Review, 2013. **49**(1): p. 14-26.

103. Ribeiro, C., et al., *Piezoelectric poly(vinylidene fluoride) microstructure and poling state in active tissue engineering.* Engineering in Life Sciences, 2015. **15**(4): p. 351-356.

104. Zamani, M., M.P. Prabhakaran, and S. Ramakrishna, *Advances in drug delivery via electrospun and electrosprayed nanomaterials.* International Journal of Nanomedicine, 2013. **8**: p. 2997-3017.

105. Wei, G. and P.X. Ma, *2 - Polymeric biomaterials for tissue engineering*, in *Tissue Engineering Using Ceramics and Polymers (Second Edition)*, A.R. Boccaccini and P.X. Ma, Editors. 2014, Woodhead Publishing. p. 35-66.

106. Fallahiarezoudar, E., et al., *A review of: Application of synthetic scaffold in tissue engineering heart valves.* Materials Science and Engineering C, 2015. **48**: p. 556-565.

107. Hikosaka, S., H. Ishikawa, and Y. Ohki, *Effects of crystallinity on dielectric properties of poly(L-lactide).* Electronics and Communications in Japan, 2011. **94**(7): p. 1-8.

108. Ochiai, T. and E. Fukada, *Electromechanical Properties of Poly-L-Lactic Acid.* Journal of Japanese Applied Physics, 1998. **37**(Part 1, No. 6A): p. 3374-3376.

109. Malmonge, J.A., et al., *Piezo and dielectric properties of PHB–PZT composite.* Polymer Composites, 2009. **30**(9): p. 1333-1337.

110. Fukada, E. and Y. Ando, *Piezoelectric properties of poly-β-hydroxybutyrate and copolymers of β-hydroxybutyrate and β-hydroxyvalerate.* International Journal of Biological Macromolecules, 1986. **8**(6): p. 361-366.

111. Gomes, J., et al., *Influence of the β-phase content and degree of crystallinity on the piezo-and ferroelectric properties of poly(vinylidene fluoride).* Smart Materials and Structures, 2010. **19**(6): p. 065010.

112. Martins, P., A.C. Lopes, and S. Lanceros-Mendez, *Electroactive phases of poly(vinylidene fluoride): Determination, processing and applications.* Progress in Polymer Science, 2014. **39**(4): p. 683-706.

113. Frubing, P., et al., *Relaxation processes at the glass transition in polyamide 11: From rigidity to viscoelasticity.* The Journal of Chemical Physics, 2006. **125**(21): p. 214701-214708.

114. Serrado Nunes, J., et al., *Relationship between the microstructure and the microscopic piezoelectric response of the α - and β -phases of poly(vinylidene fluoride).* Applied Physics A: Materials Science & Processing, 2009. **95**(3): p. 875-880.

115. Nalwa, H.S., *Ferroelectric Polymers: Chemistry, Physics, and Applications*, 1995, Marcel Dekker, Inc: New York.

116. Frias, C., et al., *Polymeric piezoelectric actuator substrate for osteoblast mechanical stimulation.* Journal of Biomechanics, 2010. **43**(6): p. 1061-1066.

117. Reis, J., et al., *A new piezoelectric actuator induces bone formation in vivo: a preliminary study.* Journal of biomedicine & biotechnology, 2012. **2012**: p. 613403-613403.

118. Ribeiro, C., et al., *Enhanced proliferation of pre-osteoblastic cells by dynamic piezoelectric stimulation.* Rsc Advances, 2012. **2**(30): p. 11504-11509.

119. Rodrigues, M.T., et al., *beta-PVDF Membranes Induce Cellular Proliferation and Differentiation in Static and Dynamic Conditions*, in *Advanced Materials Forum Iv*, A.T. Marques, et al., Editors. 2008. p. 72-76.

120. Damaraju, S.M., et al., *Structural changes in PVDF fibers due to electrospinning and its effect on biological function.* Biomedical Materials, 2013. **8**(4): p. 045007.

121. Marques, L., et al., *Subcutaneous tissue reaction and cytotoxicity of polyvinylidene fluoride and polyvinylidene fluoride-trifluoroethylene blends associated with natural polymers.* Journal of Biomedical Materials Research Part B-Applied Biomaterials, 2013. **101**(7): p. 1284-1293.

122. Ikada, Y., et al., *Enhancement of bone formation by drawn poly(L-lactide).* Journal of Biomedical Materials Research, 1996. **30**(4): p. 553-558.

123. Prabhakaran, M.P., J. Venugopal, and S. Ramakrishna, *Electrospun nanostructured scaffolds for bone tissue engineering.* Acta Biomaterialia, 2009. **5**(8): p. 2884-2893.

124. Ko, E.K., et al., *In Vitro Osteogenic Differentiation of Human Mesenchymal Stem Cells and In Vivo Bone Formation in Composite Nanofiber Meshes.* Tissue Engineering Part A, 2008. **14**(12): p. 2105-2119.

125. Wang, Y.-W., et al., *Evaluation of three-dimensional scaffolds made of blends of hydroxyapatite and poly(3-hydroxybutyrate-co-3-hydroxyhexanoate) for bone reconstruction.* Biomaterials, 2005. **26**(8): p. 899-904.

126. Paşcu, E.I., J. Stokes, and G.B. McGuinness, *Electrospun composites of PHBV, silk fibroin and nano-hydroxyapatite for bone tissue engineering.* Materials Science and Engineering: C, 2013. **33**(8): p. 4905-4916.

127. Mota, C., et al., *Additive manufacturing of poly[(R)-3-hydroxybutyrate-co-(R)-3-hydroxyhexanoate] scaffolds for engineered bone development.* Journal of Tissue Engineering and Regenerative Medicine, 2014: DOI: 10.1002/term.1897.

128. Denning, D., et al., *Electromechanical properties of dried tendon and isoelectrically focused collagen hydrogels.* Acta Biomaterialia, 2012. **8**(8): p. 3073-3079.

129. Moreira, P.L., et al., *In vitro analysis of anionic collagen scaffolds for bone repair.* Journal of Biomedical Materials Research - Part B Applied Biomaterials, 2004. **71**(2): p. 229-237.

130. Kakudo, N., et al., *Bone tissue engineering using human adipose-derived stem cells and honeycomb collagen scaffold.* Journal of Biomedical Materials Research Part A, 2008. **84A**(1): p. 191-197.

131. Gimenes, R., et al., *Composites PVDF-TrFE/BT used as bioactive membranes for enhancing bone regeneration*, in *Smart Structures and Materials 2004: Electroactive Polymer Actuators and Devices*, Y. BarCohen, Editor. 2004. p. 539-547.

132. Teixeira, L.N., et al., *Response of human alveolar bone-derived cells to a novel poly(vinylidene fluoride-trifluoroethylene)/barium titanate membrane.* Journal of Materials Science-Materials in Medicine, 2011. **22**(1): p. 151-158.

133. Beloti, M.M., et al., *In vitro biocompatibility of a novel membrane of the composite poly(vinylidene-trifluoroethylene)/barium titanate.* Journal of Biomedical Materials Research Part A, 2006. **79A**(2): p. 282-288.

134. Teixeira, L.N., et al., *In vitro biocompatibility of poly(vinylidene fluoride-trifluoroethylene)/barium titanate composite using cultures of human periodontal ligament fibroblasts and keratinocytes.* Acta Biomaterialia, 2010. **6**(3): p. 979-989.

135. Chen, Y., et al., *PLLA scaffolds with biomimetic apatite coating and biomimetic apatite/collagen composite coating to enhance osteoblast-like cells attachment and activity.* Surface & Coatings Technology, 2006. **201**(3-4): p. 575-580.

136. Valentini, R.F., et al., *Patterned neuronal attachment and outgrowth on surface modified, electrically charged fluoropolymer substrates.* Journal of Biomaterials Science, Polymer Edition, 1994. **5**(1-2): p. 13-36.

137. Royo-Gascon, N., et al., *Piezoelectric substrates promote neurite growth in rat spinal cord neurons.* Annals of Biomedical Engineering, 2013. **41**(1): p. 112-122.

138. Young, T.-H., et al., *Surface modification of microporous PVDF membranes for neuron culture.* Journal of Membrane Science, 2010. **350**(1-2): p. 32-41.

139. Aebischer, P., et al., *Piezoelectric guidance channels enhance regeneration in the mouse sciatic nerve after axotomy.* Brain Research, 1987. **436**(1): p. 165-168.

140. Delaviz, H., et al., *Repair of peripheral nerve defects using a polyvinylidene fluoride channel containing nerve growth factor and collagen gel in adult rats.* Cell Journal, 2011. **13**(3): p. 137-142.

141. Lee, Y.S. and T.L. Arinzeh, *The influence of piezoelectric scaffolds on neural differentiation of human neural stem/progenitor cells.* Tissue Engineering - Part A, 2012. **18**(19-20): p. 2063-2072.

142. Lee, Y.S., G. Collins, and T. Livingston Arinzeh, *Neurite extension of primary neurons on electrospun piezoelectric scaffolds.* Acta Biomaterialia, 2011. **7**(11): p. 3877-3886.

143. Fine, E.G., et al., *Improved nerve regeneration through piezoelectric vinylidenefluoride-trifluoroethylene copolymer guidance channels.* Biomaterials, 1991. **12**(8): p. 775-780.

144. Evans, G.R.D., et al., *Clinical long-term in vivo evaluation of poly(L-lactic acid) porous conduits for peripheral nerve regeneration.* Journal of Biomaterials Science, Polymer Edition, 2000. **11**(8): p. 869-878.

145. de Guzman, R.C., J.A. Loeb, and P.J. VandeVord, *Electrospinning of Matrigel to Deposit a Basal Lamina-Like Nanofiber Surface.* Journal of Biomaterials Science -- Polymer Edition, 2010. **21**(8/9): p. 1081-1101.

146. O'Shaughnessy, T.J., H.J. Lin, and W. Ma, *Functional synapse formation among rat cortical neurons grown on three-dimensional collagen gels.* Neuroscience Letters, 2003. **340**(3): p. 169-172.

147. Martins, P.M., et al., *Effect of poling state and morphology of piezoelectric poly(vinylidene fluoride) membranes for skeletal muscle tissue engineering.* Rsc Advances, 2013. **3**(39): p. 17938-17944.

148. Jansen, P.L., et al., *Surgical mesh as a scaffold for tissue regeneration in the esophagus.* European Surgical Research, 2004. **36**(2): p. 104-111.

149. Inui, A., et al., *Potency of double-layered Poly L-lactic Acid scaffold in tissue engineering of tendon tissue.* International Orthopaedics, 2010. **34**(8): p. 1327-1332.

150. McKeon-Fischer, K.D. and J.W. Freeman, *Characterization of electrospun poly(L-lactide) and gold nanoparticle composite scaffolds for skeletal muscle*

tissue engineering. Journal of Tissue Engineering and Regenerative Medicine, 2011. **5**(7): p. 560-568.

151. Ye, C., et al., *PHB/PHBHHx scaffolds and human adipose-derived stem cells for cartilage tissue engineering.* Biomaterials, 2009. **30**(26): p. 4401-4406.

152. Klink, C.D., et al., *Comparison of Long-Term Biocompability of PVDF and PP Meshes.* Journal of Investigative Surgery, 2011. **24**(6): p. 292-299.

153. Klinge, U., et al., *PVDF as a new polymer for the construction of surgical meshes.* Biomaterials, 2002. **23**(16): p. 3487-3493.

154. Laroche, G., et al., *Polyvinylidene fluoride monofilament sutures - can they be used safely for long-term anastomoses in the thoracic aorta.* Artificial Organs, 1995. **19**(11): p. 1190-1199.

155. Conze, J., et al., *New Polymer for Intra-Abdominal Meshes-PVDF Copolymer.* Journal of Biomedical Materials Research Part B-Applied Biomaterials, 2008. **87B**(2): p. 321-328.

156. Ribeiro-Samy, S., et al., *Development and characterization of a PHB-HV-based 3D scaffold for a tissue engineering and cell-therapy combinatorial approach for spinal cord injury regeneration.* Macromolecular Bioscience, 2013. **13**(11): p. 1576-1592.

157. Rouabhia, M., et al., *Electrical Stimulation Promotes Wound Healing by Enhancing Dermal Fibroblast Activity and Promoting Myofibroblast Transdifferentiation.* Plos One, 2013. **8**(8): p. e71660.

158. Weber, N., et al., *Characterization and in vitro cytocompatibility of piezoelectric electrospun scaffolds.* Acta Biomaterialia, 2010. **6**(9): p. 3550-3556.

159. Gallego, D., N.J. Ferrell, and D.J. Hansford, *Fabrication of Piezoelectric Polyvinylidene Fluoride (PVDF) Microstructures by Soft Lithography for Tissue Engineering and Cell Biology Applications.* MRS Online Proceedings Library, 2007. **1002**: p. 1002-N04-05.

160. Ribeiro, C., et al., *Dynamic piezoelectric stimulation enhances osteogenic differentiation of human adipose stem cells.* Journal of Biomedical Materials Research Part A, 2015. **103**(6): p. 2172-2175.

161. Guo, H.-F., et al., *Piezoelectric PU/PVDF electrospun scaffolds for wound healing applications.* Colloids and Surfaces B: Biointerfaces, 2012. **96**: p. 29-36.

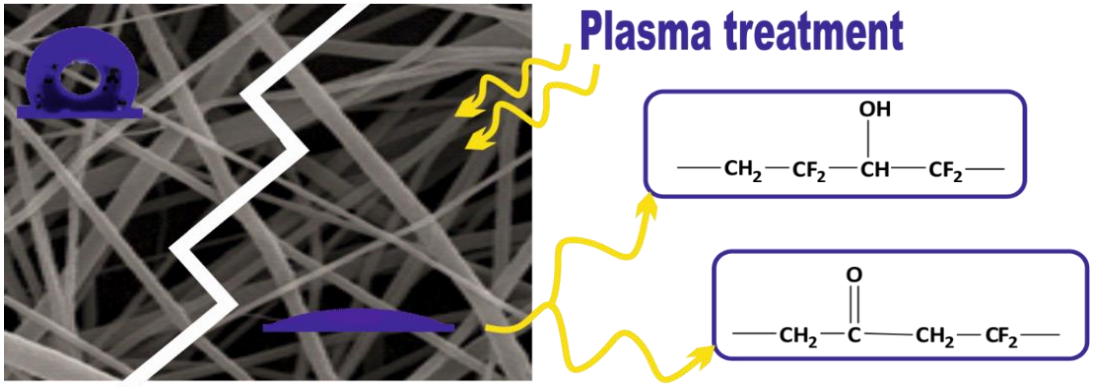

2. Influence of oxygen plasma treatment parameters on poly(vinylidene fluoride) electrospun fiber mats wettability

PVDF membranes with excellent properties can be processed by electrospinning method. However, due to the hydrophobic nature of PVDF presents limited applicability. This chapter is based on the study of the surface wettability of PVDF membranes produced by electrospinning. Oxygen plasma treatment has been applied in order to modify the surface wettability of PVDF fiber mats. The influence of the surface treatment in fiber morphology, average size and physical-chemical properties of PVDF was evaluated, together with its influence on membrane wettability.

This chapter is based on the following publication: D. M. Correia, C. Ribeiro, V. Sencadas, G.Botelho, S.A.C. Carabineiro, J.L. Gomez-Ribelles, S. Lanceroz-Méndez. *Influence of oxygen plasma treatment parameters on poly(vinylidene fluoride) electrospun fiber mats wettability*. Progress in Organic Coatings. 2015. 85:151-158.

2.1. Introduction

PVDF is a semi-crystalline polymer with strong piezoelectric properties, high mechanical strength, thermal stability, high electric and chemical resistance and good processability [1-5]. This polymer has at least four known crystalline phases (α, β, γ and δ), being the β-phase the one with the largest piezoelectric response [3,6].

PVDF has been used in various fields including tissue engineering, filtration, air cleaning, rechargeable batteries and sensors, among others [2,7,8]. In particular, electrospun PVDF fiber mats have attracted a large interest due to their high surface area, small fiber diameters and porous structure [2]. However, the high hydrophobicity, poor wettability and low surface energy characteristic of PVDF are major drawbacks for several applications [2,7]. In order to overcome these limitations, surface modification by introducing specific functional groups on the surface is often used in order to tailor polymer wettability [2,7,9].

A wide range of surface modification methodologies have been used to modify the properties of materials, including surface hydrolysis, chemical grafting, self-assembly or plasma treatment [10,11].

Plasma treatment is one of the most extensively used techniques to modify surface properties of polymers [11,12]. Gas plasma represents a reactive chemical environment in which different plasma-surface reactions occur [12].

Plasma treatment is typically used for modifying the chemical and physical surface properties of polymers without affecting their bulk characteristics [11]. It is thus commonly used to tailor surface adhesion and wetting properties by changing the surface chemical composition of the polymers [11]. With plasma surface modification and deposition it is possible to introduce functional groups, to control surface roughness and crosslinking, graft polymerization and thin film coating adhesion [11]. Generally, plasma treatment has been used to insert chemically reactive functional groups on polymer surface changing the surface chemical composition and to promote covalent immobilization of different components onto the polymer surface [2,11]. A careful selection of plasma source types, time and gas are the key issues. In this sense, plasma treatments by oxygen, ammonia or air could generate carboxyl or amine groups on polymer surfaces [11]. The application of oxygen plasma on different polymer substrates has generated promising results on promoting cell growth owing to the incorporation of hydrophilic and oxygen functional groups [13].

Plasma treatment has been used to promote surface modifications on PVDF [7,13-19]. Duca *et al.* [20] investigated the surface modifications of PVDF under RF Argon (Ar) plasma, and the results showed an improvement of the PVDF surface wettability under plasma exposure. The surface of PVDF can be also modified by Ar, He (helium) and O_2 (oxygen) plasma, however, O_2 plasma was not effective in decreasing the contact angle of PVDF sheet surface [15]. Plasma-induced free radical polymerization was used to modify PVDF membranes prepared by solvent casting [18] to support neural cell culture.

To the best of our knowledge, few studies exist on PVDF electrospun fiber surface modification by plasma in order to improve hydrophilicity. Furthermore, it has been demonstrated that Ar plasma-induced grafting of acrylic acid significantly improved the wetting behavior of electrospun PVDF nanofiber membranes [2].

This work reports the modification of electrospun PVDF fibers wettability by oxygen plasma to improve hydrophilicity of the polymeric membranes. The influence of different parameters such as treatment time (s), O_2 flow rate ($mL.min^{-1}$) and the power (W) were studied. Furthermore, the influence of plasma treatment on fiber morphology, degree of crystallinity and polymer phase were evaluated, as these are also relevant for the different application of this electroactive material.

2.2. Experimental

2.2.1. Materials

PVDF with reference Solef 1010 was acquired from Solvay. Analytical grade N,N-Dimethyl Formamide (DMF) was purchased from Merck.

2.2.2. Electrospinning processing

PVDF electrospun fibers were processed according to the previously reported method of Ribeiro *et. al.* [21]. Briefly, a 20 % (w/w) solution of PVDF in DMF was prepared under magnetic stirring at room temperature until complete dissolution of the polymer. Then, the polymer solution was placed in a plastic syringe (10 mL) fitted with a steel needle with inner diameter of 0.5 mm. The electrospinning procedure was conducted at 20 kV with a high voltage power supply from Glassman (model PS/FC30P04) with a

solution feed rate of 1 $mL.h^{-1}$ applied with the help of a syringe pump (from Syringepump). The electrospun fibers were collected in an aluminum plate.

2.2.3. Surface modification

Surface treatment was conducted in a plasma chamber (Plasma-Electronic PICCOLO) equipped with 13.56 MHz radio frequency plasma generator. Plasma treatments were performed under different conditions with the plasma power varying between 120 to 600 W, the flow rate varying from 20 to 100 $mL.min^{-1}$and from 60 to 900 s under a total pressure of 20 Pa.

2.2.4. Characterization

Fiber morphology was analyzed using a scanning electron microscopy (SEM, Quanta 650, from FEI) with an accelerating voltage of 5 kV. The samples were previously coated with a thin gold layer using a sputter coating (Polaron, model SC502).
Infrared measurements (FTIR) were performed at room temperature in a Bruker alpha apparatus in ATR mode from 4000 to 400 cm^{-1}. FTIR spectra were collected after 24 scans with a resolution of 4 cm^{-1}. Differential scanning calorimetry measurements (DSC) were performed in a Mettler Toledo 823e apparatus using a heating rate of 10 $^{o}C.min^{-1}$ under nitrogen purge. Wettability of the samples was determined by measuring the contact angle of distilled water at room temperature, using an OCA15 Dataphysics contact angle analyzer. Six measurements were carried out for each sample at different places. The porosity (ε) of the PVDF fiber mats was measured by liquid displacement method using a pycnometer. The weight of the pycnometer filled with ethanol, was measured and labeled as $\mathbf{W}_1$; the PVDF fibers, whose weight was $\mathbf{W}_s$, were immersed in ethanol. After the sample was saturated by ethanol, additional ethanol was added to complete the volume of the pycnometer. Then, the pycnometer was weighted and labeled as $\mathbf{W}_2$; the sample filled with ethanol was then taken out of the pycnometer [22]. The residual weight of the ethanol and the pycnometer was labeled $\mathbf{W}_3$. The porosity of the membrane was calculated according to Equation 2.1:

$$\varepsilon = \frac{W_2 - W_3 - W_S}{W_1 - W_3} \quad (2.1)$$

The mean porosity of each membrane was obtained as the average of the values determined in three samples. Absolute ethanol (Merck), as a non-solvent of PVDF, was used as a displacement liquid since it can penetrate among the fibers not inducing shrinking or swelling in the fiber mat [23].

X-ray photoelectron spectroscopy (XPS) was performed using a Kratos AXIS Ultra HSA, with VISION software for data acquisition and CASAXPS software for data analysis in order to evaluate the surface elemental composition and atomic concentration of the samples. The analysis was carried out with a monochromatic Al Kα X-ray source (1486.7 eV), operating at 15 kV (90 W), in FAT mode (Fixed Analyser Transmission), with a pass energy of 40 eV for regions ROI and 80 eV for survey. Data acquisition was performed with a pressure lower than 1×10^{-6} Pa, and it was used a charge neutralization system. The effect of the electric charge was corrected by the reference of the carbon peak (284.6 eV). All binding energies (BEs) were referenced to the C1s hydrocarbon peak at 286.4 eV. Spectra were analyzed using XPSPEAK software (version 4.1). Curve fitting of the high resolution spectra used 30 % Gaussian/70 % Lorentzian mixed line shapes for each component.

2.3. Results and Discussion

2.3.1. Effect of plasma treatment on PVDF fiber morphology

Pristine PVDF electrospun fibers were electrospun into a highly porous non-woven mesh with interconnected pores and smooth fiber surface: no beads were observed in the fiber mats (Figure 2.1a). PVDF membrane porosity was estimated using the pycnometer method and an overall membrane porosity of 79 ± 4 % was obtained.

The effect of the different plasma treatments on PVDF fiber morphology was assessed by SEM. The influence of plasma power was investigated by keeping constant a rich oxygen atmosphere of 120 $mL.min^{-1}$ during 120 s. The SEM pictures of Figure 2.1 show the effect of the applied plasma power on the size of the electrospun fibrils.

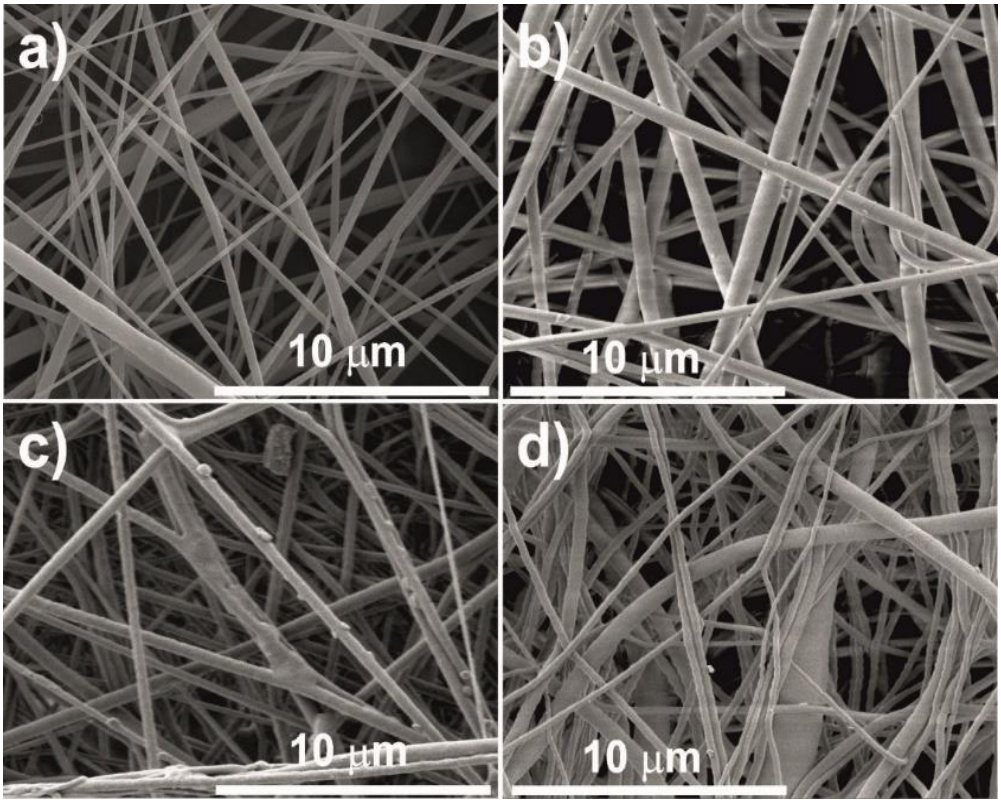

Figure 2.1. SEM images of electrospun PVDF fibers: a) without treatment and treated with O_2 plasma as a function of the applied power: b) 240 W, c) 360 W and d) 480 W for 120 s using a constant O_2 flow rate of 120 mL.min^{-1}.

The fiber roughness increased with increasing plasma power (Figure 2.1). Small "*bumps*" appeared on the fibrils surface leading to some eventual fiber joining, especially for the highest plasma power (Figure 2.1) which probably is related to surface polymer melting due to the high energy supplied by the plasma source. In spite of the mentioned, fiber surface effects the overall appearance of fiber meshes are similar to that of the pristine ones. Furthermore, no complete fiber melting was detected after plasma treatments, the membranes showing still open spaces between fibers.

The effect of plasma exposure time and oxygen flow rate for a fixed plasma power was also characterized and the variations in fiber morphology are similar to the ones observed after plasma power variation. The influence of different plasma parameters on fiber mean diameter was determined (Figure 2.2). Pristine polymer mats present a mean fiber diameter of ~400±200 nm both before and after plasma treatment (Figure 2.2), indicating that the plasma treatment induce physical-chemical variations on the fiber surface, without variations of the bulk properties.

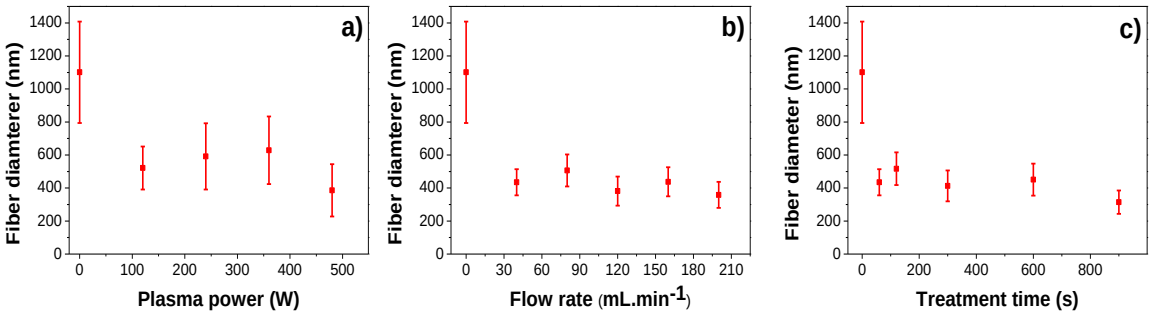

Figure 2.2. Influence of different plasma treatment parameters in PVDF average fiber diameter: a) plasma power (t=120 s; O_2 flow rate of 120 mL.min^{-1}); b) O_2 flow rate (t=120 s and power of 480 W) and c) time (power of 480 W; O_2 flow rate of 120 mL.min^{-1}).

2.3.2. Surface chemical characterization and phase content

In order to evaluate the influence of plasma treatment in the chemical surface of PVDF and on the electroactive β-phase content, FTIR-ATR of non-treated and plasma treated polymer fiber mats were measured (Figure 2.3a).

PVDF chemical structure is composed by the repetition unit -CH_2-CF_2- along the polymer chain and the characteristic vibrational modes can be used to identify the presence of different polymorphs [6]. Figure 2.3a shows the infrared spectra of the pristine sample and the plasma treated ones after different applied powers. The results are representative of the FTIR spectra obtained for the samples prepared with different O_2 flow rates and different exposure time to plasma treatment. Neither modes are totally suppressed nor do new ones appear due to the change of the plasma processing parameters, compared to the pristine fiber mats. The characteristic absorption modes for the α-phase (855, 795 and 766 cm^{-1}) and the β-phase (840 cm^{-1}) are detected (Figure 2.3a) and no traces of the γ-phase (776, 812, 833, 838 and 1234 cm^{-1} modes) appears [6, 21].

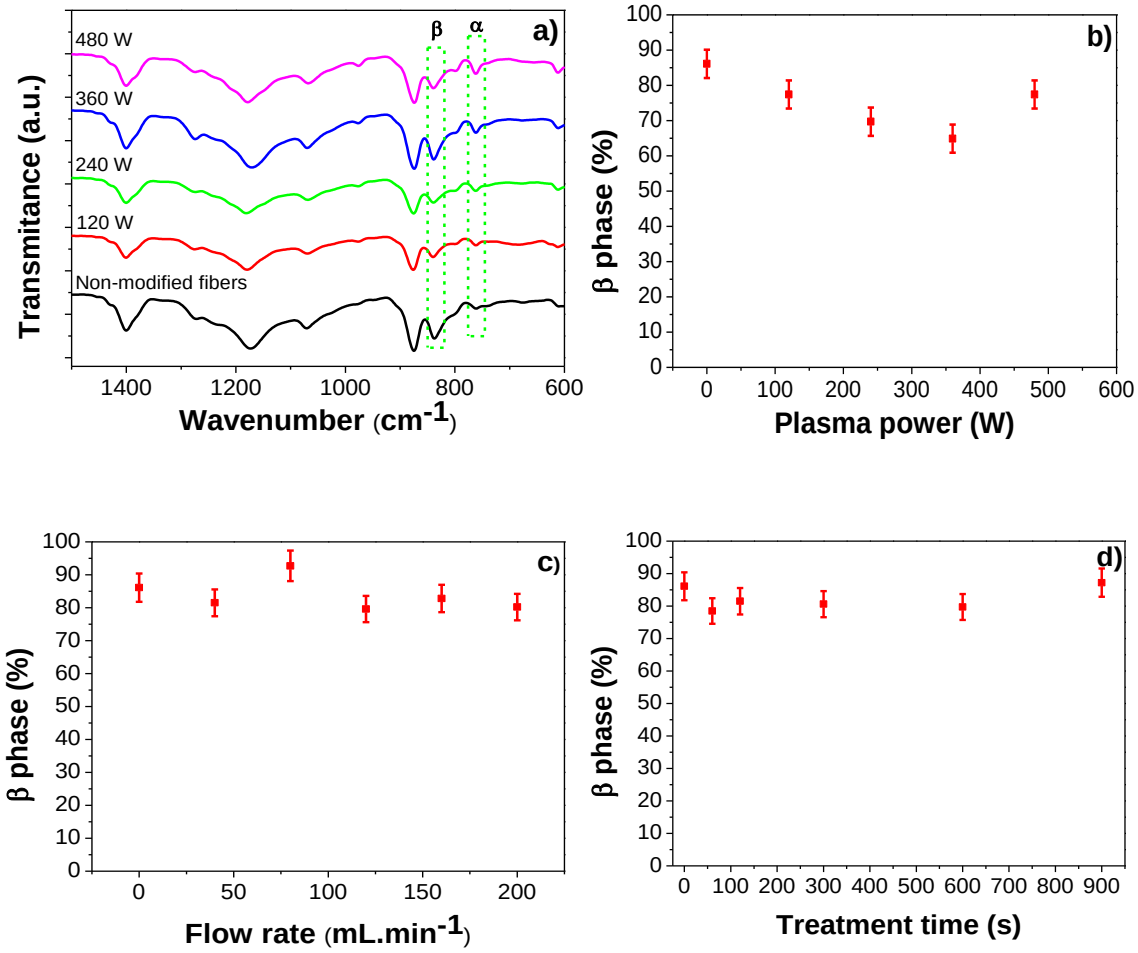

Figure 2.3. a) FTIR-ATR spectra of non-modified and plasma modified fiber at different plasma power applied for 120 s at a O_2 flow rate of 120 mL.min^{-1}; b) and d) variation of β-phase content with the applied plasma power, c) O_2 flow rate and d) treatment time**.**

The electrospinning method favors the formation of PVDF fibers crystallized in the electroactive β-phase [6, 21], due to the fact of being a low temperature solvent casting process. Moreover, the use of higher electric fields during processing contribute to dipole alignment and consequently to electrical poling of the PVDF fibers [24], leading to high responsive piezoelectric fibers. The quantification of the β-phase content of the electrospun samples can be performed from the FTIR spectra applying (Equation 2.2) and following the procedure explained in [6, 21]:

$$F(\beta) = \frac{A_\beta}{\left(\frac{K_\beta}{K_\alpha}\right) A_\alpha + A_\beta} \quad (2.2)$$

where *F(β)* represents the β-phase content, K_α and K_β the absorption coefficient for each phase and A_α and A_β the absorbance at 766 and 840 cm^{-1}, respectively. The absorption coefficient value is 7.7×10^4 $cm^2.mol^{-1}$ and 6.1×10^4 $cm^2.mol^{-1}$ for K_β and K_α, respectively [25].

It was observed that increasing the applied plasma power leads to a decrease of the electroactive β-phase (Figure 2.3b) while the O_2 flow rate and plasma treatment time have no significant effect on the β-phase content present in the samples (Figure 2.3c and 2.3d). The decrease of the β-phase content with the increase of the applied plasma power can be related to local sample temperature increase during surface plasma treatment, leading to β to α-phase transformation [26]. This phase transformation has been reported to take place at temperatures above 70 ºC in PVDF and has been related to the increase of cooperative segmental motions within the crystalline fraction [27]. It is to notice, nevertheless, that this decrease of ~20 % of the β-phase content does not represent a significant reduction of the electroactive performance of the material. Gomes *et al.* [28] reported that the piezoelectric coefficient is proportional to the amount of oriented dipoles, and therefore the number of β-phase present in PVDF films influence the piezoelectric response of the material. Typically, the decrease of the β-phase content promoted by plasma treatment is equivalent to a reduction of ~20 % in the piezoelectric coefficient, from 34 down to 28 $pC.N^{-1}$.

2.3.3. Thermal Characterization

DSC measurements were performed in order to detect possible modifications in thermal stability and melting behavior. DSC data reveal that all plasma treated fiber mats showed a similar trend, regardless the plasma treatment condition, with a broader melting transition (Figure 2.4) than in the non-treated samples.

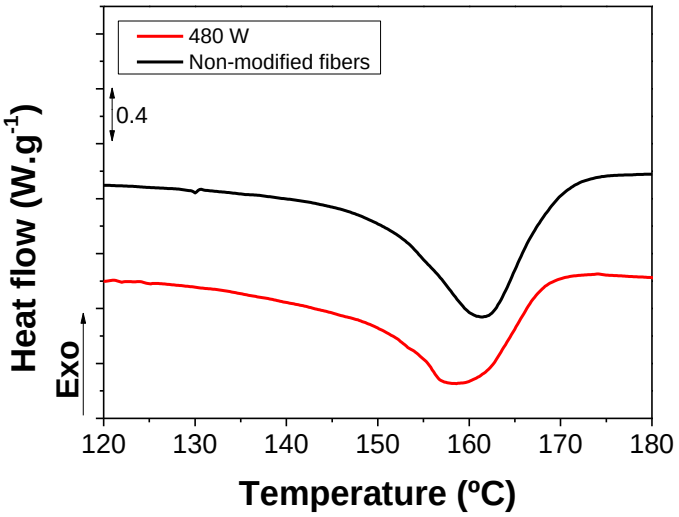

Figure 2.4. DSC curves for the electrospun PVDF non-modified and oxygen plasma modified fibers at a plasma power applied of 480 W for 120 s and an O_2 flow rate of 120 mL.min^{-1}.

FTIR results probe the coexistence of both α- and β-crystalline phases among the sample, which suggests that the broad melting peak corresponds to the melting of both phases, which is clearly observed for the sample with higher amount of α-phase (sample treated at 480 W plasma power, Figure 2.3b. Nevertheless, these kind of results have to be considered with care since DSC heating curves recorded at low heating rates can present more than one endotherm due to the recrystallization taking place during the scan itself after first melting and also a distribution of crystal sizes could produce the same effect [29]. The degree of crystallinity (X_c) of the samples was determined from the DSC thermograms using Equation 2.3 [21]:

$$X_c = \frac{\Delta H}{x\Delta H_\alpha + y\Delta H_\beta} \tag{2.3}$$

where ΔH is the melting enthalpy of the sample; ΔH_α and ΔH_β are the melting enthalpies of a 100 % crystalline sample in the α- and β-phase and the x and y the amount of the α- and β-phase present in the sample, respectively. In this study, the value of 93.07 J.g^{-1} and 103.4 J.g^{-1} were used for ΔH_α and ΔH_β, respectively [21].

Comparing pristine electrospun samples with plasma modified ones, no significant changes were detected in the degree of crystallinity, independently of the plasma treatment conditions and a crystalline fraction of 42 ± 2 % was obtained for all samples, in accordance to other studies with electrospun mats [21, 30].

2.3.4. Surface wettability

Figure 2.5 shows the variation of the contact angle of the plasma modified PVDF fibers as a function of different applied plasma power. The surface water contact angle of the non-modified fibers is 134 ± 6º being in agreement with the strong hydrophobicity of PVDF materials [2]. Changes in water contact angle were observed when the applied plasma power is applied. In particular, for plasma powers above 360 W, the surface contact angle cannot be measured as the water drop is rapidly absorbed by the membrane, indicating a superhydrophilic behavior (Figure 2.5a).

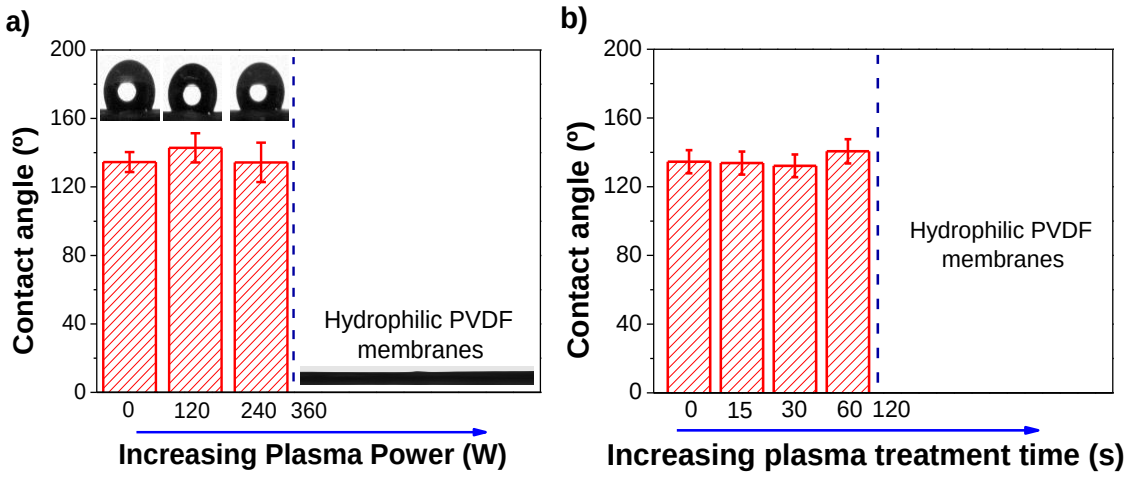

Figure 2.5. Influence of the (a) oxygen plasma power in the contact angle of PVDF fiber membranes with a treatment time of 120 s and an O_2 flow rate of 120 mL.min^{-1} and (b) influence of the treatment time at an applied power of 360 W and O_2 flow rate of 120 mL.min^{-1}. The bars in the graph are the standard deviation of the contact angle distribution.

The influence of oxygen plasma treatment and oxygen flow rate on the surface wettability of PVDF fibers are also studied (results not shown). Treatment times between 60 and 900 s and flow rates between 40 and 200 mL.min^{-1} at a plasma power ≥360 W leaded to PVDF membranes with superhydrophilic behavior, and the water

drop when in contact with PVDF surface almost immediately absorbed by the membrane.

In order to obtain the optimal values for improving the hydrophilicity of the PVDF membranes at an applied power of 360 W (minimum power applied that improves hydrophilicity of electrospun PVDF membranes), the treatment time and oxygen flow rate parameters were studied. The results allowed to conclude that for treatment times and oxygen flow rate below 120 s (Figure 2.5b) and 60 $mL.min^{-1}$, respectively, the plasma did not induce the hydrophilicity of the PVDF membranes. The optimal values to obtain hydrophilic membranes are summarized in Table 2.1.

Table 2.1. Optimal values of plasma parameters in order to obtain hydrophilic membranes.

Plasma parameter	Optimal value
Treatment time (s)	120
Flow rate ($mL.min^{-1}$)	120
Power (W)	360

The literature data show that oxygen plasma treatment reduces contact angle up to 20º, depending on the plasma conditions [7, 13, 15]. In the present case, the fact of obtaining hydrophilic membranes is associated to the variation of the contact angle of the polymer and the capillarity of the membranes. Reduction of the polymer fiber contact angles, as observed in the polymer films [7, 13, 15] lead to an associated variation of the surface tension of the membrane, leading thus to a penetration of the water drop in the membrane and the consequent hydrophilic behavior.

2.3.5. Chemical composition of electrospun PVDF fibers surface

Plasma treatment typically leads to degradation of the polymer surface. The degradation process is accompanied by cleavage of molecular chains and by the formation of free radicals that activate the surface and double bonds that will react forming new oxygen structures [31].

In order to obtain quantitative information about the elemental composition of the non-modified and modified PVDF membranes, XPS analysis was performed. Figure 2.6 shows the XPS results of PVDF surface elemental compositions at different applied

plasma powers. Carbon, fluorine and oxygen were detected in the samples (Figure 2.6a).

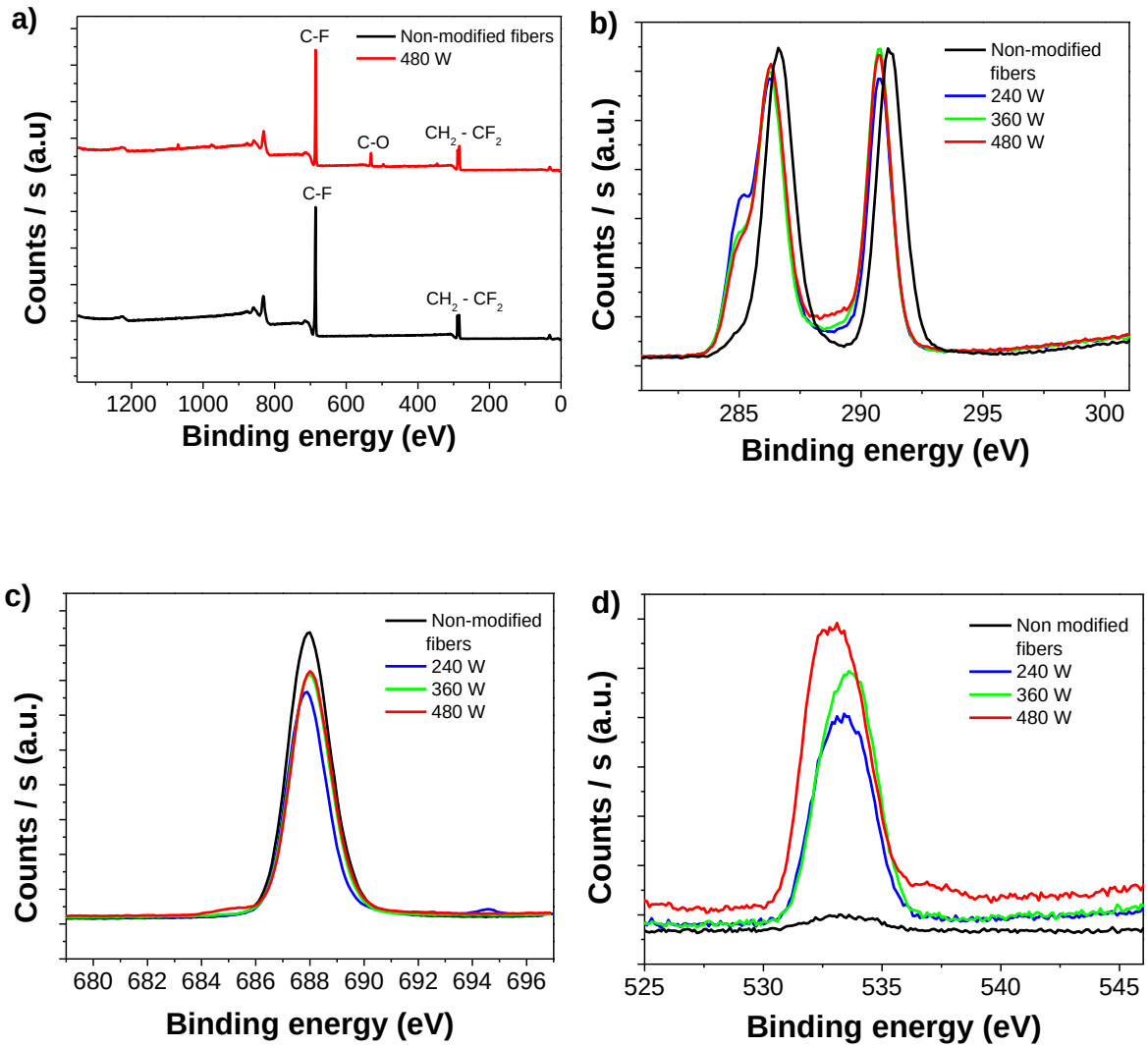

Figure 2.6. XPS results of non-modified PVDF fibers and oxygen plasma treated fibers for 120s with an O_2 flow rate of 120 mL.min^{-1}: a) XPS scans b) C1s scan spectra, c) F1s spectra and d) O1s spectra.

The atomic surface composition for the PVDF surfaces was evaluated from C1s, F1s and O1s scanning spectra. Figure 2.6b shows typical C1s spectra for the non-modified and modified PVDF fibers with oxygen plasma. Deconvolution of Figure 2.6b was performed to show the individual components of the C1s peak (Figure 2.7).

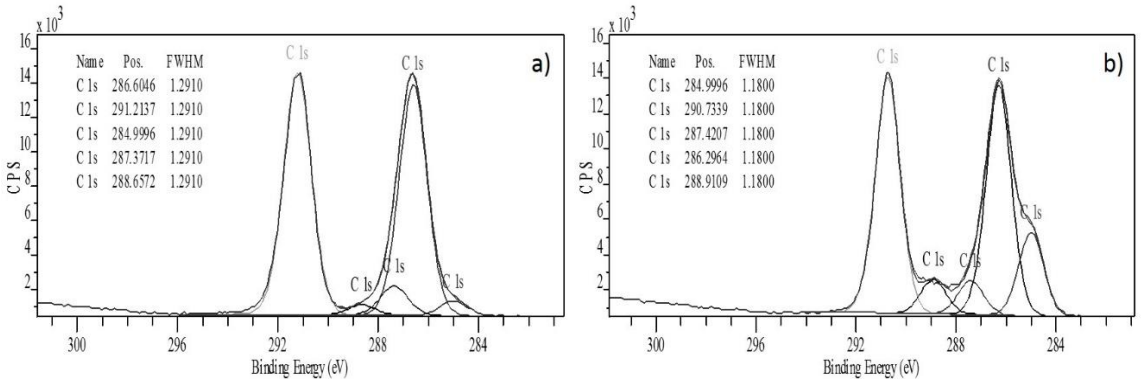

Figure 2.7. C1s scan spectra of a) untreated fibers and b) fibers submitted to O_2 flow of 120 $mL.min^{-1}$, treatment time of 120 s and a power of 480 W.

It is observed that the PVDF fibers showed two main C1s peaks at 291.4 eV assigned to CF_2 groups and at 286.4 eV due to CH_2 component (Table 2.2). Plasma treated fibers also show a peak with bending energy of about 285.0 eV attributed do C-C group (Figure 2.6b). The F1s peak at 688 eV is assigned to C-F bond. Plasma treated fibers shows an O1s peak at 533 eV assigned to C-O bond (Figure 2.6c).

Table 2.2. C 1s, F 1s and O 1s components of non-modified electrospun PVDF fibers and oxygen plasma modified fibers [7].

Peak	Binding energy (eV)	Chemical function
C 1s	285	C-C
C 1s	286	C-H
C 1s	291	C-F
O 1s	533	C-O
F 1s	688	C-F

These changes indicates that oxygen plasma exposure promotes defluorination and oxidation reactions by the incorporation of oxygen onto the polymer fiber surface. Table 2.3 summarizes the XPS analysis for the fluorine to carbon ratio (F/C) and oxygen to carbon ratio (O/C) atom ratios for non-modified and treated PVDF fiber membranes. Though, surface of non-modified PVDF fibers is composed of carbon (51.3 %), and fluorine atoms (48.3 %).

Table 2.3. Surface chemical composition of pristine PVDF fibers and O_2 plasma treated fibers at different applied plasma powers.

	Elemental composition (%)				
Surface	**C**	**O**	**F**	**O/C**	**F/C**
Pristine fibers	51.30	0.35	48.30	0.01	0.94
Plasma treated fibers					
240 W	56.70	5.20	38.10	0.09	0.67
360 W	53.60	5.80	40.60	0.11	0.76
480 W	52.80	6.80	40.40	0.13	0.77

The presence of a quite small oxygen amount (0.35 %) may arise from the exposure of the PVDF fibers to the air or due to solvent contaminants [19]. Nevertheless, modified polymer fibers reflected clear alterations in its surface elemental compositions. The signal corresponding to F being higher on the non-modified fibers than in plasma modified fibers plasma treatment leads to a substantial decrease on fluorine content and an increases in oxygen content as a result of the presence of carboxyl groups in the surface of the fibers generated by the O_2 plasma treatment [32]. The oxygen to carbon ratio O/C increases from 0.007 to approximately 0.1 while F/C decreases from 0.54 to approximately 0.21. Results indicate the success of the plasma activation in the surface of PVDF fibers.

It is reported that oxygen plasma surface modification enriches the surface with oxygen species [33]. The surface modifications of PVDF fibers after the plasma treatment, leading to an overall increase of membrane hydrophilicity, are explained by the cleavage of C-F and C-H hydrophobic groups followed by the formation of C=O, OH and COOH hydrophilic groups on PVDF fibers surface during the interaction between the plasma and the samples. Plasma environments have neutral species, energetic ions, photons and electrons that interact with the polymer causing chemical and physical modifications in the polymer surface and not on the polymer bulk properties. Particularly, the electrons present in plasma have sufficiently high kinetic energy to break the covalent bonds, inducing chemical reactions that will change the polarity of the surface [34]. Fluorinated polymers like PVDF are known to be resistant to oxygen species attack that difficult the abstraction of fluorine atoms. However, the results showed that oxygen atoms are detected in PVDF fibers, indicating that some oxidation reactions occurs in the PVDF fibers after oxygen plasma treatment [15, 35]. This can be explained by the possible recombination of fluorine with carbon radicals. It is known

that the stability of the gas product is an important factor in the modification process than bond energy [15]. Figure 2.8 demonstrates the possible modifications that occur on PVDF surface by oxygen plasma treatment. During the plasma treatment radicals are formed primarily by the scission of carbon-hydrogen bond (C-H), due to the strength of the C-H (410 kJ.mol^{-1}) bond when compared to the C-F bond (460 kJ.mol^{-1}), into the polymer surface which can react with the atmospheric oxygen after plasma treatment forming hydroperoxides. These compounds can thermally decompose producing secondary radicals that subsequently are able to react with the air exposure. As it is possible to observe in Figure 2.6 and Table 2.3, the fluorine content decreases when the plasma modification occurs. In this sense, the step 1 present in Figure 2.8 occurs predominantly originating newly formed C-O and C=O groups. The later was not observed in the XPS results indicating that, if formed, it would be a residual product [35].

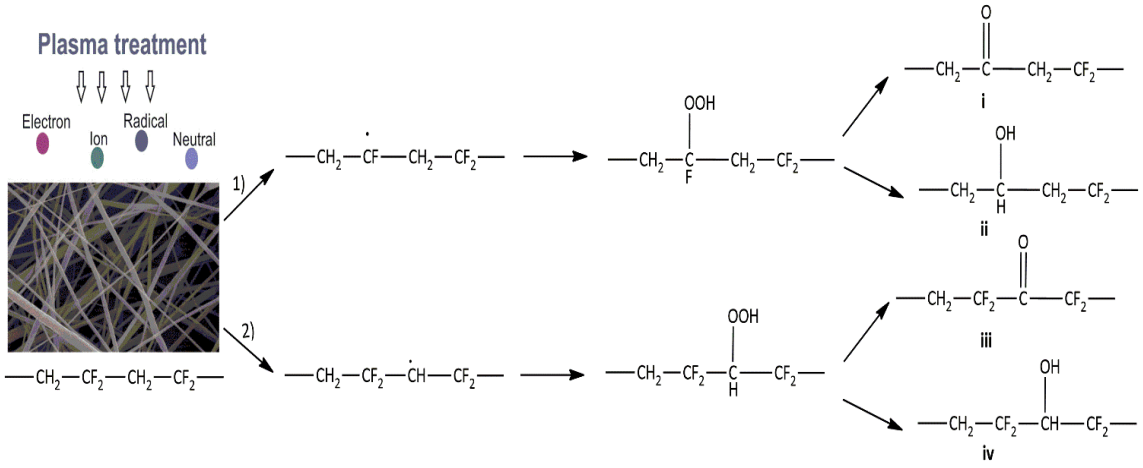

Figure 2.8. Schematic representation of O_2 plasma treatment on electrospun PVDF fibers. Plasma introduces free radicals which can react with oxygen.

2.4. Conclusions

Oxygen plasma treatment has been applied in order to modify the wettability of PVDF membranes. It was observed that plasma treatment does not produce significant variation in average diameter, being ~400 ± 200 nm thus being independent of plasma processing parameters. However, an increase in plasma power increases fiber roughness and small bumps appear on fiber surface leading to some eventual fiber joining without

change membrane overall porosity. Increase plasma power leads to a decrease of the electroactive β-phase from ~85 to 70 % ,O_2 flow rate and plasma treatment time having no influence on β-phase content of the polymer fiber mats. Also no significant changes were detected on degree of crystallinity, independently of the plasma treatment conditions, being ~ 42 ± 2 %.

The plasma treatment showed to be effective to change polymer membrane wettability turning the neat hydrophobic membranes into superhydrophilic ones. This effect is attributed to the introduction of oxygen compounds and a decrease of fluorine content onto the polymer fibers surface and a mechanism is proposed. This fact leads to a reduction of the contact angle of the polymer fibers and an overall decrease of the surface tension of the membranes, which in turn improves capillarity and water absorption of the membrane. PVDF superhydrophilic surfaces can be achieved applying a plasma power bellow 360 W for a treatment time of 120 s and a flow rate of 120 $mL.min^{-1}$.

2.5. References

1. Bormashenko, E., et al., *Polyvinylidene fluoride—piezoelectric polymer for integrated infrared optics applications.* Optical Materials, 2004. **27**(3): p. 429-434.
2. Huang, F.L., et al., *Dynamic wettability and contact angles of poly(vinylidene fluoride) nanofiber membranes grafted with acrylic acid.* Express Polymer Letters, 2010. **4**(9): p. 551-558.
3. Coster, H.G.L., T.D. Farahani, and T.C. Chilcott, *Production and characterization of piezo-electric membranes.* Desalination, 2011. **283**: p. 52-57.
4. Liu, F., et al., *Progress in the production and modification of PVDF membranes.* Journal of Membrane Science, 2011. **375**(1–2): p. 1-27.
5. Zhang, X., et al., *Effects of surface modification on the properties of magnetic nanoparticles/PLA composite drug carriers and in vitro controlled release study.* Colloids and Surfaces A: Physicochemical and Engineering Aspects, 2013. **431**: p. 80-86.
6. Martins, P., A.C. Lopes, and S. Lanceros-Mendez, *Electroactive phases of poly(vinylidene fluoride): Determination, processing and applications.* Progress in Polymer Science, 2014. **39**(4): p. 683-706.
7. Kaynak, A., et al., *Study of Radio Frequency Plasma Treatment of PVDF Film Using Ar, O_2 and (Ar + O_2) Gases for Improved Polypyrrole Adhesion.* Materials, 2013. **6**(8): p. 3482-3493.
8. Martins, P.M., et al., *Effect of poling state and morphology of piezoelectric poly(vinylidene fluoride) membranes for skeletal muscle tissue engineering.* Rsc Advances, 2013. **3**(39): p. 17938-17944.
9. Klee, D., et al., *Surface modification of poly(vinylidenefluoride) to improve the osteoblast adhesion.* Biomaterials, 2003. **24**(21): p. 3663-3670.
10. Valence, S.d., et al., *Plasma treatment for improving cell biocompatibility of a biodegradable polymer scaffold for vascular graft applications.* European Journal of Pharmaceutics and Biopharmaceutics, 2013. **85**(1): p. 78-86.
11. Yoshida, S., et al., *Surface modification of polymers by plasma treatments for the enhancement of biocompatibility and controlled drug release.* Surface and Coatings Technology, 2013. **233**: p. 99-107.
12. Chu, P.K., et al., *Plasma-surface modification of biomaterials.* Materials Science and Engineering: R: Reports, 2002. **36**(5–6): p. 143-206.
13. Mangindaan, D., et al., *Modulation of biocompatibility on poly(vinylidene fluoride) and polysulfone by oxygen plasma treatment and dopamine coating.* Journal of Biomedical Materials Research Part A, 2012. **100A**(11): p. 3177-3188.
14. Gil'man, A.B., *Low-Temperature Plasma Treatment as an Effective Method for Surface Modification of Polymeric Materials.* High Energy Chemistry, 2003. **37**(1): p. 17-23.

15. Park, Y.W. and N. Inagaki, *Surface modification of poly(vinylidene fluoride) film by remote Ar, H2, and O2 plasmas.* Polymer, 2003. **44**(5): p. 1569-1575.

16. Noeske, M., et al., *Plasma jet treatment of five polymers at atmospheric pressure: surface modifications and the relevance for adhesion.* International Journal of Adhesion and Adhesives, 2004. **24**(2): p. 171-177.

17. Vandencasteele, N., D. Merche, and F. Reniers, *XPS and contact angle study of N_2 and O_2 plasma-modified PTFE, PVDF and PVF surfaces.* Surface and Interface Analysis, 2006. **38**(4): p. 526-530.

18. Young, T.-H., et al., *Surface modification of microporous PVDF membranes for neuron culture.* Journal of Membrane Science, 2010. **350**(1–2): p. 32-41.

19. Liu, X., et al., *Amphiphobicity of polyvinylidene fluoride porous films after atmospheric pressure plasma intermittent etching.* Applied Surface Science, 2011. **257**(21): p. 8828-8835.

20. Duca, M.D., C.L. Plosceanu, and T. Pop, *Surface modifications of polyvinylidene fluoride (PVDF) under rf Ar plasma.* Polymer Degradation and Stability, 1998. **61**(1): p. 65-72.

21. Ribeiro, C., et al., *Influence of Processing Conditions on Polymorphism and Nanofiber Morphology of Electroactive Poly(vinylidene fluoride) Electrospun Membranes.* Soft Materials, 2010. **8**(3): p. 274-287.

22. Costa, C.M., et al., *Effect of degree of porosity on the properties of poly(vinylidene fluoride–trifluorethylene) for Li-ion battery separators.* Journal of Membrane Science, 2012. **407**–**408**: p. 193-201.

23. Tan, Q., et al., *Fabrication of Porous Scaffolds with a Controllable Microstructure and Mechanical Properties by Porogen Fusion Technique.* International Journal of Molecular Sciences, 2011. **12**(2): p. 890-904.

24. Sencadas, V., et al., *Local piezoelectric response of single poly(vinylidene fluoride) electrospun fibers.* physica status solidi (a), 2012. **209**(12): p. 2605-2609.

25. Gonçalves, R., et al., *Nucleation of the electroactive β-phase, dielectric and magnetic response of poly(vinylidene fluoride) composites with Fe_2O_3 nanoparticles.* Journal of Non-Crystalline Solids, 2013. **361**: p. 93-99.

26. Silva, M.P., et al., *Degradation of the dielectric and piezoelectric response of β-poly(vinylidene fluoride) after temperature annealing.* Journal of Polymer Research, 2011. **18**(6): p. 1451-1457.

27. Sencadas, V., et al., *Relaxation dynamics of poly(vinylidene fluoride) studied by dynamical mechanical measurements and dielectric spectroscopy.* The European Physical Journal E, 2012. **35**(5): p. 1-11.

28. Gomes, J., et al., *Influence of the β-phase content and degree of crystallinity on the piezo and ferroelectric properties of poly(vinylidene fluoride).* Smart Materials and Structures, 2010. **19**(6): p. 065010.

29. Sencadas, V., R. Gregorio, and S. Lanceros-Méndez, *α to β Phase Transformation and Microestructural Changes of PVDF Films Induced by*

Uniaxial Stretch. Journal of Macromolecular Science, Part B, 2009. **48**(3): p. 514-525.

30. Lopes, A.C., et al., *Effect of filler content on morphology and physical–chemical characteristics of poly(vinylidene fluoride)/NaY zeolite-filled membranes.* Journal of Materials Science, 2014. **49**(9): p. 3361-3370.

31. Slepičková Kasálková, N., et al., *Biocompatibility of plasma nanostructured biopolymers.* Nuclear Instruments and Methods in Physics Research Section B: Beam Interactions with Materials and Atoms, 2013. **307**: p. 642-646.

32. Yoo, H.S., T.G. Kim, and T.G. Park, *Surface-functionalized electrospun nanofibers for tissue engineering and drug delivery.* Advanced Drug Delivery Reviews, 2009. **61**(12): p. 1033-1042.

33. Zandén, C., et al., *Surface characterisation of oxygen plasma treated electrospun polyurethane fibres and their interaction with red blood cells.* European Polymer Journal, 2012. **48**(3): p. 472-482.

34. Pawde, S.M. and K. Deshmukh, *Surface characterization of air plasma treated poly vinylidene fluoride and poly methyl methacrylate films.* Polymer Engineering & Science, 2009. **49**(4): p. 808-818.

35. Akashi, N. and S.-i. Kuroda, *Protein immobilization onto poly (vinylidene fluoride) microporous membranes activated by the atmospheric pressure low temperature plasma.* Polymer, 2014. **55**(12): p. 2780-2791.

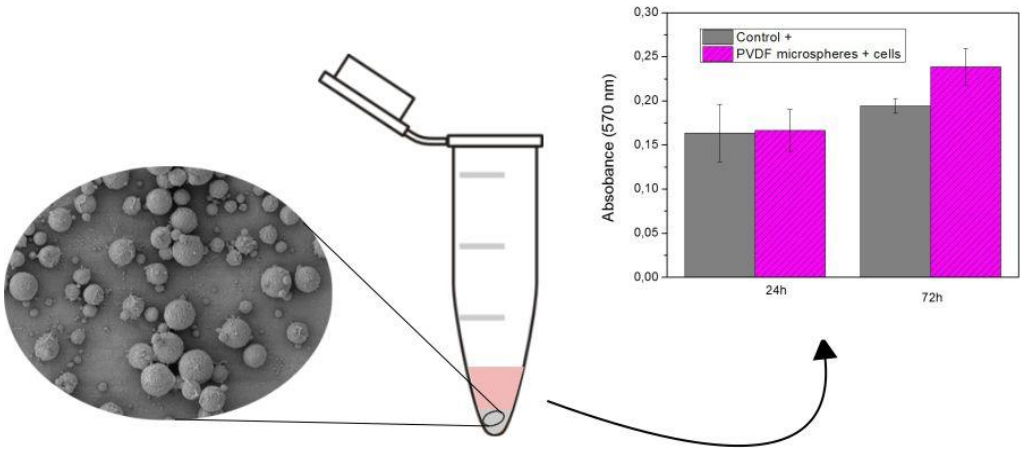

3. Electrosprayed poly(vinylidene fluoride) microspheres for tissue engineering applications

This chapter describes the production of PVDF microspheres by electrospray as a suitable substrate for tissue engineering applications. The influence of polymer solution concentration and processing parameters such as electric field, flow rate and inner needle diameter on sphere size and distribution has been studied. The physico-chemical properties and the electroactive β-phase content were evaluated. MC-3T3-E1 cell adhesion on the PVDF microspheres was assessed, to study their potential use for biomedical applications.

This chapter is based on the following publication: D. M. Correia, R. Gonçalves, C. Ribeiro, V. Sencadas, G.Botelho, J.L. Gomez-Ribelles, S. Lanceroz-Méndez. *Electrosprayed poly(vinylidene fluoride) microparticles for tissue engineering applications*. RSC Advances. 2014. 4:33013.

3.1. Introduction

Polymer microspheres have found applicability in biomedical engineering for drug delivery systems [1, 2] and are increasingly being used as supports for cell expansion and differentiation, which implies the control over micro and macrostructure features of the polymer substrate [3], scaffolds formed by polymer microspheres allowing to hold and populate more cells than the traditional 3D scaffolds [3].

Electrospray is a promising technique for preparation of polymeric micro- and nanoparticles [4]. This method might overcome some of the drawbacks associated with conventional microspheres-producing methods such as solvent casting, single and double emulsion, spray-drying, porous glass membrane emulsification and coacervation [4].

The principles of electrospray are similar to the ones of the electrospinning process. In electrospray, polymeric microspheres can be produced from a polymer solution in a conductive enough solvent. The variation of solution properties such as concentration, viscosity and surface tension, and processing parameters, such as flow rate, needle diameter, distance of the needle to the collector and applied voltage, promotes the formation of a continuous jet that can be broken down into droplets, resulting in microspheres of different size [4]. The advantage of electrospray is the fact that the droplet size can be controlled by adjusting solution and processing parameters [5].

Natural and synthetic polymers have been processed in the form of microspheres by electrospray [6]. The most common natural polymers produced by electrospray are gelatin [7], chitosan [6, 8] and elastin [6]. Gelatin [7] and chitosan [8] microspheres aggregates have been used as a 3D scaffold in cartilage tissue engineering produced. Synthetic polymers including polylactides (PLAs), PLGA and PCL have also been electrosprayed [6]. Among other studies, PLGA microparticles of 4-5 μm in average diameter have been used as a drug delivery system for bone tissue regeneration [9].

Despite to the interest of using electroactive microspheres for several applications, in particular PVDF microspheres due to its strong piezoelectric properties as reported in chapter 2, to our knowledge, there is just one report on the use of electrospray to prepare thin PVDF films composed by PVDF microspheres with diameters in the range of 61 to 250 nm [5].

Thus, this work reports on the production of PVDF microspheres by electrospray. By controlling solution parameters, namely polymer concentration, a stable process has

been achieved allowing to obtaining microspheres with controlled size. The suitability of the developed microspheres as a substrate for tissue engineering application was proven by cell viability studies performed with osteoblast-like MC3T3-E1 cells.

3.2. Experimental

3.2.1. Materials

PVDF reference Solef 1010, was acquired from Solvay. Analytical grade tetrahydrofuran (THF) and DMF were purchased from Panreac and Merck, respectively. The main characteristics of the solvents are summarized in Table 3.1.

The polymer was dissolved in a DMF/THF co-solvent system with a volume ratio of 85/15 (v/v) for PVDF concentrations of 5, 7 and 10 % (w/v). THF is known for the lower boiling point, when compared to the DMF solvent. The ratio DMF/THF was chosen after a series of experimental measurements taken into account the polymer microspheres integrity and jet stability. The solutions were kept under agitation with a magnetic stirrer at room temperature until complete dissolution of the polymer.

Table 3.1. Physical and thermal properties of the solvents used in the present work. Data collected from the datasheets supplied by the manufacturers.

Solvent	Boiling point (^{0}C)	Melting point (^{0}C)	Vapor pressure (Pa)	Dipole moment (Debye)	Dielectric constant	Density (g.cm^{-3})
DMF	146	-61	1300	382	38.2	0.944
THF	65	-108	17530	1.75	7.6	0.889

3.2.2. Electrospray processing

The polymer solution was placed in a commercial plastic syringe fitted with a steel needle with inner diameter of 0.2, 0.5, 1 or 1.7 mm, respectively. Electrospray was conducted by applying a voltage ranging from 15 to 25 kV with a PS/FC30P04 power source from Glassman. A syringe pump (Syringepump) feed the polymer solution into the tip at a rate between 0.2 and 4 mL.h^{-1}. The electrosprayed samples were collected on a grounded collecting plate placed at 20 cm from the needle tip.

3.2.3. Characterization

Microsphere morphology was analyzed by SEM in the same conditions of the samples described in the experimental section of the chapter 2 (see section 2.2.4). Microsphere average diameter and distribution was calculated over approximately 30 microspheres using the SEM images (10000 and 30000 X magnification) and the ImageJ software. Statistical differences were determined by ANOVA with *P* values <0.05 being statistically significant. The physico-chemical properties of the microspheres were evaluated by FTIR and DSC measurements, as described in the experimental section of the chapter 2 (see section 2.2.4).

3.2.4. Cell culture

MC3T3-E1 cells (Riken cell bank, Japan) were cultivated in Dulbecco's modified Eagle's medium (DMEM) 1g.L^{-1} glucose (Gibco) containing 10 % Fetal Bovine Serum (FBS) (Fisher) and 1 % penicillin/streptomycin (P/S) at 37 ºC in a 5 % CO_2 incubator.
For cell culture, 10 mg of microspheres obtained by electrospray (7 % w/v) were placed in a 2 mL *Eppendorf*. For sterilization purposes, the microspheres were immersed in 70 % ethanol, followed by washing with phosphate-buffered saline solution (PBS) 5 times for 10 min under constant shaking. Before cell seeding, fibronectin (FN) was adsorbed by immersing the microspheres in a FN solution of 20 µg.mL^{-1} overnight under constant shaking.
For the cell viability study, MC3T3-E1 (pre-osteoblast) cells (density of 1.5 x 10^5 cells/eppendorf) were mixed with the microspheres up to 3 days. Cell pellets without any microspheres were used as reference (control +) and only microspheres as used as negative control. For the quantification of cell viability, (3-(4, 5-Dimethylthiazol-2-yl)-2, 5-diphenyltetrazolium bromide) (MTT, Sigma-Aldrich) assay was carried out. MTT is used to measure the number of metabolic active cells based on the quantification of the activity of living cells via mitochondrial dehydrogenases. At each time point, the supernatant was removed and fresh medium containing MTT solution was added to each Eppendorf. After 3 h of incubation, the supernatant was removed and dimethyl sulfoxide (DMSO) was added to dissolve the MTT formazan crystals. Thereafter, the solution of each Eppendorf was mixed in a shaker in order to exclude the microspheres

and the supernatant was used to determine the absorbance at 570 nm. Three measurements were performed for each sample.

3.3. Results and discussion

3.3.1. Microsphere morphology

3.3.1.1.Effect of polymer concentration

During electrospray, several parameters related to process and solvent properties play a key role in the stability of the process. The solution should fulfill some requirements related to polymer solubility, proper values for the relative permittivity, surface tension, density, viscosity and conductivity [5]. Additionally, some parameters such as flow rate, electric field, needle inner diameter and distance from the needle tip to collector have influence on the morphology and size of the obtained microspheres [4]. These parameters need to be controlled and optimized in order to obtain microspheres of the desired diameter.

Figure 3.1 shows representative SEM images of the PVDF microspheres prepared by electrospray from a 2, 5, 7 and 10 % (w/v) solution concentration using a solvent mixture of THF and DMF. The corresponding microsphere size distribution is also shown in Figure 3.1. Electrospray from low polymer concentration solution (2 % w/v) did not result in microspheres with spherical geometry (Figure 3.1a), a fact that can be ascribed to the low polymer content in the jet leading to low solution viscosity and high surface tensions of the solution. Under those conditions no polymer entanglement is achieved [10]. Further, more diluted polymer concentrations solutions favors the formation of tailed microspheres (Figure 3.1a) due to the lack of sufficiently strong polymer chain entanglements [10]. On the other hand, spherical PVDF microspheres with different size distributions were obtained with polymer concentrations 5 % (w/v) or more, as reported in [11].

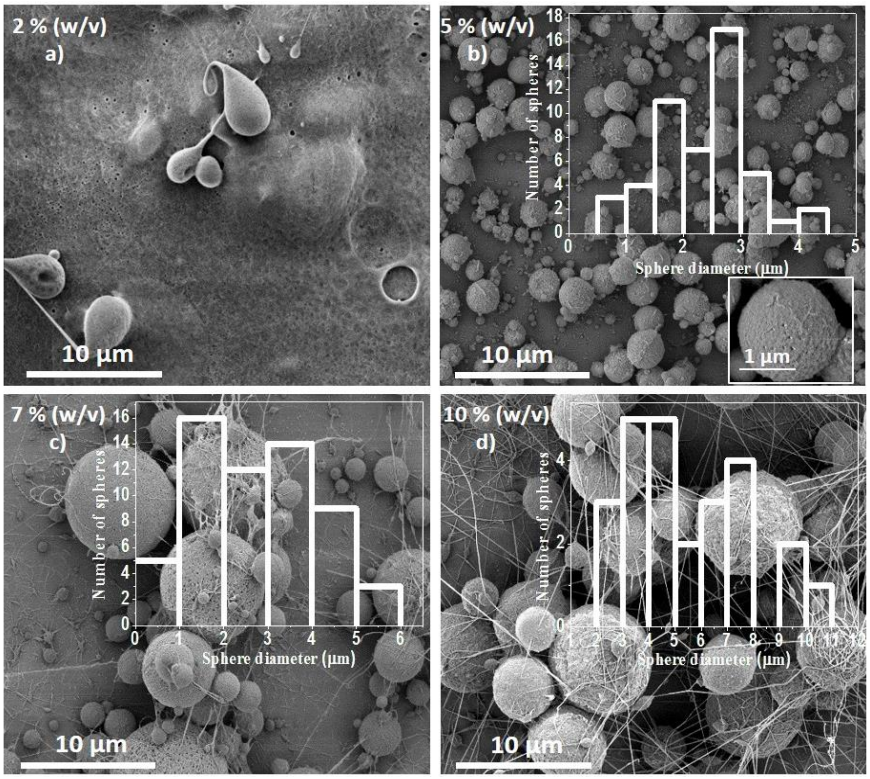

Figure 3.1. Morphology of the PVDF spheres for the samples obtained with a) 2, b) 5, c) 7 and d) 10 % (w/v) polymer solution obtained at an applied electric field of 1 $kV.cm^{-1}$ with a needle diameter of 0.2 mm, flow rate of 2 $mL.h^{-1}$. The particle distribution obtained from each processing condition is presented as an inset.

The spherical morphology of the PVDF microspheres is attributed to the complete solvent evaporation from the droplets before reaching the collector, complementary to the polymer diffusion during solvent evaporation. A rapid polymer diffusion ensures the achievement of solid and dense microspheres but does not necessarily lead to the spherical morphology [2, 6].

PVDF microspheres obtained from the dissolution of PVDF in the co-solvents of DMF/THF are compact due the low boiling point of THF that allows fast polymer crystallization from the liquid jet surface. The high boiling point and low vapor pressure of DMF hinders fast solvent evaporation and promotes a decrease of the mean microspheres size, leading to dense polymer microspheres (Figure 3.1) [6]. Moreover, moisture present in the atmosphere when the electrospray is carried on, also contributes to the high surface roughness observed in Figure 3.1. It has been shown in different polymer systems that high moisture levels present during electrospinning favors the presence of circular pores on top of the electrospun fibers, that become larger with

increasing humidity until they coalescence to form large, non-uniform shaped structures [12, 13].

At a concentration of 7 % (w/v) and more some thin fibers were detected among polymer microspheres and it was observed that when the polymer concentration increases, the amount of fibers in the collector increases and, consequently, the amount of polymer microspheres decreases. This is related to the facts observed in [14] in which smooth and beadles PVDF fibers were obtained for polymer concentrations above 20 % (w/v), leading to some beads in the fiber mats for lower polymer concentrations. Fiber formation has been also reported for polymer concentrations above 10 % (w/v) [11], attributed to enough solution viscosity and surface tension that favors polymer chain entanglement. Our results suggest that dilute or semi-dilutes solutions favor the formation of polymer microspheres while fibers are formed for concentrated solutions above 10 % (w/v).

In this sense, polymer concentration plays a central role in fiber or microspheres formation and therefore in process optimization [6]. Thus, the ideal regime of polymer solution to obtain microspheres is the semi-dilute moderately entangled, where a significant degree of entanglement is observed and dense, solid and reproducible microspheres are obtained [6]. In this state, it is essential that the concentration of the solution (c) is larger than the critical entanglement concentration (c_{ent}) but lower than the critical chain overlap concentration (c_{ov}): for $c > 3c_{ov}$ the regime is defined as semi-dilute highly entangled regime and characterized by the presence of beaded fibers or fibers. In this sense, for a PVDF concentration of 10 % (w/v), the solution is in a semi-dilute highly entangled regime [2, 6] and the critical entanglement concentration is 5 % (w/v), in order to achieve PVDF spherical microspheres. The critical chain overlap is observed when the droplet carries enough polymer to overlap, but not sufficient to generate a significant degree of entanglement, giving origin to deformed spheres and non-uniform and non-reproducible morphology. According to our results the c_{ov} is around 2 % (w/v). The influence of polymer concentration (5, 7 and 10 % (w/v)) in the average size of the PVDF microspheres is shown in Figure 3.2, resulting in an increase in the average microsphere diameter from 2.5 to 5.5 μm, with the increasing polymer concentration.

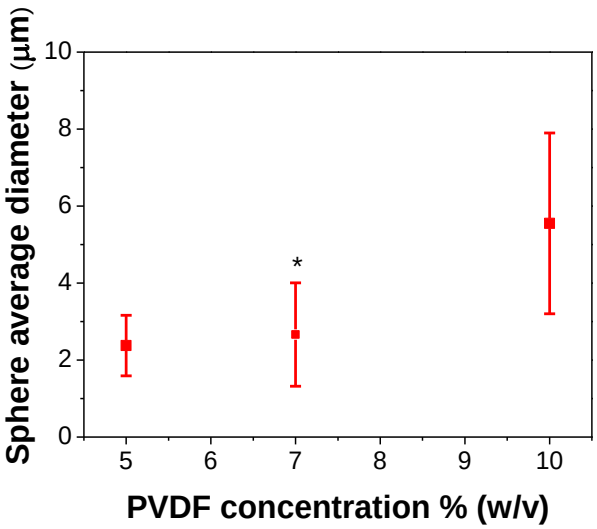

Figure 3.2. Influence of the PVDF solution concentration % (w/v) on microspheres average diameter. The bars in the graph are the standard deviation of the fiber diameter distribution. *P ≤ 0.05 *vs*. PVDF concentration of 10 % (w/v).

3.3.1.2.Effect of electric field on microsphere size

The electrospray process will be initiated when the electrostatic force in the solution overcomes the surface tension of the solution and consequently the amount of polymer sprayed during the electrospray process will increase. In this sense, the effect of the applied electric field in polymer average diameter and microsphere size distribution was evaluated for applied electric fields between 0.75 to 1.25 $kV.cm^{-1}$ (Figure 3.3). For larger applied electric fields elongated microspheres or fibers are formed. On the other hand, when lower electric fields are applied to the polymer solution, the main droplet will be maintained more stable, and ejection of smaller jets from the main one will promote PVDF microspheres with larger size distribution (Figure 3.3c).

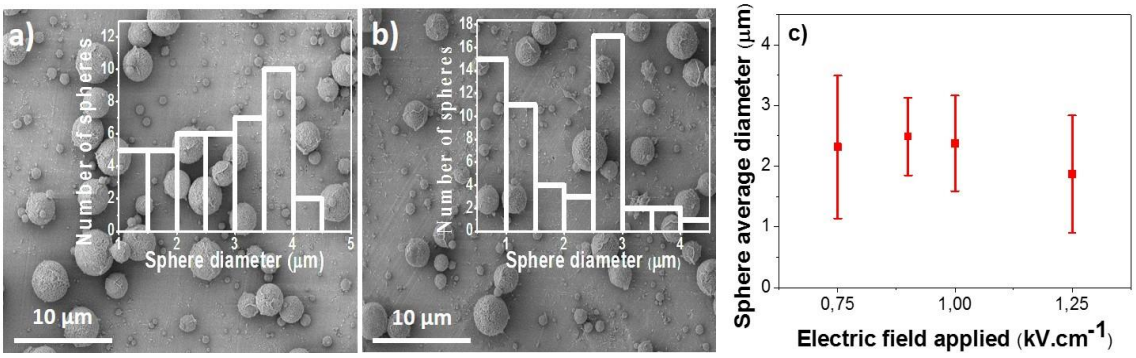

Figure 3.3. a) Morphology of the PVDF microspheres for the samples obtained with a 5 % (w/v) polymer solution at different applied voltages: a) E = 0.75 kV.cm^{-1} b) 1.25 kV.cm^{-1} and c) Influence of the applied electrical field (kV.cm^{-1}) on the microspheres average diameter. Samples prepared with needle diameter of 0.2 mm, flow rate of 2 mL.h^{-1} at a traveling distance of 20 cm. The bars in the graph are the standard deviation of the microsphere diameter distribution.

3.3.1.3.Effect of flow rate on microsphere size

Flow rate will determine the amount of polymer solution available for electrospraying. Moreover, for higher feed rates, solvent total evaporation during the travel from the needle tip to the ground collector is not possible and consequently microspheres are partially solvated when they impact the collector, leading to a deformed and non-consistent morphology [6]. Figure 3.4a shows that flow rate was noticeable determinant in the production of PVDF microspheres. For low flow rates of 0.2 mL.h^{-1}, microspheres have smaller average diameter, while for higher polymer feed rates microspheres with a higher average diameter was obtained (Figure 3.4b), that are independent on the flow rate. These results are explained by the competing mechanism of Coulomb fission and chain entanglements undergoing solvent evaporation. The phenomenon of Coulomb fission, a process by which charge droplet emits a cloud of highly charged small droplets, occurs when a charged drop approach the Rayleigh limit (φ_{Ray}), the limit value at which the drop cannot hold more charge. For higher polymer solution feed rates (> 4 mL.h^{-1}), it was observed that due to the higher amount of the solution that is drawn from the needle tip, the jet takes more time to dry, and consequently the solvent present in the deposited particles has not time enough to evaporate at the same flight time, promoting particle adhesion to each other in the metallic ground collector.

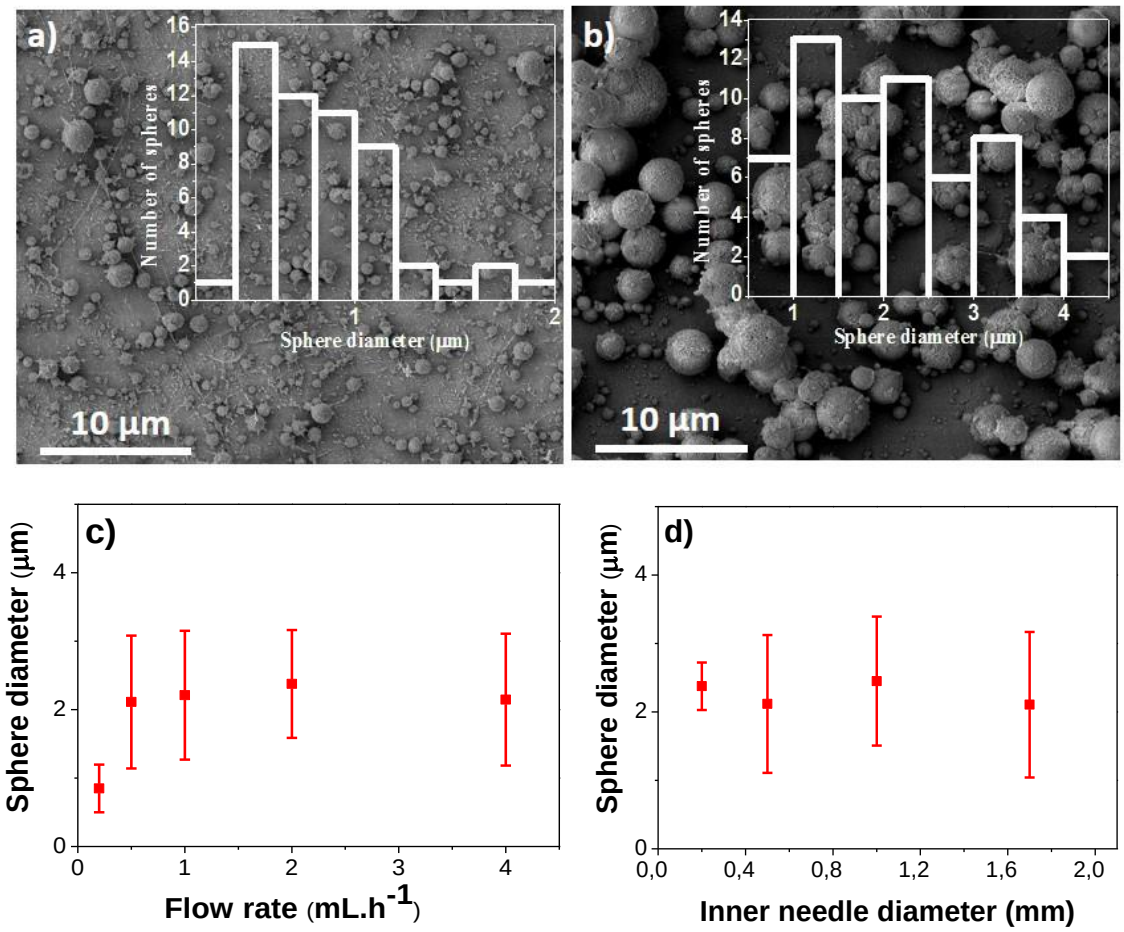

Figure 3.4. Morphology of the PVDF microspheres for the samples obtained with a 5 % (w/v) polymer solution at different flow rates: a) 0.2 $mL.h^{-1}$ and b) 4 $mL.h^{-1}$ with a needle diameter of 0.2 mm, electric applied field of 20 $kV.cm^{-1}$ at a traveling distance of 20 cm. The microparticle diameter histograms of the corresponding figures are also given in the figure. c) and d) Influence of the flow rate ($mL.h^{-1}$) and inner needle diameter (mm) respectively on the microsphere average diameter. The bars in the graph are the standard deviation of the diameter distribution.

The average size of microspheres for the different needle inner diameters was evaluated (Figure 3.4c) and the results show a quite similar particle diameter for all the different samples with an average size diameter between 2.0 and 2.5 µm, being therefore independent of the needle inner diameter.

Figure 3.5 summarizes the influence of the polymer concentration on the size of electrosprayed polymer microspheres, as this is the parameter that mainly influences microsphere formation and diameter (Figure 3.1). Morphology and size of microspheres can be further tuned by the additional parameters described above in order to obtain fibers without beads and in the case of microspheres the absence of fibers.

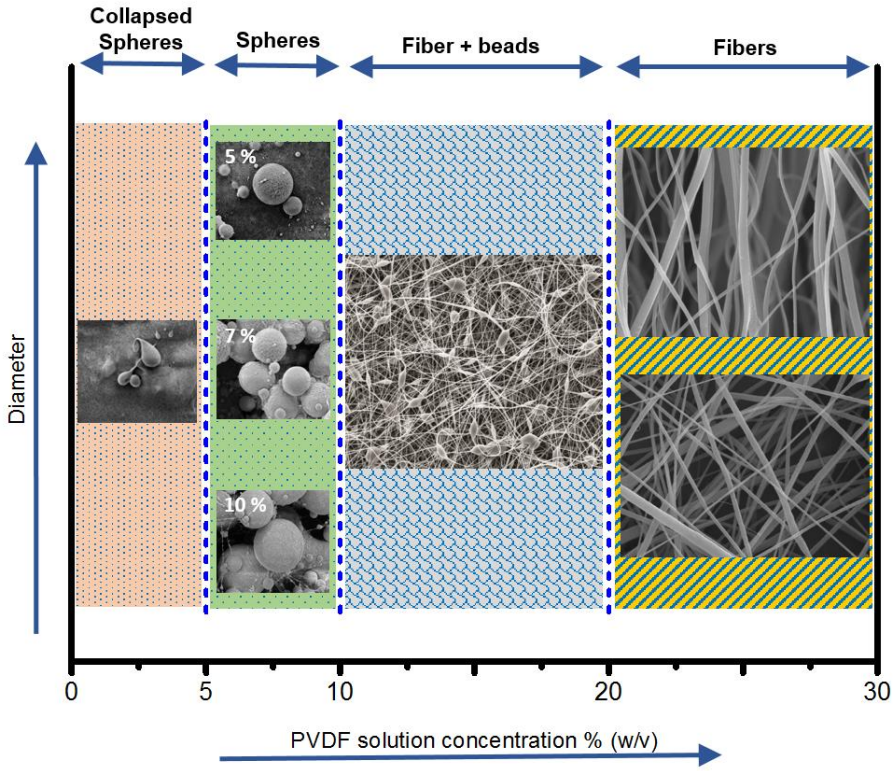

Figure 3.5. Schematic diagram of the influence of PVDF solution concentration in the production of microspheres and fibers by electrospray.

3.3.2. Surface chemical characterization and phase content

FTIR spectroscopy is a characterization technique useful for the identification and quantification of the different crystalline phases of PVDF [15, 16].

The chemical structure of PVDF is composed by the repetition unit–CH_2-CF_2- along the polymer chain and characteristic vibrational modes can be used to the identification of the α- and β-phases [15, 17] The α-phase can be identified by the presence of absorption bands at 489, 530, 615 and 766 cm^{-1} attributed to stretching of the group CF_2, at 795 cm^{-1} corresponding to the CH_2 stretching and at 855 and 976 cm^{-1} resulting of the CH group stretching [18]. The β-phase content present in the sample can be determined by the absorption infrared band at 840 cm^{-1} corresponding to the stretching of the CH_2 absorption band and by 511 and 600 cm^{-1} characteristic of CF_2 and CF stretching, respectively [15, 18].

Figure 3.6a shows FTIR-ATR spectrum of representative PVDF electropray microparticles and α-PVDF film for comparison. Electroactive β-phase is desired for

sensor and actuator applications as well as for tissue and biomedical engineering due to its piezoelectric properties that enhances cell growth and proliferation [19, 20]. Figure 3.6a shows that the characteristic bands of β-PVDF and α-phase are present in the polymer microparticles. This fact has been previously reported for electrospun PVDF fibers and their composites [14, 15] and was attributed to the combination of low solvent evaporation and electric field stretching of the fibers [21]. It the case of microspheres produced by electrospray the presence of the electroactive phase is due to the low temperature solvent evaporation.

The β-phase content of the microspheres was determined applying Equation 2.2 (see section 2.3.2). The variation of β-phase content with polymer concentration and applied electric field is present in Figure 3.6b and 3.6c.

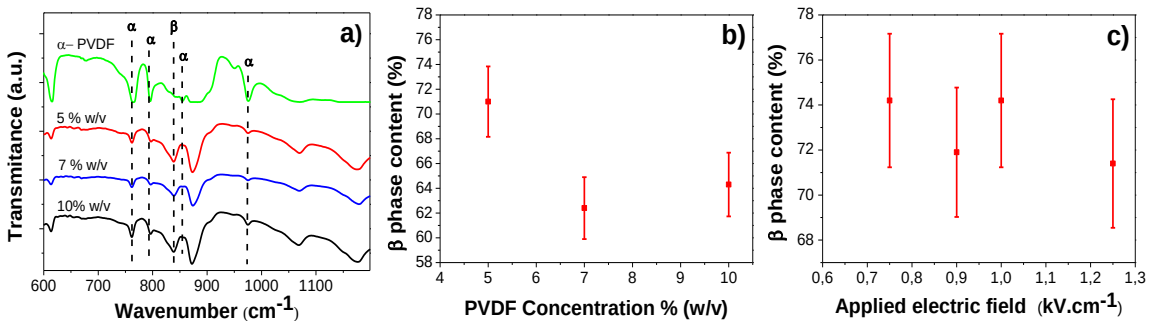

Figure 3.6. a) FTIR spectrums of 5, 7 and 10 % (w/v) PVDF microspheres and α-PVDF film; b) the variation of β-phase content with the concentration and c) the applied electric field for 5 % (w/v) samples.

Figure 3.6b and c shows that electrospray processing parameters does not influence substantially the amount of β-phase content present in the sample as phase content is mainly determined by the low crystallization temperature (room temperature) that favors polymer crystallization in the electroactive phase [16].

3.3.3. Thermal Characterization

DSC has been often used in the identification and in the quantification of the PVDF crystalline phases [15, 16]. The characteristic melting peaks depends both on crystalline phase and morphology of the polymeric structure [15]. It is thus stated that the melting

temperature of the α- and β-PVDF occurs in the range of 167 ºC to 172 ºC [15]. Figure 3.7a and 3.7b show the characteristic DSC thermographs of the microspheres, showing single melting peaks with a melting temperature *(T_m)* of 170 ºC for the samples prepared for 5, 7 and 10 % (w/v) solution concentrations and for microspheres obtained at different applied electric fields. The degree of crystallinity of the samples was determined from the DSC curves using Equation 2.3 (see section 2.3.3).

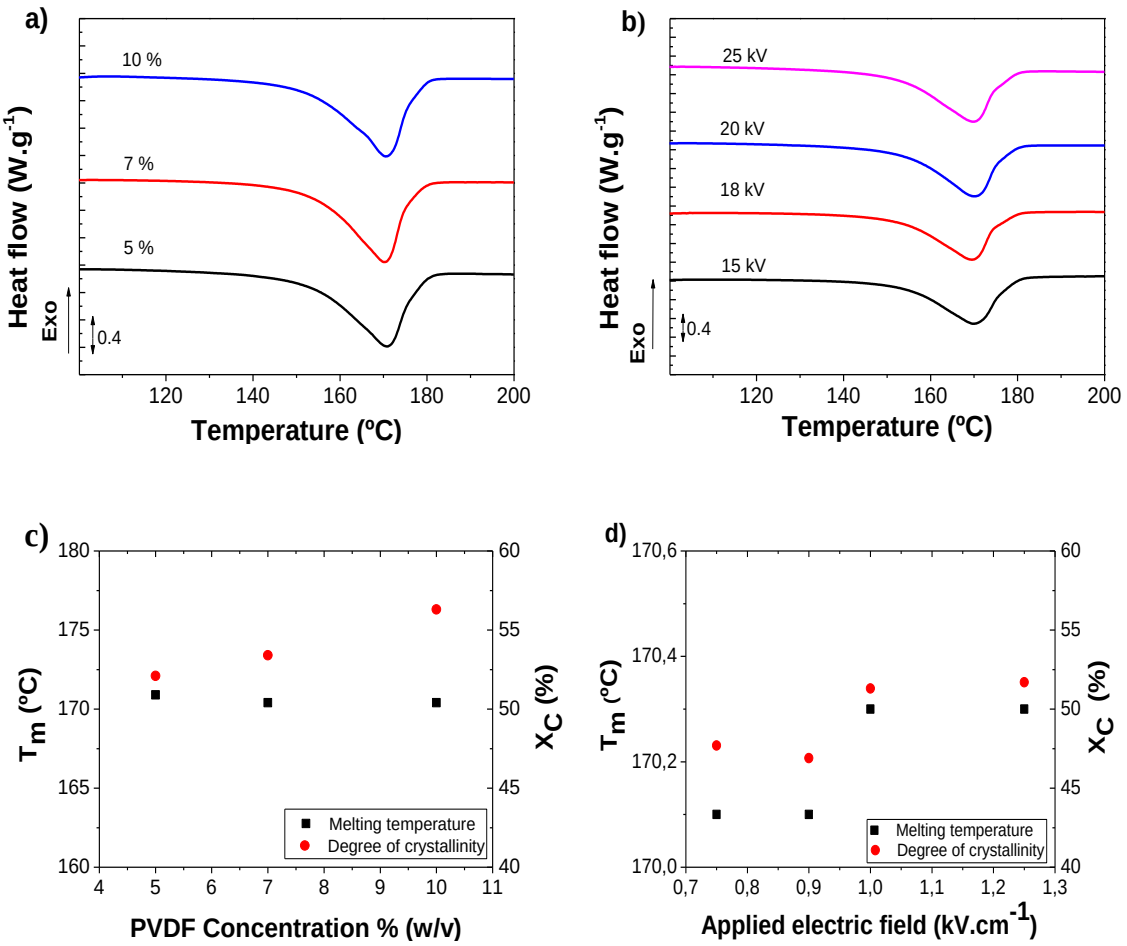

Figure 3.7. DSC thermographs of the PVDF microspheres obtained from a) 5, 7 and 10 % (w/v) polymer solutions and b) for 5 % (w/v) at different applied electric fields. Variation of the sample melting temperature and degree of crystallinity with c) the solution concentration and d) applied electric field.

It was observed that processing parameters led to variation in the degree of crystallinity between 47 and 57 %, the melting temperature being independent on the processing

conditions (Figure 3.7c and 3.7d). These results are similar to the ones observed for electrospun PVDF fiber mats [14].

3.3.4. Cell viability

Figure 3.8 shows the scheme and also the macroscopic figures of MC3T3-E1 cells with and without PVDF microspheres cultured in vitro after 24 h incubation. Is possible observe that, after 24 h, PVDF microspheres mixed with MC3T3-E1 pre-osteoblast formed a cell/microspheres pellet in the bottom of the eppendorf (Figure 3.8a). On the other hand, the positive control didn't form a stable structure and the cells remain dispersed in the eppendorf or forming small aggregates in the walls of the eppendorf.

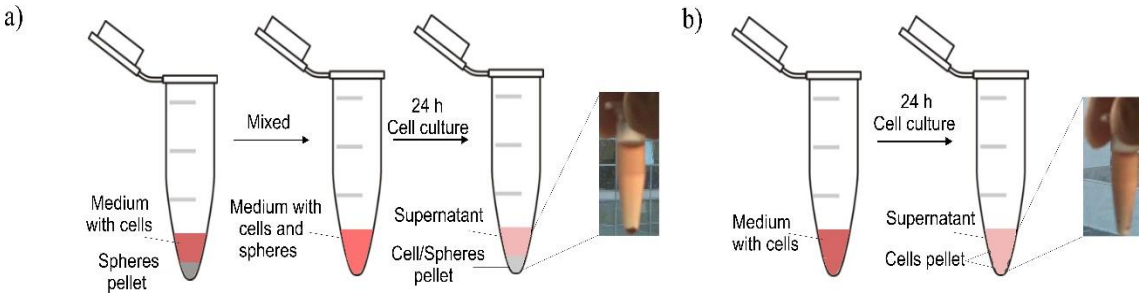

Figure 3.8. Scheme and macroscopic figures of MC3T3-E1 cells with and without PVDF microspheres cultured in vitro after 24 h incubation: a) MC3T3-E1 cells mixed with microspheres; b) Cells without microspheres used as control.

The viability of MC3T3-E1 cells seeded in an Eppendorf with and without PVDF particles was examined by MTT assay (Figure 3.9). The cell viability percentage was calculated after Equation 3.1 [22]:

$$Cell\ viability\ (\%) = \frac{Absorbance\ of\ sample}{Absorbance\ of\ negative\ control} x100 \quad (3.1)$$

The obtained results reveal that the cell agglomerates are viable for both. Comparing the PVDF microspheres/cells pellet with the cell pellet used as control it is possible to verify a higher number of cells after 72 h on the pellet with microspheres. This result shows that the PVDF microspheres can provide a suitable environment for cell growth,

than can be further explored through suitable mechanical stimulation leading to electromechanical response of the microspheres [20].

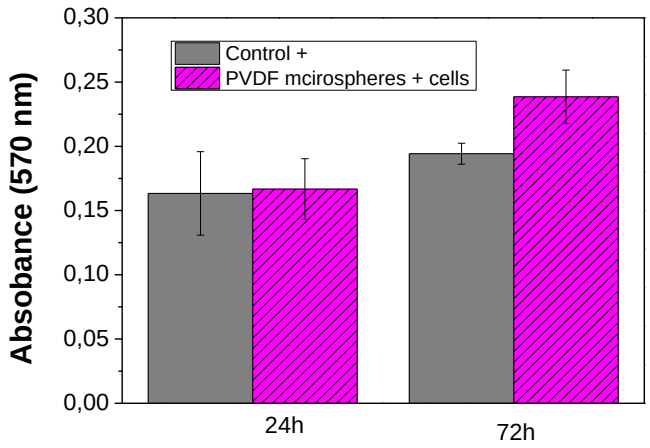

Figure 3.9. MTT assay for PVDF microspheres/cells and cells pellets (control +). Results are expressed as mean ± standard deviation with $n = 3$.

3.4. Conclusions

PVDF microspheres with spherical morphology have been prepared from a PVDF solution concentration using DMF/ THF mixture solutions by a stable electrospray process. It was observed that dilute or semi dilute concentrations favored the formation of PVDF microspheres, with average diameters ranging between 0.81 ± 0.34 and 5.55 ± 2.34 μm for concentrations between 2 and 7 % (w/v) respectively, while higher concentration promotes fibers formation. No significant differences occur in the average microspheres diameter with the variation of the electrospray processing parameters.

Infrared spectroscopy showed that electrospray allows the processing of the PVDF particles in the β-phase, with electroactive phase contents of around 70 %. Moreover, processing parameters does not influence substantially the amount of β-phase content.

DSC results of the PVDF microspheres show that the mixture of solvents used during the PVDF dissolution and the varying electrospray processing conditions allow variations in the degree of crystallinity between 47 and 57 %, being the melting temperature of the samples independent on the processing conditions.

MC-3T3-E1cell adhesion was not inhibited by the PVDF microspheres preparation, indicating the suitability of the material for the development of electroactive scaffold for biomedical applications.

Thus, this work reports on the production of PVDF microspheres by electrospray. By controlling solution parameters, namely polymer concentration, a stable process has been achieved allowing to obtaining microspheres with controlled size. The suitability of the developed microspheres as a substrate for tissue engineering application was proven by cell viability studies performed with osteoblast-like MC3T3-E1 cells.

3.5. References

1. Bhamidipati, M., et al., *Subcritical CO_2 sintering of microspheres of different polymeric materials to fabricate scaffolds for tissue engineering.* Materials Science and Engineering: C, 2013. **33**(8): p. 4892-4899.
2. Bock, N., et al., *Electrospraying, a Reproducible Method for Production of Polymeric Microspheres for Biomedical Applications.* Polymers, 2011. **3**(1): p. 131-149.
3. Hong, S.J., H.S. Yu, and H.W. Kim, *Preparation of porous bioactive ceramic microspheres and in vitro osteoblastic culturing for tissue engineering application.* Acta Biomaterialia, 2009. **5**(5): p. 1725-1731.
4. Zamani, M., M.P. Prabhakaran, and S. Ramakrishna, *Advances in drug delivery via electrospun and electrosprayed nanomaterials.* International Journal of Nanomedicine, 2013. **8**: p. 2997-3017.
5. Rietveld, I.B., et al., *Morphology control of poly(vinylidene fluoride) thin film made with electrospray.* Journal of Colloid and Interface Science, 2006. **298**(2): p. 639-651.
6. Bock, N., T.R. Dargaville, and M.A. Woodruff, *Electrospraying of polymers with therapeutic molecules: State of the art.* Progress in Polymer Science, 2012. **37**(11): p. 1510-1551.
7. García Cruz, D.M., et al., *Gelatin microparticles aggregates as three-dimensional scaffolding system in cartilage engineering.* Journal of Materials Science: Materials in Medicine, 2013. **24**(2): p. 503-513.
8. Garcia-Giralt, N., et al., *Chitosan microparticles for "in vitro" 3D culture of human chondrocytes.* Rsc Advances, 2013. **3**(18): p. 6362-6368.
9. Nath, S.D., et al., *Preparation and characterization of PLGA microspheres by the electrospraying method for delivering simvastatin for bone regeneration.* International Journal of Pharmaceutics, 2013. **443**(1–2): p. 87-94.
10. Deitzel, J.M., et al., *The effect of processing variables on the morphology of electrospun nanofibers and textiles.* Polymer, 2001. **42**(1): p. 261-272.
11. Nasir, M., et al., *Control of diameter, morphology, and structure of PVDF nanofiber fabricated by electrospray deposition.* Journal of Polymer Science Part B: Polymer Physics, 2006. **44**(5): p. 779-786.
12. Casper, C.L., et al., *Controlling Surface Morphology of Electrospun Polystyrene Fibers: Effect of Humidity and Molecular Weight in the Electrospinning Process.* Macromolecules, 2003. **37**(2): p. 573-578.
13. Rungswang, W., et al., *Existence of microdomain orientation in thermoplastic elastomer through a case study of SEBS electrospun fibers.* Polymer, 2011. **52**(3): p. 844-853.
14. Ribeiro, C., et al., *Influence of Processing Conditions on Polymorphism and Nanofiber Morphology of Electroactive Poly(vinylidene fluoride) Electrospun Membranes.* Soft Materials, 2010. **8**(3): p. 274-287.

15. Martins, P., A.C. Lopes, and S. Lanceros-Mendez, *Electroactive phases of poly(vinylidene fluoride): Determination, processing and applications.* Progress in Polymer Science, 2013. **39**(4): p. 683 - 706.

16. Sencadas, V., R. Gregorio Filho, and S. Lanceros-Mendez, *Processing and characterization of a novel nonporous poly(vinilidene fluoride) films in the β phase.* Journal of Non-Crystalline Solids, 2006. **352**(21–22): p. 2226-2229.

17. Sencadas, V., R. Gregorio, and S. Lanceros-Méndez, *α to β Phase Transformation and Microestructural Changes of PVDF Films Induced by Uniaxial Stretch.* Journal of Macromolecular Science, Part B, 2009. **48**(3): p. 514-525.

18. Bormashenko, Y., et al., *Vibrational spectrum of PVDF and its interpretation.* Polymer Testing, 2004. **23**(7): p. 791-796.

19. Martins, P.M., et al., *Effect of poling state and morphology of piezoelectric poly(vinylidene fluoride) membranes for skeletal muscle tissue engineering.* Rsc Advances, 2013. **3**(39): p. 17938-17944.

20. Ribeiro, C., et al., *Enhanced proliferation of pre-osteoblastic cells by dynamic piezoelectric stimulation.* Rsc Advances, 2012. **2**(30): p. 11504-11509.

21. Lopes, A., et al., *Effect of filler content on morphology and physical-chemical characteristics of poly(vinylidene fluoride)/NaY zeolite-filled membranes.* Journal of Materials Science, 2014. **49**(9): p. 3361-3370.

22. Fischer, D., et al., *In vitro cytotoxicity testing of polycations: Influence of polymer structure on cell viability and hemolysis.* Biomaterials, 2003. **24**(7): p. 1121-1131.

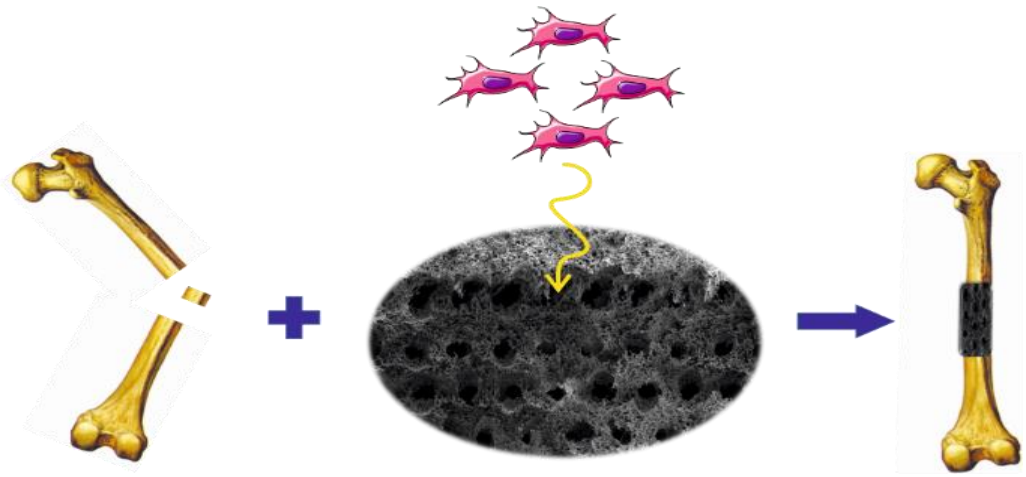

4. Strategies for the development of three dimensional scaffolds from piezoelectric poly(vinylidene fluoride)

PVDF has been proven to be a suitable as a substrate for tissue engineering in the form of microspheres and two dimensional membranes. On the other hand, many tissue engineering strategies require three-dimensional scaffolds in order to be implanted. This chapter describes several strategies for developing three dimensional scaffolds from PVDF. Three processing methods, including solvent casting, solvent casting with particulate leaching and freeze extraction with 3D nylon and PVA printed templates are presented in order to obtain three-dimensional scaffolds with different architectures and interconnected porosity. The morphology, physico-chemical properties and the electroactive β-phase content were evaluated. Quasi-static mechanical measurements were also performed to evaluate the mechanical performance of the scaffolds.

This chapter is based on the following publication: D. M. Correia, C. Ribeiro, V. Sencadas, L. Vikingsson, M. Oliver Gasch, J. L. Gómez Ribelles, G. Botelho, S. Lanceros-Méndez. *Strategies for the development of three dimensional scaffolds from piezoelectric poly(vinylidene fluoride)*. Submitted. 2015.

4.1. Introduction

Different processing techniques are being applied to tailor the shape of the scaffolds for temporary or permanent cell supports in tissue engineering (TE) applications [1, 2]. The versatility of these scaffolds is associated with variables such as composition, size and shape, degree of porosity and pore size that can be modeled to obtain an optimized system for specific cells and/or tissues [3]. These natural or synthetic functional scaffolds are used for culturing cells in order to generate tissues that can be later implanted in the human body [2].

Strong efforts are being performed in the development of 3D scaffolds as support for tissue engineering applications. They offer important advantages comparatively to two dimensional (2D) structures such as, films and fiber mats, as they allow a biomimetic environment for cell-cell interaction, cell migration and morphogenesis, promoting a better interconnection between cells and tissues [4]. In this sense, the scaffolds should present a pore size enabling the accommodation of cells, promoting/allowing cellular adhesion, growth and migration. Furthermore, a suitable pore interconnectivity is essential for the transport of nutrients and metabolites [4], as well as, an appropriate microenvironment, allowing the transmission of biochemical and/or mechanical and/or electrical clues.

Several methods have been proposed for 3D scaffolds production, conventional methods including etching, template-assisted synthesis, solvent casting, particulate leaching, gas foaming, contact printing, wet-chemical approach and electrospinning [4, 5]. More recently, rapid prototyping (RP) technologies including fused deposition modeling (FDM), precision extrusion deposition (PED), selective laser sintering (SLS), stereolithography (STL) and 3D printing have been used to overcome the drawbacks of conventional methods, including inaccurate control over the micro- and macro-scale features, allowing the fabrication of scaffolds with a controlled microstructure and porosity [6].

3D structures based on smart and functional biomaterials are increasingly playing an important role in TE applications once they do not work just as passive supports, but can also play a relevant role in the development of tissues and cells [7] by triggering/stimulating specific cues on both cells and tissues [8]. Also in order to promote a better compatibility between cells and the biomaterial, different strategies have been used, including surface tailoring with bio-mimetic molecules such as peptides

and adhesive proteins, tuning chemical and physical properties to produce similarity to native ECM, to modulate the surface and bulk properties or providing external therapeutic molecules in order to stimulate the surrounding cells and tissues [8]. The internal modulation mainly involves biomimetic modification of chemical, physical and/or biological properties in order to mimic the native tissue and provide a more friendly environment and enhance target functions such as adhesion, proliferation, migration and differentiation [8]. Among the most interesting clues to be provided to specific cells, such as mechanical [9] and (bio) chemical [10], electrical clues have already proven to be important in TE applications [11]. In that sense, piezoelectric polymers, materials that generate a voltage under mechanical loading without the need of electrodes or external power source, offer a unique opportunity to deliver electrical cues directly to cells [12]. The relevance of this effect for biomedical applications is that several tissues such as bone, cannot only take advantage of this effect, as they are subjected to electromechanical functions, but they are piezoelectric themselves [13], suggesting the biomimetic need of this effect in the scaffold. Previous studies have shown that electroactive polymers, in particular piezoelectric PVDF, are suitable for the development of electro-mechanically bioactive supports [14, 15].

Different techniques have been used to process PVDF and its polymer/composites based in different strategies (Table 4.1) to obtain various morphologies including particles [16, 17], films [18-21] and fibers [14, 22-27] in order to better suit specific tissue engineering strategies. Further, it has been shown that substrates based on PVDF have different influence on cell adhesion, proliferation and differentiation [7] depending on their morphology.

Table 4.1 summarizes the different PVDF structures used as supports for cell viability studies. To the best of our knowledge no studies regarding 3D structures based on piezoelectric materials and, in particular, in PVDF have been reported in the literature.

Table 4.1. PVDF structures, processing method and tissue engineering applications reported in the literature.

Polymeric structure	Composition	Method	Application	Ref.
Particles	PVDF	Electrospray	Tissue engineering	[17]
Films	PVDF	Stretching of α-phase	Fibronectin adsorption	[28]
			Enhanced proliferation of pre-osteoblastic cells	[28]
			Skeletal muscle tissue engineering	[29]
		Solution cast	Homogeneous cell distribution and more significant deposition of fibronectin	[30]
Fibers	PVDF	Electrospinning	Skeletal muscle tissue engineering	[29]
		Electrospinning	Promoting the neuronal differentiation and neurite extension.	[31]
	PVDF-TrFe	Electrospinning	Promising base material for manipulating cell behavior and proliferation in a three dimensional matrix	[15]
		Electrospinning	Neurite extension of primary neurons	[32]
	PVDF/PU	Electrospinning	Wound healing	[14]
	PVDF	Electrospinning	Bone	[33]

Thus, in order to extend the applicability of the material for effective tissue engineering applications, this work reports on three different strategies for the preparation of electroactive 3D PVDF scaffolds with tailored porosity and pore size. Further, the influence of the processing technique on polymer porosity, electroactive phase, crystallinity and mechanical properties, were systematically studied.

4.2. Experimental section

4.2.1. Materials

PVDF (Solef 1010/1001) was acquired from Solvay. Analytical grade DMF was purchased from Merck and formic acid and ethanol were purchased from Sigma

Aldrich. PVA filaments with 1.75 mm were supplied by Plastic2Print (Netherlands). Sodium chloride (NaCl), 99 % was purchased from Fisher Scientific.

4.2.2. Scaffolds production methods

4.2.2.1.Solvent-casting particulate leaching

PVDF scaffolds were prepared via solvent casting method. The polymer was dissolved in a DMF solution (10 % w/v) under mechanical stirring. After complete dissolution of PVDF, 5, 10 and 20 g of NaCl was added to the solution. After solvent evaporation at room temperature, the membranes were placed under vacuum and allow drying at room temperature. After solvent evaporation, the membranes were washed thoroughly with distilled water until complete salt removal. The resultant microporous membranes were again vacuum dried, until a constant weight was obtained.

4.2.2.2.Solvent casting with a 3D nylon template

For this procedure, nylon plates (Saatilon) with a pore diameter of 60 and 150 μm (NT-60 and NT-150) were cut into $2 \times 2\ cm^2$ samples and piled up on top of each other (5 layers) inside a Teflon Petri dish. The PVDF solution (prepared as indicated above) was carefully added to the nylon plate assembly. After solvent evaporation at room temperature, the scaffolds were rinsed with formic acid to remove the nylon plates in order to obtain the porous scaffold. Finally, the scaffolds were rinsed with water and dried in the same conditions as the solvent casting samples reported above.

4.2.2.3.Freeze extraction with a 3D PVA template

PVA templates were fabricated in the 3D printer Bits from Bytes 3D Touch. The printer parameters were optimized to obtain different porous structures. Four PVA templates with different filament distances were fabricated. The designation of each template is presented in Table 4.2.

Table 4.2. PVA template designation with corresponding distance between filaments.

Templates	Filaments distance (mm)
M1	0.6
M2	0.8
M3	1
M4	1.2

PVDF scaffolds were produced by two different approaches. The PVDF solution (prepared as indicated above) was casted into a PVA template to completely fill the porous structure. Afterwards, DMF solvent evaporation was performed at 60 ºC in a Homo Vacuo-Temp. After complete solvent evaporation, the PVA template was extracted with deionized water in order to obtain the porous structure in the form of interconnected channels. The PVA washing step was performed 3 times daily during 3 days. Furthermore, a freeze extraction method was used to prepare highly porous scaffolds. After introducing the PVDF solution into the free space of the PVA template, it was quickly frozen by immersion in liquid nitrogen and then stored at -80 ºC to induce crystallization and phase separation between PVDF and DMF. Then, ethanol precooled at -80 ºC was poured on top of the template containing the frozen polymer solution in order to extract DMF while the whole system is kept at -80 ºC. The ethanol was changed twice a day during 3 days to fully remove the DMF solvent. After solvent removal, the PVA template was extracted by washing repeatedly with deionized water at room temperature, as described above.

Figure 4.1 schematizes the procedures used for the PVDF three dimensional scaffolds production.

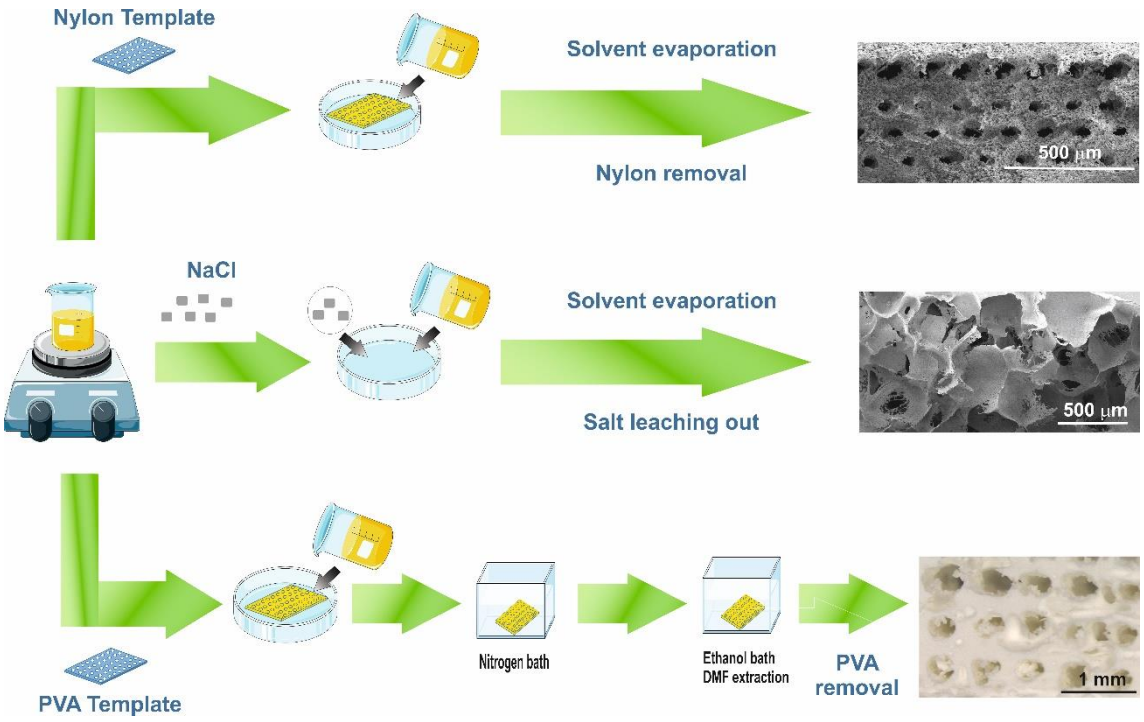

Figure 4.1. Schematic representation of the different procedures for PVDF three dimensional scaffolds production.

A neat porous PVDF membrane (10 % w/v in DMF) prepared via solvent casting [34] method was used to compare with the tridimensional structures.

4.2.3. Sample characterization

PVDF scaffolds morphology and porosity were analyzed by SEM and pycnometer method as described in chapter 2 (section 2.2.4). Pore size distribution was examined by ImageJ software.

The crystalline phase or phases present in the scaffolds were confirmed by FTIR and the degree of crystallinity by DSC as previously mentioned in chapter 2 (section 2.2.4).

Mechanical experiments were performed on cylindrical samples with approximately 6 mm diameter and 3 mm height in a Shimadzu AG-IS universal testing machine in compression mode at a test velocity of 1 $mm.min^{-1}$. The samples were submitted to a compressive-strain cycle load up to 10 cycles at a strain of 15 % with a 500 N load cell. Strain deformation was measured by machine cross-head displacement. The Young's modulus was calculated from the slope at the initial linear stage of the stress–strain curves and the tensile strength was determined from the maximum load.

4.3. Results and discussion

4.3.1. Scaffolds morphology

In order to produce piezoelectric PVDF scaffolds, the polymer was dissolved in DMF solvent and different strategies were applied to tailor the final porosity and pore interconnectivity of the polymer structures. The PVDF scaffold obtained through solvent casting with NaCl as a sacrificial material (Figure 4.2a) shows a porous structure with the bigger porous with approximately 300 - 400 μm (Figure 4.3a), which are of the same size range as pristine NaCl crystals (262 to 370 μm). The porous formation occurs after polymer crystallization in places previously occupied by the porogen, and the pore size is controlled by the size of the sacrificial particle size. However, the salt leaching method does not allow the design of structures with completely interconnected pores with a regular and reproducible morphology.

3D PVDF structures with high porosity and interconnected pores can be achieved by solvent casting with a 3D nylon template and freeze extraction with a PVA template (Figure 4.2b and 4.2c). As shown in Figure 4.2b and 4.2c, scaffolds fabricated using a 3D template present a good interconnected porous structure (Figure 4.2c) with well distributed pores. When nylon templates were used porous structures with approximately 60 μm and 130 μm can be obtained (Figure 4.2b and 4.3b). The size of the pores was governed by the sacrificial filament geometry and the space between the filaments was fully filled with the polymer solution. Then, crystallization leads to small interconnected porous (below 5 μm) within the major ones (Figure 4.2c), corresponding to the former filament places. The samples prepared by freeze drying extraction show the pores left by the sacrificial PVA filaments, with an inner diameter between 300 – 400 μm (Figure 4.2c).

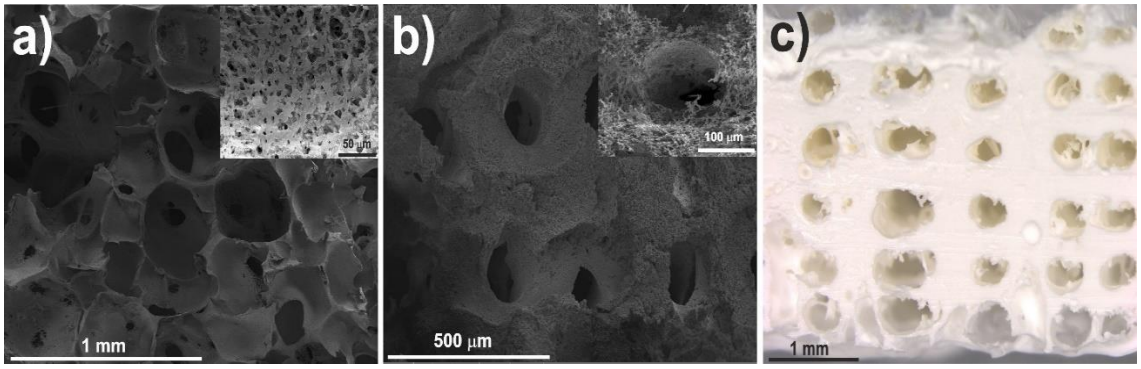

Figure 4.2. SEM images of the morphology of the PVDF scaffolds obtained by a) salt leaching method, b) using nylon templates and c) using PVA templates and freeze extraction.

The same procedure was not feasible when a PVA template obtained by 3D printing was used, due to the larger diameter of the PVA filaments. Further, even increasing the solvent temperature during solvent evaporation to 60 ºC, followed by the dissolution of PVA in water, it was not possible to achieve a tridimensional porous structure (results not shown). To overcome this issue, the solution was immersed in liquid nitrogen to immediately freeze the solution and stored at -80 ºC with ethanol, to improve the DMF solvent dissolution by the ethanol, while the polymer chains remained frozen (Figure 4.2d). After the samples were washed with water to PVA removal and dried at room temperature, the space initially occupied by the non-solvent became micropores and the pore architecture finally obtained consists in an orthotropic structure of interconnected channels whose walls are in turn connected by micropores. Figure 4.3c shows that the channels in the scaffolds are well interconnected and their average diameter ranging between 316 and 413 μm corresponds to the diameter of the sacrificial PVA filament obtained by 3D printing (Table 4.2).

The influence of the adopted processing technique and the porogen used on the overall porosity was assessed by gravimetric method, while the pore size and its distribution was measured through the SEM images (Figure 4.2). In general, all samples show pores in the same range of the sacrificial material used (Figure 4.3). The highest overall porosity was achieved for the samples with NaCl as porogen, being the sample with the highest porosity the ones with the highest amount of sacrificial material (Figure 4.3).

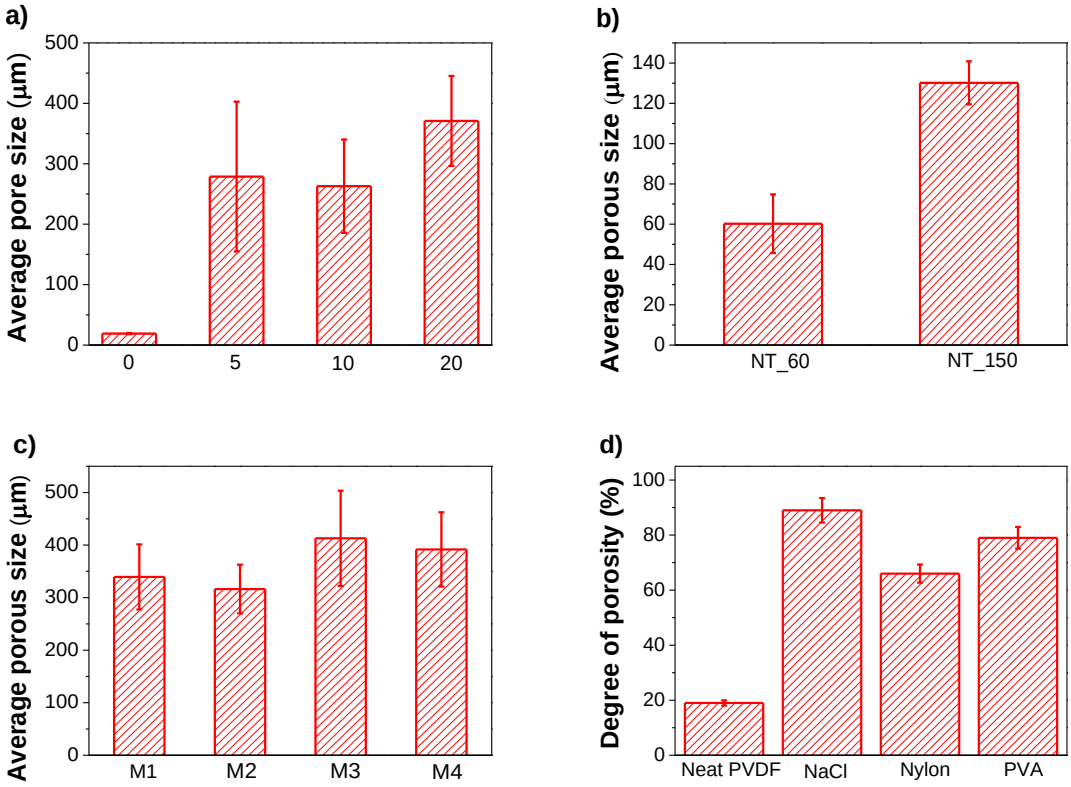

Figure 4.3. Pore size distribution of the PVDF scaffolds obtained by a) solvent casting with NaCl leaching, b) solvent casting with a 3D nylon template and c) freeze extraction with a 3D PVA template d) Degree of porosity of the PVDF scaffolds.

4.3.2. Surface chemical characterization and phase content

FTIR-ATR spectroscopy was performed in order to study possible chemical modifications induced by the processing technique in the PVDF scaffolds. Moreover, this method provides valuable information to distinguish between the different PVDF polymorphs [35] and, in particular, to quantify the piezoelectric β-phase content present in the scaffolds.

Figure 4.4a shows the main absorption band at 840 cm^{-1} characteristic of the β-phase of PVDF [35]. Also absorption bands at 765, 795 and 855 cm^{-1}, relative to α-PVDF are also observed, independently of the processing technique. Further, no absorption bands corresponding to the different porogen materials or solvents were detected, which suggests that the removal of the sacrificial materials was complete.

Figure 4.4b shows that the scaffolds production methods does not influence significantly the amount of β-phase content determined applying Equation 2.2 (see

section 2.3.2). Comparatively to PVDF membranes which present a β-phase content of 91 %, scaffolds produced by salt leaching, solvent casting and freeze extraction show β-phase contents of 86, 90 and 94 %, respectively. In this sense, as low crystallization temperature (e.g. room temperature) favors the PVDF crystallization in the β-phase, also freeze extraction method induces the formation of the polymer electroactive phase.

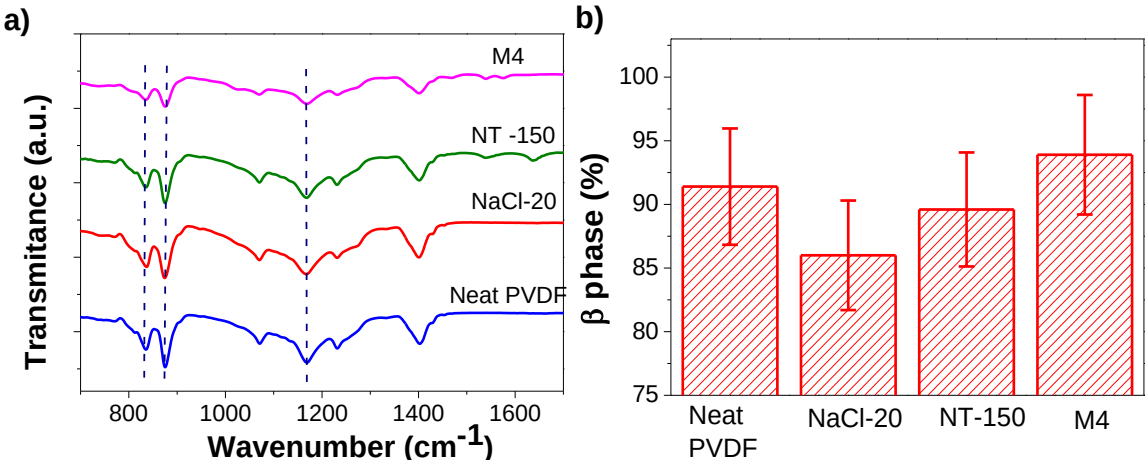

Figure 4.4. a) FTIR spectra of neat PVDF and the scaffolds processed by different methods and b) variation of β-phase content for the same samples.

4.3.3. Thermal characterization

DSC was performed to assess the influence of the processing technique and porogen in the polymer degree of crystallinity. It was observed that the incorporation of different fillers leads to a shift towards lower temperatures of the melting transition, when compared to the neat PVDF sample obtained from solvent casting, particularly noticed when NaCl is used (Figure 4.5). In this way, the strong ionic character of the salt, lead to strong interaction with the highly polar polymer chain, reducing the stability region of the crystalline structure [36]. Moreover, the meting transition appears as a broad endothermic peak for all samples, suggesting a distribution of crystal sizes among the polymer matrix.

The degree of crystallinity of the PVDF samples was determined from the DSC curves and Equation 2.3 (see section 2.3.3). Different porogen materials show different effects on polymer degree of crystallinity. Pristine PVDF polymer shows a degree of

crystallinity ~ 45 %, but for the sample prepared with NaCl, the sample shows an X_c around 33 %. Low *et al.* [37] showed that when small amounts of NaCl are added to the PVDF solution, the salt, combined with free radicals near the crystalline surface promotes an increase of sample crystallinity [37]. However, beyond a critical concentration, the excess of salt will interact with the PVDF on the crystallite surface and promotes atoms dislocation, resulting in a decrease of the crystallinity degree of the PVDF sample (Figure 4.5b). Most relevant, the large amounts of filler used in the present investigation act as defective structures, leading to hindered spherulite growth during polymer crystallization [38]. On the other hand, when a nylon mesh was used as a template, an increase of the degree of crystallinity of the sample was observed up to 55 %, while for the PVDF prepared with PVA porogen, the degree of crystallinity present in the sample is similar to the observed for the pristine PVDF (Figure 4.5b).

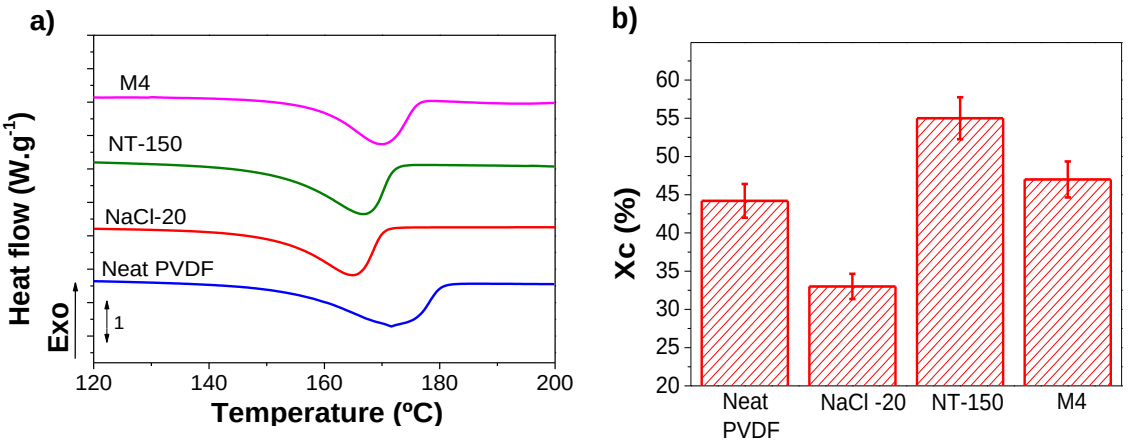

Figure 4.5. a) DSC thermographs of neat PVDF and PVDF scaffolds obtained from solvent-casting particle leaching and with nylon and PVA templates; b) variation of the degree of crystallinity for the different scaffolds.

4.3.4. Mechanical characterization

Various cellular activities are influenced by mechanical properties of surrounding tissues and scaffolds [39]. Cyclic stress *vs* strain measurements obtained under compressive mode and for a strain of 15 %, for the different PVDF structures are shown in Figure 4.6. The final mechanical strain of 15 % was defined to match the characteristic deformation of the natural cartilage and it is also used as the target strain in experiments with bioreactors for chondrogenic differentiation [40, 41].

The mechanical performance of the scaffolds obtained for different NaCl concentrations show a similar behavior, attributed to the similar porosity (Figure 4.2) present in the sample (data not shown). For all tested samples, the difference between the first and the second cycle is related to the processing history and to the surface of the mechanical pin accommodation among the sample surface. Further, some permanent deformation during the first compression cycle was observed (Figure 4.6). In successive load-unload compression cycles, it was observed an increase of the irreversible processes, leading to permanent deformation, reflected by the slight decrease of the maximum stress reached in the stress-strain loop (Figure 4.6). The samples prepared by nylon template meshes collapse after three consecutive mechanical loading-unloading cycles (data not show), but the maximum stress for the first cycles was quite higher when compared to the rest of the porous samples obtained by different methods. This behavior is probably related to the microstructure and distribution of the pores among the sample, which is characterized by perpendicular channels with an overall porosity of ~ 66 ± 3.3 % (Figure 4.3). When the mechanical cycle is applied to the sample, the stress is not uniformly distributed among the polymer bulk due to the dual porosity e.g. small pores of 2 μm diameter and pores with 60 and 150 μm, which leads to a collapse of the channels formed by the nylon mesh, due to the small polymer thickness when compared to the bulk PVDF polymer structure.

For the rest of the samples it was observed that the maximum stress decreases with increasing mechanical loading-unloading cycle, showing the samples obtained from salt leaching and the freeze dried M1 (distance between filaments of 0.6 mm) similar mechanical hysteresis patterns (Figure 4.6). The sample M4 (filaments placed at 1.2 mm between each other) is the one with the lowest maximum stress at the end of each cycle. This behavior is related to the big size of the channels when compared to sample M1 that locally induces a poor mechanical load distribution due to the decrease of the thickness in the region between the channels.

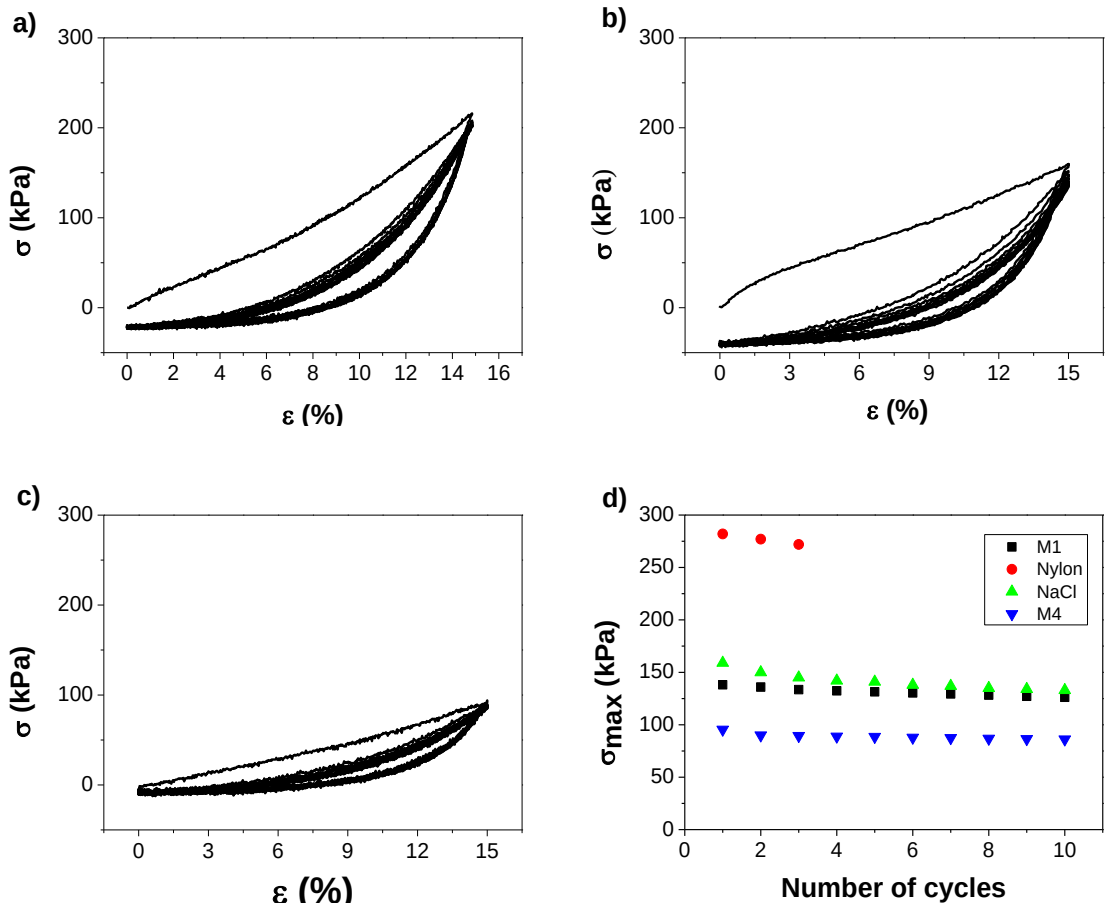

Figure 4.6. Characteristics stress–strain curves of PVDF scaffolds for compression assays at 15 %. PVDF scaffolds obtained by a) solvent-casting NaCl leaching, b) freeze extraction with a M1 template c) freeze extraction with a M4 template. d) Evolution of the maximum stress obtained up to 10 cycles.

The apparent elastic modulus (E) was calculated from the stress-strain data at 1 % deformation and the results are shown in Table 4.3. The scaffolds prepared by NaCl leaching show a higher E when compared to the rest of the samples. This result is interesting due to the high porosity present in these samples, being explained by the fact that the pore walls in such samples are homogeneously distributed among the polymer bulk, which promotes an evenly distribution of the mechanical load between the polymer walls. The samples prepared by PVA template and freeze drying, as well as the ones obtained by nylon mesh show a similar morphology, characterized by the big channels from the template. This leads to a dual distribution of the mechanical stress, one part being supported by the bulk polymer with pore size of ≤ 2 μm and the other by

the channels with small wall thickness, which ultimately leads to a decrease of the mechanical properties, as observed in Figure 4.6, and to a decrease of E (Table 4.3).

Table 4.3. Tangent modulus (MPa) of scaffolds at 15 % of strain presented as average ± standard deviation.

Sample	Young Modulus (MPa)
NaCl leaching	2.2 ± 0.3
Nylon template	0.4 ± 0.1
M1	0.79 ± 0.08
M2	0.94 ± 0.03
M3	1.02 ± 0.01
M4	1.5 ± 0.3

Thus, Figure 4.7 shows the PVDF structures with different morphologies and geometries that can be obtained using different processing methods, the PVDF scaffolds with different pore sizes being the ones presented in this work and obtained by three different methods.

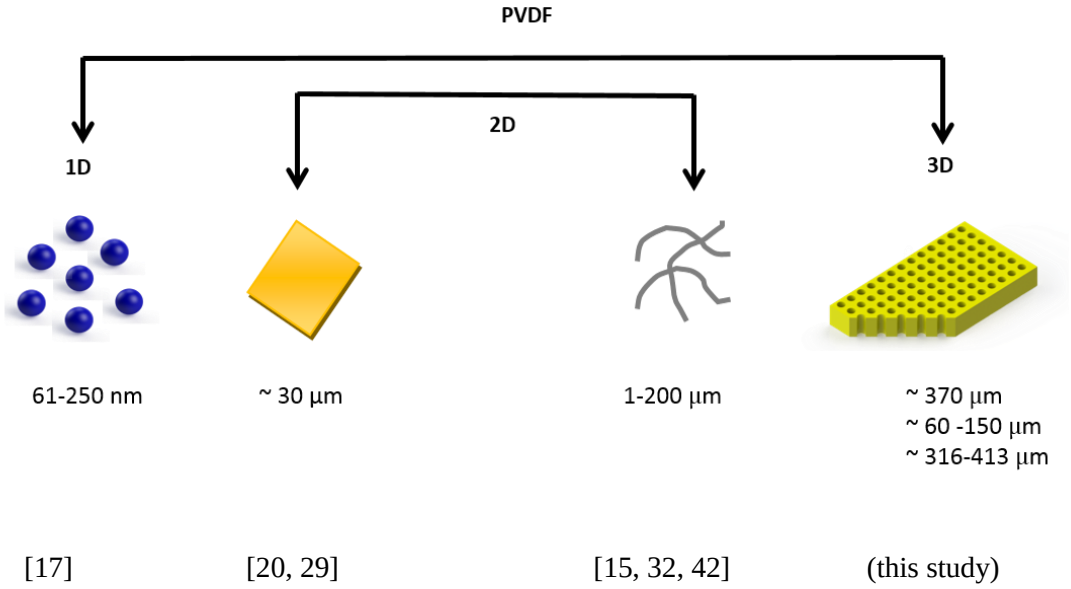

Figure 4.7. Different structures and morphologies of PVDF for tissue engineering applications.

4.4. Conclusions

PVDF three dimensional scaffolds can be obtained by NaCl salt leaching, solvent casting and freeze extraction with nylon and PVA templates, respectively. The different preparation methods allow tuning pore size, interconnectivity and porosity. Thus, varying the ratio of NaCl/porogen and the distance between the filaments of the templates allows to control the porosity of the scaffold. The structure of the 3D templates allows obtaining scaffolds with well interconnected pores. Infrared spectroscopy showed that all processing methods result in scaffolds mainly in the piezoelectric β-phase of PVDF (between 86 and 94 %) and with a degree of crystallinity between 33 and 47 %. The characterization of the scaffolds by mechanical compression tests and the relation between scaffold porosity and mechanical properties showed that higher porosities promotes a significant decrease in the tensile strengths and the Young's Modulus, the overall results indicating the suitability of the PVDF scaffolds for tissue engineering applications.

4.5. References

1. García Cruz, D.M., et al., *Gelatin microparticles aggregates as three-dimensional scaffolding system in cartilage engineering.* Journal of Materials Science: Materials in Medicine, 2013. **24**(2): p. 503-513.
2. Seidi, A., et al., *Gradient biomaterials for soft-to-hard interface tissue engineering.* Acta Biomaterialia, 2011. **7**(4): p. 1441-1451.
3. Oliveira, M.B. and J.F. Mano, *Polymer-based microparticles in tissue engineering and regenerative medicine.* Biotechnology Progress, 2011. **27**(4): p. 897-912.
4. Sun, B., et al., *Advances in three-dimensional nanofibrous macrostructures via electrospinning.* Progress in Polymer Science, 2014. **39**(5): p. 862-890.
5. Schmidt, C.E., et al., *Stimulation of neurite outgrowth using an electrically conducting polymer.* Proceedings of the National Academy of Sciences, 1997. **94**(17): p. 8948-8953.
6. Rana, D., et al., *Chapter 10 - Considerations on Designing Scaffold for Tissue Engineering*, in *Stem Cell Biology and Tissue Engineering in Dental Sciences*, A.V.S.S. Ramalingam, Editor. 2015, Academic Press: Boston. p. 133-148.
7. Ribeiro, C., et al., *Piezoelectric poly(vinylidene fluoride) microstructure and poling state in active tissue engineering.* Engineering in Life Sciences, 2015. **15** (4): p. 351–356.
8. Pérez, R.A., et al., *Naturally and synthetic smart composite biomaterials for tissue regeneration.* Advanced Drug Delivery Reviews, 2013. **65**(4): p. 471-496.
9. Chan, B.P. and K.W. Leong, *Scaffolding in tissue engineering: General approaches and tissue-specific considerations.* European Spine Journal, 2008. **17**(SUPPL. 4): p. S467-S479.
10. Vrana, N.E., et al., *Cell/tissue microenvironment engineering and monitoring in tissue engineering, regenerative medicine, and in vitro tissue models.* BioMed research international, 2014. **2014**: p. 951626.
11. Qazi, T.H., R. Rai, and A.R. Boccaccini, *Tissue engineering of electrically responsive tissues using polyaniline based polymers: A review.* Biomaterials, 2014. **35**(33): p. 9068-9086.
12. Kochervinskiĭ, V.V., *Piezoelectricity in crystallizing ferroelectric polymers: Poly(vinylidene fluoride) and its copolymers (a review).* Crystallography Reports, 2003. **48**(4): p. 649-675.
13. Shamos, M.H. and L.S. Lavine, *Piezoelectricity as a Fundamental Property of Biological Tissues.* Nature, 1967. **213**(5073): p. 267-269.
14. Guo, H.-F., et al., *Piezoelectric PU/PVDF electrospun scaffolds for wound healing applications.* Colloids and Surfaces B: Biointerfaces, 2012. **96**: p. 29-36.
15. Weber, N., et al., *Characterization and in vitro cytocompatibility of piezoelectric electrospun scaffolds.* Acta Biomaterialia, 2010. **6**(9): p. 3550-3556.

16. Rietveld, I.B., et al., *Morphology control of poly(vinylidene fluoride) thin film made with electrospray.* Journal of Colloid and Interface Science, 2006. **298**(2): p. 639-651.

17. Correia, D.M., et al., *Electrosprayed poly(vinylidene fluoride) microparticles for tissue engineering applications.* Rsc Advances, 2014. **4**(62): p. 33013-33021.

18. Sencadas, V., R. Gregorio, and S. Lanceros-Méndez, *α to β Phase Transformation and Microestructural Changes of PVDF Films Induced by Uniaxial Stretch.* Journal of Macromolecular Science, Part B, 2009. **48**(3): p. 514-525.

19. Hong, S.J., H.S. Yu, and H.W. Kim, *Preparation of porous bioactive ceramic microspheres and in vitro osteoblastic culturing for tissue engineering application.* Acta Biomaterialia, 2009. **5**(5): p. 1725-1731.

20. Sencadas, V., S. Lanceros-Méndez, and J.F. Mano, *Characterization of poled and non-poled β-PVDF films using thermal analysis techniques.* Thermochimica Acta, 2004. **424**(1–2): p. 201-207.

21. Ribeiro, C., et al., *Fibronectin adsorption and cell response on electroactive poly(vinylidene fluoride) films.* Biomedical Materials, 2012. **7**(3): p. 035004.

22. Liu, Z.H., et al., *Piezoelectric properties of PVDF/MWCNT nanofiber using near-field electrospinning.* Sensors and Actuators A: Physical, 2013. **193**: p. 13-24.

23. Na, H., et al., *Formation of core/shell ultrafine fibers of PVDF/PC by electrospinning via introduction of PMMA or BTEAC.* Polymer, 2009. **50**(26): p. 6340-6349.

24. Ketpang, K. and J.S. Park, *Electrospinning PVDF/PPy/MWCNTs conducting composites.* Synthetic Metals, 2010. **160**(15–16): p. 1603-1608.

25. Bormashenko, E., et al., *Polyvinylidene fluoride—piezoelectric polymer for integrated infrared optics applications.* Optical Materials, 2004. **27**(3): p. 429-434.

26. Zhang, H., et al., *Role of wettability in interfacial polymerization based on PVDF electrospun nanofibrous scaffolds.* Journal of Membrane Science, 2013. **442**: p. 124-130.

27. Bhamidipati, M., et al., *Subcritical CO_2 sintering of microspheres of different polymeric materials to fabricate scaffolds for tissue engineering.* Materials Science and Engineering: C, 2013. **33**(8): p. 4892-4899.

28. Ribeiro, C., et al., *Enhanced proliferation of pre-osteoblastic cells by dynamic piezoelectric stimulation.* Rsc Advances, 2012. **2**(30): p. 11504-11509.

29. Martins, P.M., et al., *Effect of poling state and morphology of piezoelectric poly(vinylidene fluoride) membranes for skeletal muscle tissue engineering.* Rsc Advances, 2013. **3**(39): p. 17938-17944.

30. Low, Y.K.A., et al., *beta-Phase poly(vinylidene fluoride) films encouraged more homogeneous cell distribution and more significant deposition of fibronectin towards the cell-material interface compared to alpha-phase poly(vinylidene*

fluoride) films. Materials science & engineering. C, Materials for biological applications, 2014. **34**: p. 345-53.

31. Lee, Y.S., et al., *Neural Differentiation of Human Neural Stem/Progenitor Cells on Piezoelectric Scaffolds,* in *2010 Ieee 36th Annual Northeast Bioengineering Conference*. 2010.

32. Lee, Y.-S., G. Collins, and T. Livingston Arinzeh, *Neurite extension of primary neurons on electrospun piezoelectric scaffolds.* Acta Biomaterialia, 2011. **7**(11): p. 3877-3886.

33. Damaraju, S.M., et al., *Structural changes in PVDF fibers due to electrospinning and its effect on biological function.* Biomedical materials, 2013. **8**(4): p. 045007-045007.

34. Nunes-Pereira, J., et al., *Poly(vinylidene fluoride) and copolymers as porous membranes for tissue engineering applications.* Polymer Testing, 2015. **44**: p. 234-241.

35. Martins, P., A.C. Lopes, and S. Lanceros-Mendez, *Electroactive phases of poly(vinylidene fluoride): Determination, processing and applications.* Progress in Polymer Science, 2014. **39**(4): p. 683-706.

36. Martins, P., et al., *On the origin of the electroactive poly(vinylidene fluoride) β-phase nucleation by ferrite nanoparticles via surface electrostatic interactions.* CrystEngComm, 2012. **14**(8): p. 2807-2811.

37. Low, Y.K.A., et al., *Increasing solvent polarity and addition of salts promote β-phase poly(vinylidene fluoride) formation.* Journal of Applied Polymer Science, 2013. **128**(5): p. 2902-2910.

38. Sencadas, V., et al., *Influence of ferrite nanoparticle type and content on the crystallization kinetics and electroactive phase nucleation of poly(vinylidene fluoride).* Langmuir, 2011. **27**(11): p. 7241-7249.

39. Yang, G.-H., M. Kim, and G. Kim, *A hybrid PCL/collagen scaffold consisting of solid freeform-fabricated struts and EHD-direct-jet-processed fibrous threads for tissue regeneration.* Journal of Colloid and Interface Science, 2015. **450**: p. 159-167.

40. Vikingsson, L., et al., *Relationship between micro-porosity, water permeability and mechanical behavior in scaffolds for cartilage engineering.* Journal of the Mechanical Behavior of Biomedical Materials, 2015. **48**: p. 60-69.

41. Panadero, J.A., et al., *Fatigue prediction in fibrin poly-ε-caprolactone macroporous scaffolds.* Journal of the Mechanical Behavior of Biomedical Materials, 2013. **28**: p. 55-61.

42. Ribeiro, C., et al., *Influence of Processing Conditions on Polymorphism and Nanofiber Morphology of Electroactive Poly(vinylidene fluoride) Electrospun Membranes.* Soft Materials, 2010. **8**(3): p. 274-287.

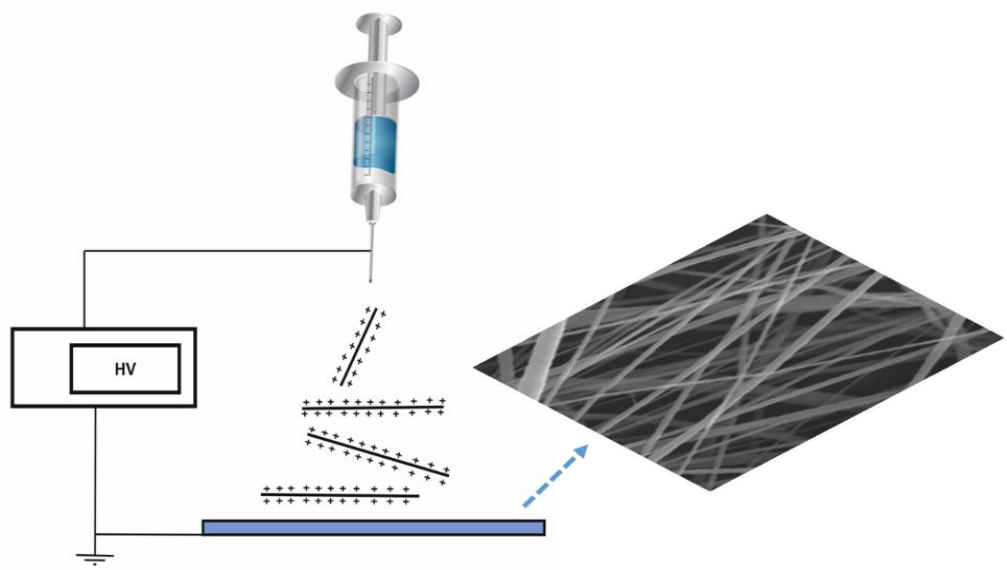

5. Influence of electrospinning parameters on poly(hydroxybutyrate) electrospun membranes fiber size and distribution

PVDF and co-polymers are the polymers with the largest piezoelectric response. There materials are biocompatible but they are not biodegradable, limiting their potential use in certain applications. This chapter reports on the production of biodegradable electrospun membranes of PHB by electrospinning. The influence of processing parameters on morphology, fiber size and distribution was systematically studied. The physico-chemical properties of the polymer, including crystalline phase and thermal degradation were evaluated. The potential of the PHB membranes for biomedical applications was also tested.

This chapter is based on the following publication: D. M. Correia, C. Ribeiro, J. C. Coelho, G. Botelho, J. L. Gomez Ribelles, S. Lanceros-Méndez and V. Sencadas. *Influence of electrospinning parameters on Poly(hydroxybutyrate) electrospun membranes fiber size and distribution*. Polym. Eng. Sci. 2014. 54: 1608–1617.

5.1. Introduction

In recent years, much attention has been paid to the production, processing and applications of polyhydroxyalkanoates (PHAs) in the biomedical field. PHAs are natural polymers synthesized by a wide variety of microorganisms such as soil bacteria, blue-green algae and genetically modified plants, being the PHB the most common type of PHAs [1].

PHB was discovered by Lemoigne in the bacterium *Bacillus megaterium* in 1926 [2, 3]. It was the first polymer of the PHAs class to be discovered and it is also the most widely studied and the best characterized PHA. PHB is a non-toxic, insoluble in water, biodegradable and biocompatible thermoplastic polymer with a high crystallinity degree and with physical properties similar to polypropylene [3-5]. The high crystallinity of PHB (almost 80 %) is a consequence of its perfect stereoregularity and high purity, resulting from its bacterial fermentation production [6].

Due to its natural origin and its properties, PHB is suitable for biomedical applications. It has been already evaluated for controlled drug release systems, surgical structures, wound dressings, orthopedic devices, tissue engineering and skin substitute materials, among others [7]. However, the high crystallinity and brittleness of PHB limits its application potential [3]. The high nucleation rate and smaller number of PHB nuclei often results, during crystallization, large spherulites that exhibit inter-spherulitic cracks. Polymer glass transition occurs near 0 ºC which is below room temperature, and secondary crystallization of the amorphous phase occurs during storage [6].

For tissue engineering applications, studies with PHB have shown that cells such as osteoblasts, epithelial cells and ovine chondrocytes adhered efficiently to PHB films synthesized by both solvent casting and solute-leaching techniques [1]. Furthermore, composites of amorphous carbonated apatite (ACP) and poly-(R)-3-hydroxybutyrate contribute to cell proliferation [6] and PHB with hydroxyapatite (HAP) composites improves osteoblasts cell growth [8].

Due to the promising application of PHB in tissue engineering applications, further studies have been conducted in electrospun PHB fibers, as electrospun polymeric membranes have attracted an increasing interest for tissue engineering applications due to their nanostructured morphology, which shall mimic the extracellular matrix components distribution like collagen [7] or elastin [9]. Furthermore, electrospun

membranes have large specific surface area and high porosity, which are desirable properties for nutrient delivery, fluid absorption excretion, and oxygen supply [7].

Ultrafine fibers of PHB, PHBV (poly(hydroxybutyrate-co-hydroxyvalerate)) and their blends have been produced using chloroform as a solvent system and its viability was evaluated with mouse fibroblasts [10], and used for bone scaffolds, especially cell attachment, proliferation and alkaline phosphatase (ALP) activity of human osteoblasts [1].

Fiber mats of PHB have been prepared under different conditions, including spinning PHB solution with chloroform as a solvent [11], producing three-dimensional nanofibers nonwoven webs from solution of PHB and dodecylbenzene sulfonic acid (DBSA) doped polyaniline in chloroform/trifluoroethanol mixture [12] and electrospinning pure PVA, PHB and their blends using a solvent system of 1, 1, 1, 3, 3, 3-hexafluoro-2-propanol (HFIP) [7].

Sucrose is available in large quantities from sugar cane industry and from the ethanol production in Brazil via microbial cultivations in bioreactors. Rodrigues *et al.* [13] found that *Burkholderia* sp. strains (IPT64 and IPT77B), which grew faster in sucrose and were able to accumulate PHA as intracellular storage compounds. After extraction and purification of the polymer, it can be successfully processed by conventional polymer techniques such extrusion or solvent casting [14]. Up to our knowledge, the use of such PHB obtained from the sugar cane waste and processed into electrospun fibers meshes was not reported. Finally, despite the aforementioned investigations and the large application potential of these materials for tissue and biomedical engineering, there is a lack of systematic study on how processing parameters modify membrane fiber dimensions which is one of the key features for tailoring membranes for specific applications. In the present work PHB obtained from sugar cane residues was processed by electrospinning and a systematic study of the influence of electrospinning parameters such as applied voltage, needle inner diameter and solution flow rate on fiber morphology is presented. The suitability of the developed membranes for biomedical applications was proven by cell viability studies performed with osteoblast-like MC3T3-E1 cells.

5.2. Experimental

5.2.1. Materials

PHB (molecular weight of ~ 531112 Da) from sugar cane was supplied by PHB Industrial and dissolved in a blend of DMF, from *Merck,* and Chloroform (CF, from M*erck)* (3/7 v/v), at 60 ºC under stirring until complete polymer dissolution, to achieve a polymer concentration of 7 and 10 % (w/w) of the final solution.

5.2.2. Electrospinning processing

The polymer solution was placed in a commercial plastic syringe (10 mL) fitted with a steel needle with different diameters (from 0.5 mm up to 1.7 mm). Electrospinning was conducted at 40 ºC in a home-made controlled temperature chamber with a relative humidity of 55 %, at different electrical fields created by a high voltage power supply from *Glassman* (model PS/FC30P04). A syringe pump (from *Syringepump*) was used to feed the polymer solutions into the needle tip at a rate between 5 and 20 $mL.h^{-1}$. The as-spun random oriented fibers were collected in grounded collecting plate.
A PHB film was produced by solvent casting from the same solution at 60 ºC, because films crystallized during solvent evaporation at temperatures below that presented high porosity and were unstable due to their poor mechanical properties.

5.2.3. Characterization

Electrospun fibers were coated with a thin gold layer using a sputter coating (*Polaron,* model SC502) and their morphology was analyzed using SEM (Cambridge, *Leica*) with an accelerating voltage of 15 kV. The fibers average diameter and their size distribution was calculated over approximately 40 fibers using de SEM image (2000X magnification) and the ImageJ software.
FTIR were performed at room temperature in an ABB FTLA 2000 apparatus in transmission mode from 4000 to 500 cm^{-1}. FTIR spectra were collected after 32 scans with a resolution of 4 cm^{-1}. Contact angle measurements (sessile drop in dynamic mode) were performed at room temperature in a Data Physics OCA20 device using ultrapure water as test liquid. The contact angles were measured as described in the experimental section of the chapter 2 (section 2.2.4).

The thermal degradation kinetics of PHB was characterized by means of thermogravimetric analysis in a *Perkin-Elmer* Pyris-1 TGA apparatus using different heating rate scans. All experiments were performed under a nitrogen atmosphere. DSC were performed in a *Perkin-Elmer* Pyris-1 apparatus at a heating rate of 10 $^{o}C.min^{-1}$. The samples for the DSC studies were cut into small pieces from the middle region of the electrospun membranes and placed into 40 µL aluminum pans. All experiments were performed under a nitrogen purge.

5.2.4. Cell culture

For cell culture, circular PHB nanofiber membranes with 13 mm of diameter were prepared. For sterilization purposes, the nanofibers were immersed in 70 % ethanol for 30 min several times. Then, the membranes were washed 5 times for 5 min with PBS solution followed by washing 3 times with the culture medium to eliminate any residual ethanol.

MC3T3-E1 cells (Riken cell bank, Japan) were cultivated in DMEM 1 $g.L^{-1}$ glucose (Gibco) containing 10 % FBS (Fisher) and 1 % P/S.

For the study of cell viability, the osteoblast-like cells were seeded in 24-well TC plates with PHB fiber membranes at cell density of 3×10^{4} cells/well for 2 days. For the quantification of cell viability, MTT assay (Sigma-Aldrich) was carried out. The cell viability was evaluated using Equation 3.1.

5.3. Results and Discussion

5.3.1. Fiber mat morphology and average fiber diameter

The parameters having influence on the morphology and properties of the electrospun fibers can be divided in three main groups: initial polymer solution, jet formation and collection procedure [15]. Among the parameters related to the polymer solution, the most relevant are the nature of used solvent (dielectric properties, volatility, boiling point and others), the solution concentration, that controls its viscosity, and the molecular weight of the polymer (that must allow polymer entanglement). Moreover, parameters that control the jet formation, stability and solvent evaporation are the flow rate through the needle, needle inner diameter, distance from the needle to collector,

temperature, moisture and applied voltage. With respect to the collection procedure, it can be static or rotating collector, and in the last case the rotating speed of the collector is the most important parameter determining fiber orientation and diameter [15-17]. The number of parameters that influence the electrospinning process is quite high and in order to allow a broad characterization of the influence of the electrospinning parameters on fiber size and distribution some of them should be fixed.

In order to obtain well-formed fibers and samples without bead defects, a blend of CF/DMF solvents was used to dissolve the PHB polymer. CF was used to dissolve the polymer, but it has low dielectric constant and boiling point resulting in fast polymer crystallization, giving origin to needle obstruction and non-continuous electrospun polymer processing. In that sense, DMF (with higher dielectric constant and lower volatility, see Table 5.1) was added to the solution, allowing to solve the aforementioned problems and resulting in stable and continuous processing of the fiber membranes.

Table 5.1. Physical and thermal properties of the solvents used for the processing of the fibers. Data collected from the material datasheet supplied by the manufacturers.

Solvent	Melting Point (ºC)	Vapor Pressure (Pa)	Dipole moment (Debye)	Dielectric constant	Density ($g.cm^3$)
DMF	-61	1300	382	38.2	0.944
CF	-63	47.6	1.15	4.8	1.483

The influence of the applied electric field was investigated keeping constant the value of the inner needle diameter at 0.5 mm and a flow rate of 10 $mL.h^{-1}$. The morphology of the obtained samples is represented in Figure 5.1. A histogram (Figure 5.1c and 5.1d) of the fiber diameter distribution, determined from the SEM images and fiber average size and standard deviation was obtained. The as-spun membranes presented a fibrillar structure, without bead formation, with a smooth surface and with randomly oriented fibrils on the static grounded collector.

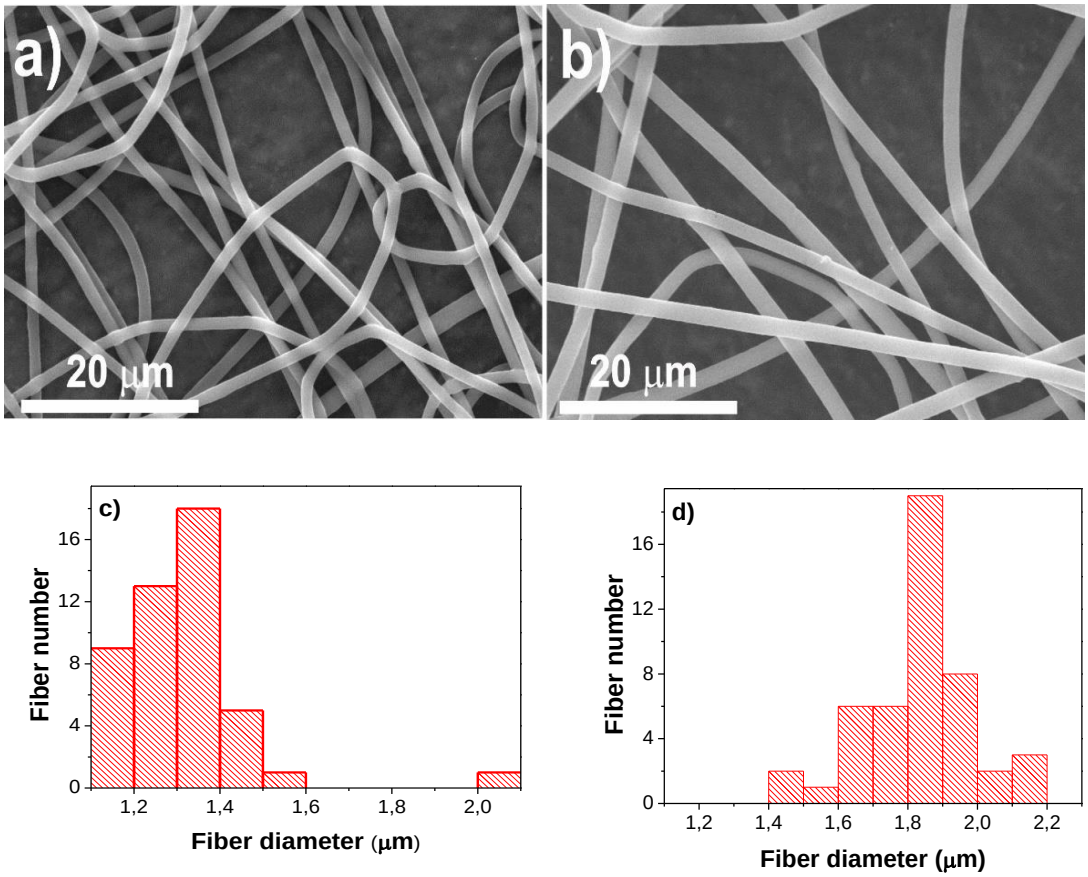

Figure 5.1. PHB electrospun membranes obtained at 10/90 (10 % PHB + 90 % solvent blend) with a needle inner diameter of 0.5 mm and a flow rate of 10 $mL.h^{-1}$ at 1 $kV.cm^{-1}$ [a) and c)] and 1.75 $kV.cm^{-1}$ [b) and d)].

Samples obtained at several applied electric fields between the needle tip and the ground metallic collector showed a mean diameter that ranges between 1.31 ± 0.13 μm and 2.01 ± 0.17 μm (Figure 5.2). An increase of the mean fiber diameter with increasing of the applied electric field was observed until 1.5 $kV.cm.^{-1}$. By further increasing the applied electric field, a decrease of the mean fiber diameter occurred (Figure 5.2a) due to changes in mass flow and jet dynamics promoted by the applied electric field [15].

The formation of the thin fibers is mainly due to the stretching and acceleration of the jets promoted by the high electric field [16, 18] which in turn will result in higher charge density on the surface of the jets, increasing jet velocity and consequently fiber stretching. In this sense, it is generally reported that the diameter of the fibers becomes gradually smaller with increasing the applied electric field [19-22]. On the other hand, as observed in the present experiments and in other cases reported in the literature [15],

this result is not general since increasing charge density within the applied electric field also affect other processing parameters such as jet traveling time, which has the opposite effect on the fiber diameter [23]. In order to promote the formation of independent and smooth fibers, most of the solvent evaporation must occur during the travel between the tip and the metallic ground collector. Increasing electric field decreases travelling time. Furthermore, increasing the applied electric field often enhances jet instability, promoting multiple fiber formation, which results in a broader distribution of the fiber diameters [16, 20, 24].

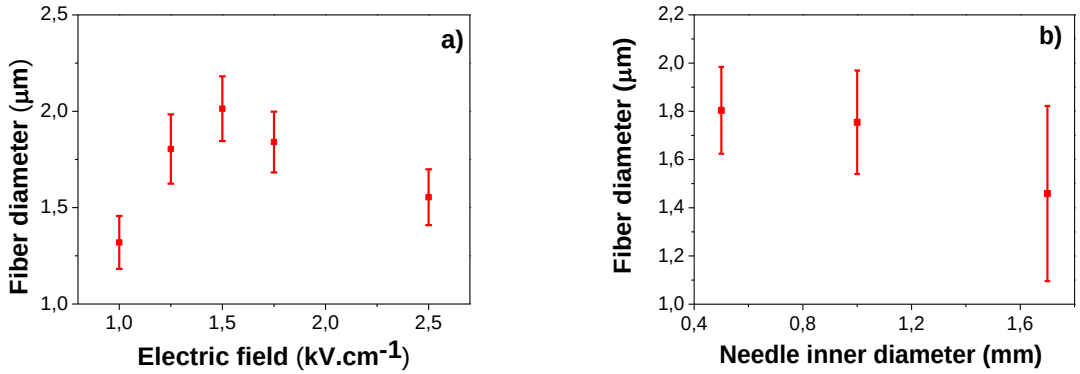

Figure 5.2. a) Influence of applied electric field and b) Influence of needle inner diameter on the mean diameter of the electrospun PHB fibers.

The inner diameter of the needle also plays an important role in the electrospun fiber size and distribution. Typically, a small internal diameter reduces clogging and prevents the formation of beads on the electrospun fibers as well due to less exposure of the solution to the atmosphere during processing [25].

For PHB it was found that increasing needle inner diameter is associated to a decrease of the fiber mean diameter and size distribution becomes broader (Figure 5.2b). Literature shows contradictory results concerning the influence of the internal needle diameter. Macossay *et al.* [15] found no influence of the needle diameter on average fiber diameter for poly(methyl methacrylate) electrospun fibers, but on the other hand, some authors report that a decrease of the needle inner diameter is associated to a reduction of the fiber diameter, and such behavior was attributed to the increasing surface tension of the droplet, which results in variations of the forces needed for jet initialization and therefore in traveling time, influencing jet stretching and solvent evaporation. For PHB electrospun fibers, the increase of the needle inner diameter

results in a higher droplet volume ate the needle tip during the electrospinning and no stable Taylor cone is achieved, and several jets arise simultaneously from the droplet, that are stretched by the electric field giving origin to smaller and broader fiber diameter (Figure 5.2b). Further, the area of the droplet expose to air increases with for higher needle diameters during processing and as a result clogging at the tip of the needle occurred easily and electrospinning terminated automatically within a very short of time before sufficient fiber could be produced. Such effect was also observed Tong and Wang [26].

The influence of the solution feed rate on electrospun fiber mean diameter and distribution was also analyzed keeping constant the applied voltage (25 kV) and the needle inner diameter (0.5 mm, Figure 5.3).

It is observed that increasing feed rate from 5 up to 10 $mL.h^{-1}$ increases the mean fiber diameter, but by further increasing flow rates a slight decrease of the mean fiber diameter occurs (Figure 5.3). On the other hand, fiber size distribution is very similar for the samples collected at different feed rates. It is generally expected increasing fiber diameters and number of beads when the feed rate increases due to the larger volume of solution that is drawn away from the needle. This increase of volume drawn from the needle tip will promote an increase of the time for the solvent to evaporate and consequently more time is needed for the polymer to crystallize, given origin to higher fiber diameters and broader distribution as observed for other polymer systems like PVDF [16], PLA [24] and chitosan [23].

For PHB, it seems that the low boiling point of the CF/DMF solvent blend (Table 5.1) allows a fast evaporation during the flight time. In this situation, full solvent evaporation occurs when the fiber reaches the grounded collector and therefore the feed rate does not have strong influence on fiber diameter. It is also observed that for feed rates higher than 20 $mL.h^{-1}$ the jet becomes instable and the fiber reaches the ground metallic collector with some solvent promoting the dissolution of the fibers already collected.

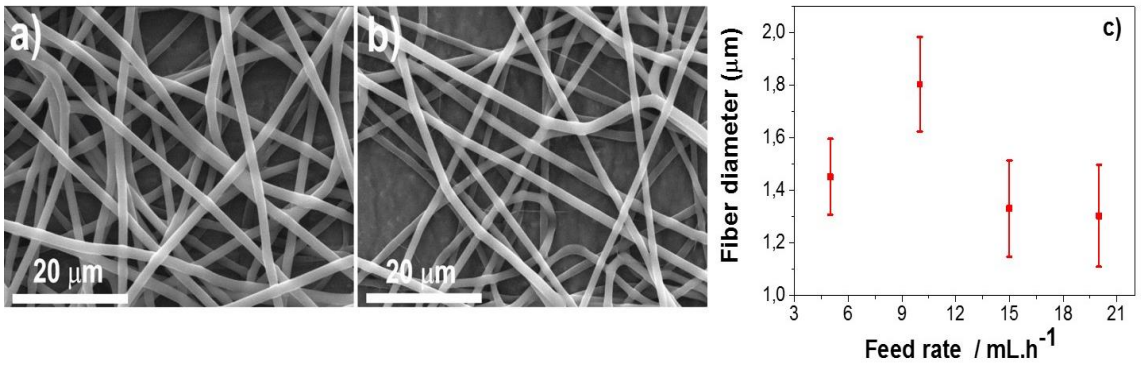

Figure 5.3. Influence of feed rate on the mean diameter of the electrospun PHB fibers. Needle inner diameter: 0.5 mm; applied field of 1.25 kV.cm^{-1}: a) sample obtained at 5 mL.h^{-1}, b) sample obtained at 20 mL.h^{-1} and c) fiber average size and distribution dependence on feed rate.

In order to study the influence of the polymer concentration of the CF/DMF solution, different polymer/solvent ratios were prepared. For an amount of 5 % PHB on solvent dissolution, electrospinning was not feasible due to the high conductivity of the solution that promotes sparks. Increasing PHB concentration to 7 % allows stable polymer electrospinning. Moreover, a decrease of the fiber diameter from 1.8 ± 0.2 μm (Figure 5.1) down to 530 ± 140 nm was observed and the fibers present same randomly distribution, with smooth fibers, without ribbons or beads (Figure 5.4) observed for the polymer concentration of 10 % (Figure 5.1)

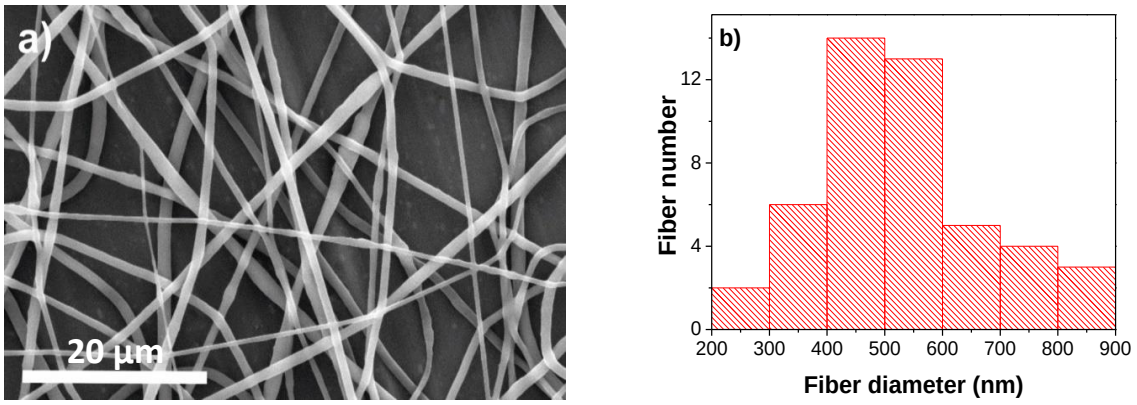

Figure 5.4. a) PHB electrospun membrane obtained at 7/93 (7 % PHB + 93 % solvent blend, v/v) for an applied field of 1.25 kV.cm^{-1}, needle inner diameter of 0.5 mm, feed rate of 10 mL.h^{-1} (scale bar is 20 μm) and b) histogram of the fiber diameter distribution.

5.3.2. Surface chemical characterization

FTIR was used to monitor variations at a molecular level that might occur due to the electrospun conditions. Figure 5.5 shows the characteristic infrared spectra observed for PHB film and for the electrospun fibers obtained at different applied electrical fields. The overall response of the FTIR spectra is quite similar, no vibration modes are totally suppressed and no new modes seems to appear due to the changes in the processing parameters (Figure 5.5), i.e. the structure and the crystalline phase of the PHB remain the same, independently of the processing conditions.

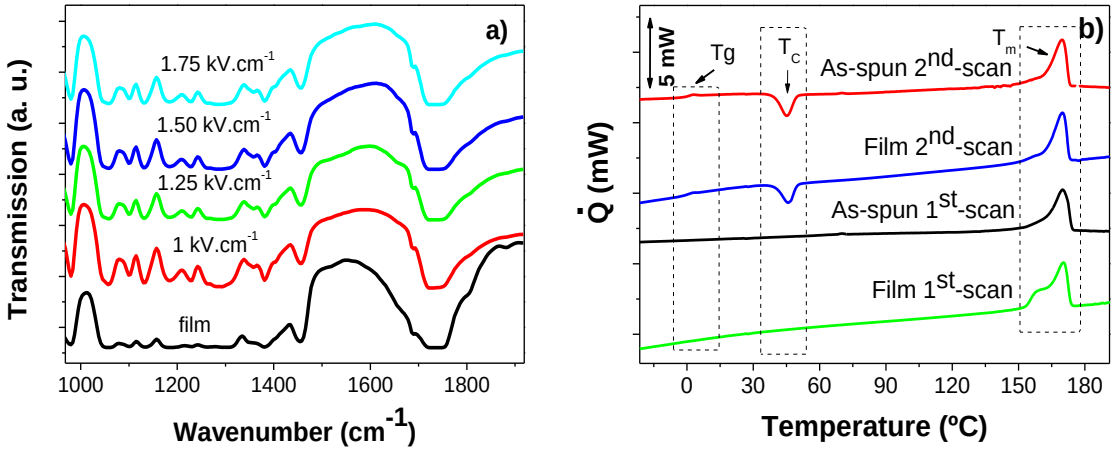

Figure 5.5. a) Infrared spectra for a PHB film and for electrospun samples prepared with tip inner diameter of 0.5 mm, a feed rate of 10 mL.h^{-1} and at different applied electric fields and b) DSC curves of PHB electrospun sample collected with tip inner diameter of 0.5mm, a feed rate of 10 mL.h^{-1} and at an applied field of 1.25 kV cm^{-1}. The film was obtained for solvent casting at 60 ºC.

PHB absorption bands and their assignments are summarized in Table 5.2. The results obtained showed that the most characteristic absorption peaks are the carbonyl and hydroxyl groups at ~1720 and 3278 cm^{-1}, respectively. Other characteristic bands for PHB polymer appear at ~1276, ~1180, and ~1057 cm^{-1}, which can be assigned to the ester groups of the polymer (Figure 5.5).

Table 5.2. Characteristic FTIR absorption bands and assignments for PHB polymer [7].

Wavenumber (cm^{-1})	Absorption bands
2976	stretching of C-CH_3
2936	asymmetric stretching of CH_2
2871	CH stretching
1720	C=O carbonyl group stretching vibration of the crystalline carbonyl group
1687	stretching of C=O (acetate group) (crystalline)
1452	asymmetric deformation of CH_3
1380	symmetric wagging of CH_3
1277	symmetric C-O-C stretching
1259	symmetric C-O-C stretching + C-H deformation
1227	C-O-C stretching
1180	asymmetric C-O-C stretching
1130	symmetric stretching vibration of C-O-C group
1101	symmetric C-O-C stretching
1057	C-O stretching and CH_2 rocking
981	C-C stretching (crystalline)

5.3.3. Thermal characterization

Differential scanning calorimetry (DSC) normalized thermograms (heat flow divided by sample mass and heating rate) are shown in Figure 5.5b. The first heating scan shows a strong endothermic peak around 170 ºC that corresponds to melting. On the second scan, recorded after cooling from the melt at 10 ºC.min^{-1}, the glass transition appears around 0 ºC, and at higher temperatures, a cold crystallization exotherm process is observed in the range of 30 ± 60 ºC, with a maximum at 45 ºC. It was observed that PHB glass transition temperature occurs around 0 ºC, and if the material is stored at room temperature (25 ºC), polymer cold crystallization occurs almost immediately (Figure 5.5b). Same effect was observed by other authors in PHB films [27, 28].

Crystallinity degree of PHB electrospun mats can be calculated according to equation 5.1.

$$\Delta X_c = \frac{\Delta H_{sample}}{\Delta H_0^f} \times 100 \quad (5.1)$$

where, ΔH_{sample} and ΔH_0^f (= 146 J.g^{-1} [27, 28]) are the experimental melting enthalpy and the thermodynamic melting enthalpy of a 100 % crystalline PHB polymer, respectively. Both PHB samples, film and electrospun membrane show the same crystallinity degree of 53 %, which is similar to the values reported in literature. Xu *et al.* [28] performed PHB annealing measurements at different temperatures above glass transition and found a maximum crystallinity degree of 56.8 %. Amico *et al.* [29] study the thermal properties of the PHB filled with clays and reported a crystallinity of 66 % for pure polymer that slightly decreases with the incorporation of the clays into the polymer matrix.

Thermal instability is one of the major drawbacks of the PHB since the decomposition temperature of the polymer is close to the melting point. Figure 5.6 shows the TGA data obtained for the PHB fiber mats at various heating rates. A major weight loss process was observed between 200 and 350 ºC. No loss of volatiles was found below 200 ºC showing the absence of solvents remains used in electrospinning process and water (due to the hydrophobic nature of the polymer). Two main temperatures were revealed: the initial degradation temperature ($T_{initial}$), which is defined as the temperature at which the experimental curves deviates from the tangent line that the mass evolution follows before degradation, and the onset temperature (T_{onset}) that is calculated by extending the pre-degradation portion of the curve to the point of the interception with a line drawn as a tangent to the steepest portion of the mass curve occurring during degradation.

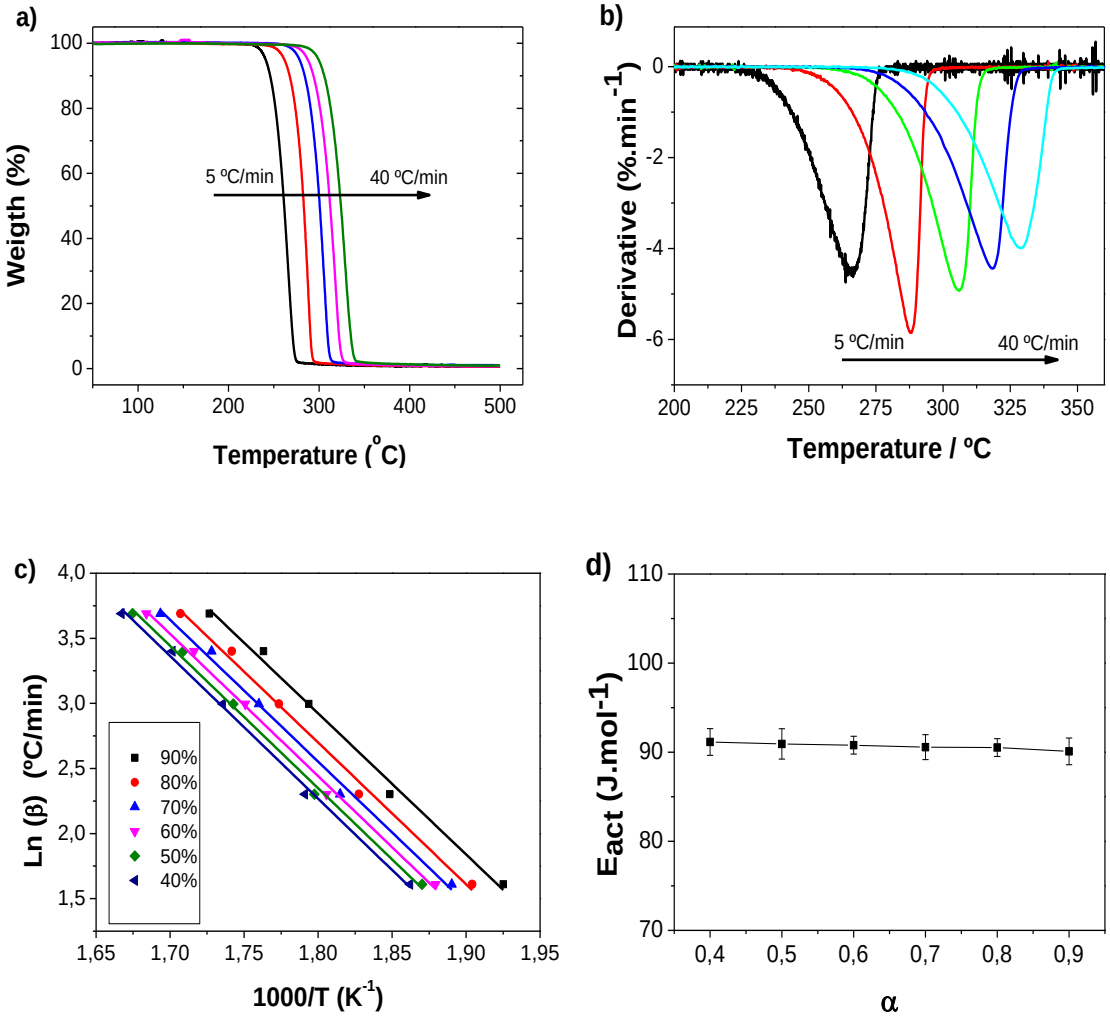

Figure 5.6. Thermal degradation of PHB electrospun mats: a) Thermogravimetric results for electrospun mats, b) Derivative, DTG, results obtained for the different heating rates, c) Ozawa-Flynn-Wall plots, and d) Evolution of the activation energy. Sample obtained with tip inner diameter of 0.5 mm, a feed rate of 10 mL.h^{-1} and an applied field of 1.25 kV.cm^{-1}.

The kinetics of the mass loss process can be investigated by analyzing experiments performed at different heating rates (Figure 5.6a and 5.6b). As expected, increasing heating rate shifts the onset temperature of the degradation process to higher temperatures, not affecting any of the main characteristics of the process itself.

A typical model for the decomposition has the following general form:

$$\frac{\partial \alpha(T)}{\partial t} = k(T) f[\alpha(T)] \qquad (5.2)$$

where, α represents the degree of conversion of the sample under degradation, defined by:

$$\alpha = {(w_0 - w_t)}\Big/{(w_0 - w_\infty)} \quad (5.3)$$

where w_0, $w_{(t)}$ and w_∞ are the weights of the sample before degradation, at a given time t and after complete degradation, respectively. The rate constant $k(T)$ changes with the absolute temperature according to the Arrhenius equation. $f(\alpha(T))$ represents the net results of elementary steps, as the polymer degradation is often a chain reaction. For the reaction model $f(\alpha(T)) = (1-\alpha)^n$, where n is the reaction order, assumed to remain constant during the degradation process.

The isoconversional method of Ozawa-Flynn-Wall (OFW) [30, 31] is a method which assumes that the conversion function $f(\alpha)$ does not change with the variation of the heating rate for all values of the degree of conversion α. It involves measuring the temperatures corresponding to fixed values of α from the experiments at different heating rates, β . In this theory:

$$\ln(\beta) = \frac{\ln(AE_{act})}{R} - \ln[f(\alpha(T))] - \frac{E_{act}}{RT} \quad (5.4)$$

where A is a pre-exponential factor (min^{-1}), R is the gas constant (8.31 $J.mol^{-1}.K^{-1}$), and E_{act} is the activation energy of the degradation process. By the plotting $\ln(\beta)$ *vs* ${1}/{T}$, activation energy can be obtain from the slope of the resulting straight line, regardless of the reaction order of the system. The validity of this model is based in the assumption that the conversion at the peak maximum is constant for the different heating rates [30, 31]. The linear fitting for the PHB as-spun mats is represented in Figure 5.6c. The evolution of the activation energy with the degree of conversion reveals to be constant and a value of 91 $kJ.mol^{-1}$ was obtained. Previous reports have shown that the activation energy value of the degradation fall within a wide range 100 - 235 $kJ.mol^{-1}$. A clear explanation for the wide variation of E_{act} has yet to be provided. Despite this uncertainty, the random β-elimination scission has been widely held as the exclusive degradation mechanism of PHB based on typical structures of pyrolysis products, i.e. crotonic acid and oligomers with a crotonate end-group [32, 33]. Recently, an E1cB

mechanism proceeding via α-deprotonation by a carboxylate anion to produce the same products was proposed [34].

5.3.4. Cell viability

Fiber mats surface energy was estimated by water contact angle measurements on a PHB film and in the as-spun membranes. The water contact angle measured for the polymeric film was 77 ± 2º, similar to the values reported in the literature [35]. For the as-spun membranes the calculated contact angle was 126 ± 3º, which reveals a strong increase of the hydrophobicity due to morphological variations. This behavior is common to other polymeric systems obtained by electrospinning such as PLA [36].

PHB shows potential for biomedical and tissue engineering applications such as bone repair and drug-carriers [37]. Electrospinning uses many times toxic solvents that could eventually prevents the use of electrospun membranes in biomedical applications. MTT tests were used to characterize proliferation and viability of cells on PHB as-spun fiber membranes throughout 3 days of culture. The absorbance (A) was measured at 570 nm for all the samples at each time. It was observed for the first 3 days that electrospun PHB fiber mats prepared under the above described method and conditions do not inhibit the adhesion of cells (Figure 5.7).

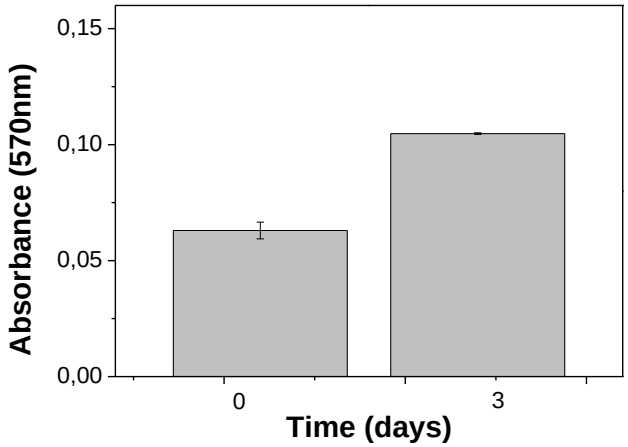

Figure 5.7. MTT absorbance results after cells seeded for 0 and 3 days on PHB fibers. Values are mean ± SD.

5.4. Conclusions

PHB was dissolved in a mixture of CF and DMF and processed by electrospinning at 40 ºC. The addition of DMF to the solvent solution turns the polymer membrane more stable. Smooth randomly oriented fibers without beads and ribbons were obtained. Moreover, it was observed that an increase of the applied electric field is associated to an increase of the fiber average diameter until a mean diameter of 2.01 μm for an applied electric field of 1.50 $kV.cm^{-1}$, but for higher electric fields, a decrease of the fiber diameter was observed, due to the jet instability and fiber stretching. On the other hand, the increase of the tip inner diameter promotes a decrease of the fiber average diameter and a broader distribution. Fiber around 500 nm was obtained by decreasing down to 7 % the concentration of PHB in the solution.

Infrared spectroscopy showed that the changes in the processing parameters do not alter the crystalline phase present in the polymer. Moreover, the crystallinity of PHB film and as-spun membranes are similar, around 53 %. Thermogravimetric results of the as-spun membranes show that polymer degradation occurs in single step degradation process, with activation energy of 91 $kJ.mol^{-1}$.

MC-3T3-E1cell adhesion was not inhibited by the fiber mats preparation, indicating the suitability of the material for biomedical applications.

5.5. References

1. Sombatmankhong, K., et al., *Bone scaffolds from electrospun fiber mats of poly(3-hydroxybutyrate), poly(3-hydroxybutyrate-co-3-hydroxyvalerate) and their blend.* Polymer, 2007. **48**(5): p. 1419-1427.
2. Wróbel, M., J. Zebrowski, and J. Szopa, *Polyhydroxybutyrate synthesis in transgenic flax.* Journal of Biotechnology, 2004. **107**(1): p. 41-54.
3. Ali, A.Q., et al., *In vitro genotoxicity tests for polyhydroxybutyrate - A synthetic biomaterial.* Toxicology in Vitro, 2008. **22**(1): p. 57-67.
4. Gouda, M.K., A.E. Swellam, and S.H. Omar, *Production of PHB by a Bacillus megaterium strain using sugarcane molasses and corn steep liquor as sole carbon and nitrogen sources.* Microbiological Research, 2001. **156**(3): p. 201-207.
5. Reis, K.C., et al., *Characterization of polyhydroxybutyrate-hydroxyvalerate (PHB-HV)/maize starch blend films.* Journal of Food Engineering, 2008. **89**(4): p. 361-369.
6. Dias, M., et al., *Blends of poly(3-hydroxybutyrate) and poly(p-dioxanone): miscibility, thermal stability and biocompatibility.* Journal of Materials Science-Materials in Medicine, 2008. **19**(12): p. 3535-3544.
7. Asran, A.S., et al., *Nanofibers from Blends of Polyvinyl Alcohol and Polyhydroxy Butyrate As Potential Scaffold Material for Tissue Engineering of Skin.* Biomacromolecules, 2010. **11**(12): p. 3413-3421.
8. Wang, Y.-W., et al., *Evaluation of three-dimensional scaffolds made of blends of hydroxyapatite and poly(3-hydroxybutyrate-co-3-hydroxyhexanoate) for bone reconstruction.* Biomaterials, 2005. **26**(8): p. 899-904.
9. Nivison-Smith, L., J. Rnjak, and A.S. Weiss, *Synthetic human elastin microfibers: Stable cross-linked tropoelastin and cell interactive constructs for tissue engineering applications.* Acta Biomaterialia, 2010. **6**(2): p. 354-359.
10. Sombatmankhong, K., et al., *Electrospun fiber mats of poly(3-hydroxybutyrate), poly(3-hydroxybutyrate-co-3-hydroxyvalerate), and their blends.* Journal of Polymer Science Part B-Polymer Physics, 2006. **44**(19): p. 2923-2933.
11. Sangsanoh, P., et al., *In vitro biocompatibility of schwann cells on surfaces of biocompatible polymeric electrospun fibrous and solution-cast film scaffolds.* Biomacromolecules, 2007. **8**(5): p. 1587-1594.
12. Fryczkowski, R. and T. Kowalczyk, *Nanofibres from polyaniline/polyhydroxybutyrate blends.* Synthetic Metals, 2009. **159**(21-22): p. 2266-2268.
13. Rodrigues, M.F.A., et al., *Biosynthesis of poly (3-hydroxybutyric acidco-3-hydroxy-4-pentenoic acid) from unrelated substrates byBurkholderia sp.* Applied Microbiology and Biotechnology, 1995. **43**(5): p. 880-886.
14. Martin Koller, et al., *Sustainable Embedding of the Bioplastic Poly-(3-Hydroxybutyrate) into the Sugarcane Industry: Principles of a Future-Oriented*

Technology in Brazil, in *The Handbook of Environmental Chemistry*, C.H. Martin Weller and O. Hutzinger, Editors. 1980, Springer-Verlag: London, UK.

15. S. Ramakrishna, et al., *An introduction to electrospinning and nanofibers*. 2005, New Jersey: World Scientific.

16. Ribeiro, C., et al., *Influence of Processing Conditions on Polymorphism and Nanofiber Morphology of Electroactive Poly(vinylidene fluoride) Electrospun Membranes.* Soft Materials, 2010. **8**(3): p. 274-287.

17. Wang, C., et al., *How to manipulate the electrospinning jet with controlled properties to obtain uniform fibers with the smallest diameter?—a brief discussion of solution electrospinning process.* Journal of Polymer Research, 2011. **18**(1): p. 111-123.

18. Qin, X.-H., et al., *Effect of LiCl on electrospinning of PAN polymer solution: theoretical analysis and experimental verification.* Polymer, 2004. **45**(18): p. 6409-6413.

19. Zhao, S., et al., *Electrospinning of ethyl–cyanoethyl cellulose/tetrahydrofuran solutions.* Journal of Applied Polymer Science, 2004. **91**(1): p. 242-246.

20. Gao, K., et al., *Crystal structures of electrospun PVDF membranes and its separator application for rechargeable lithium metal cells.* Materials Science and Engineering: B, 2006. **131**(1–3): p. 100-105.

21. Demir, M.M., et al., *Electrospinning of polyurethane fibers.* Polymer, 2002. **43**(11): p. 3303-3309.

22. Megelski, S., et al., *Micro- and Nanostructured Surface Morphology on Electrospun Polymer Fibers.* Macromolecules, 2002. **35**(22): p. 8456-8466.

23. Sencadas, V., et al., *Determination of the parameters affecting electrospun chitosan fiber size distribution and morphology.* Carbohydrate Polymers, 2012. **87**(2): p. 1295-1301.

24. Ribeiro, C., et al., *Tailoring the morphology and crystallinity of poly(L-lactide acid) electrospun membranes.* Science and Technology of Advanced Materials, 2011. **12**(1).

25. Mo, X.M., et al., *Electrospun P(LLA-CL) nanofiber: a biomimetic extracellular matrix for smooth muscle cell and endothelial cell proliferation.* Biomaterials, 2004. **25**(10): p. 1883-1890.

26. Tong, H.-W. and M. Wang, *Electrospinning of Poly(Hydroxybutyrate-co-hydroxyvalerate) Fibrous Scaffolds for Tissue Engineering Applications: Effects of Electrospinning Parameters and Solution Properties.* Journal of Macromolecular Science, Part B, 2011. **50**(8): p. 1535-1558.

27. Kemnitzer, J., et al., *Crystallization behavior of predominantly syndiotactic poly(β-hydroxybutyrate).* Journal of Polymers and the Environment, 1995. **3**(1): p. 37-47.

28. Xu, S., et al., *Blending and characterizations of microbial poly(3-hydroxybutyrate) with dendrimers.* Journal of Applied Polymer Science, 2006. **102**(4): p. 3782-3790.

29. D'Amico, D.A., L.B. Manfredi, and V.P. Cyras, *Relationship between thermal properties, morphology, and crystallinity of nanocomposites based on polyhydroxybutyrate.* Journal of Applied Polymer Science, 2012. **123**(1): p. 200-208.

30. Flynn, J.H. and L.A. Wall, *A quick, direct method for the determination of activation energy from thermogravimetric data.* Journal of Polymer Science Part B: Polymer Letters, 1966. **4**(5): p. 323-328.

31. Ozawa, T., *A new method to analyze thermogravimetric data.* Bulletin of the Chemical Society of Japan, 1965. **38**(11): p. 1881-1991.

32. Morikawa, H. and R.H. Marchessault, *Pyrolysis of bacterial polyalkanoates.* Canadian Journal of Chemistry, 1981. **59**(15): p. 2306-2313.

33. Ballistreri, A., et al., *Analytical degradation: An approach to the structural analysis of microbial polyesters by different methods.* Journal of Analytical and Applied Pyrolysis, 1989. **16**(3): p. 239-253.

34. Kawalec, M., et al., *Carboxylate-Induced Degradation of Poly(3-hydroxybutyrate)s.* Biomacromolecules, 2007. **8**(4): p. 1053-1058.

35. Zhang, D.M., et al., *Wettability improvement of bacterial polyhydroxyalkanoates via ion implantation.* Surface and Coatings Technology, 2000. **131**(1–3): p. 350-354.

36. Areias, A.C., et al., *Influence of crystallinity and fiber orientation on hydrophobicity and biological response of poly(l-lactide) electrospun mats.* Soft Matter, 2012. **8**(21): p. 5818-5825.

37. Chen, G.-Q. and Q. Wu, *The application of polyhydroxyalkanoates as tissue engineering materials.* Biomaterials, 2005. **26**(33): p. 6565-6578.

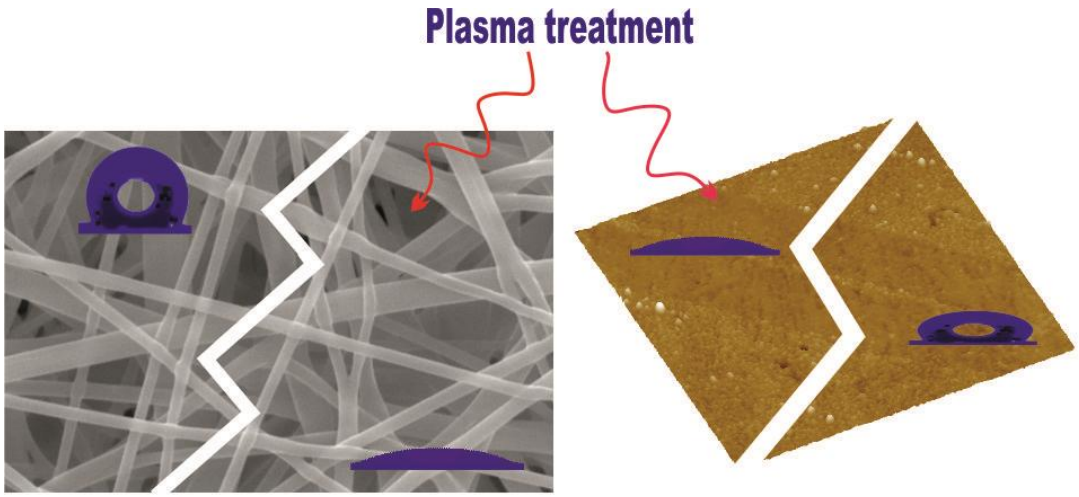

6. Superhydrophilic plasma treated poly(L-lactic acid) electrospun membranes for biomedical applications

Surface characteristics and, in particular, wettability, are very important properties of materials for tissue engineering applications. This chapter describes the surface wettability modification of electrospun PLLA membranes and films after argon and oxygen plasma treatments. The influence of the plasma treatment gas, time and power in the physico-chemical properties and contact angle were studied and superhydrophilic membranes were obtained. Cell viability studies were also performed in both plasma treated and non-treated samples.

This chapter is based on the following publication: D.M. Correia, C. Ribeiro, G. Botelho, J. Borges, C. Lopes, F. Vaz, S. Carabineiro, A. V. Machado, S. Lanceros-Méndez. *Superhydrophilic plasma treated poly(L-lactic acid) electrospun membranes for biomedical applications*. Submitted. 2015

6.1. Introduction

Biomaterials used as extracellular matrixes in tissue engineering applications play a key role in supporting cells and/or biologically active molecules to promote the repair of damage tissue and/or tissue regeneration [1]. In particular, extracellular matrixes based on biodegradable polymers such as PLLA have been extensively studied once they can be easily processed in a variety of forms [2]. PLLA is an aliphatic semi-crystalline polyester that can be produced from renewable sources, such as corn or sugar cane [3]. Due to its biocompatibility and biodegradability through hydrolytic scission of the ester groups into lactic acid, with a degradation rate that matches the healing time of damaged human tissues, low toxicity and proper mechanical characteristics, this polymer has been attracting strong interest for uses in tissue repair and regeneration [4, 5]. Moreover, its piezoelectric properties (d_{25} = 10 $pC.N^{-1}$) are also an advantage that can be used to stimulate tissue by mechano-electrical transduction [6, 7] in order to implement active scaffolds [7, 8], not just acting as passive supports for cells.

Electrospun fiber membranes based on PLLA are particularly appropriate for tissue engineering applications due to their large surface area, small fiber diameters and porous structure [2]. It was demonstrated that PLLA fibers promote cell adhesion and proliferation [9]. [10]. The major drawback of these fibrous membranes for tissue engineering are associated to the PLLA hydrophobicity, limiting their applicability, due to hindered cell-material interaction [11]. As reported in chapter 2 several methods can be used to modify the surface properties of the materials being plasma treatment one of the most extensively used methods to modify the chemical and physical properties of polymers without affecting their bulk characteristics. The success of plasma treatment is associated to the selection of plasma source type (oxygen, argon, nitrogen and acetylene, among others), treatment time and power [12, 13].

The surface of PLLA can be modified by several gases such as argon (Ar), Ar-NH_3/H_2, oxygen (O_2) and nitrogen (N_2) [14]. It has been shown that a significant decrease in contact angle occurs after Ar plasma treatment in PLLA films (~41º) due to development of oxygen-containing groups on the modified surface [15] and under Ar-NH_3/H_2 gas plasma treatment in PLLA membranes (~49º) and in electrospun fibrous scaffolds (~0º) through the introduction of nitrogen-containing surface groups, such as amine (-NH_2) [16]. Also O_2 and N_2 can be used to improve the hydrophilicity of PLLA surfaces, with a significant decrease (75 %) in contact angle due to the increase of the

number of polar groups formed during the plasma treatment [17]. However, to the best of our knowledge, there is no work reported on O_2 and Ar plasma treatment for PLLA to achieve superhydrophilic surfaces [16]. In this work, the effects of O_2 and Ar plasma treatments on PLLA electrospun PLLA membranes and films surface wettability and the variation of the treatment time were investigated. Furthermore, the influence of plasma treatment on fiber morphology, surface composition and degree of crystallinity were evaluated.

6.2. Experimental section

6.2.1. Materials

Purasorb PL18 PLLA, with an average molecular weight of 217.000–225.000 $g.mol^{-1}$, was purchased from Purac; DMF from Merck and dichloromethane (MC) from Sigma Aldrich. Materials were used as provided.

6.2.2. Sample preparation

PLLA electrospun membranes were processed according to a previously reported method [4]. Briefly, a 10 wt % solution of PLLA in DMF/MC was prepared under magnetic stirring at room temperature until complete dissolution of the polymer. Then, the polymer solution was placed in a plastic syringe (10 mL) fitted with a steel needle with inner diameter of 0.5 mm. The electrospinning procedure was conducted at 20 kV with a high voltage power supply from Glassman (model PS/FC30P04) with a solution feed rate of 0.5 $mL.h^{-1}$ applied with a syringe pump (from Syringepump). The randomly oriented electrospun membranes were collected in an aluminum plate. PLLA films were obtained by casting from the solution used for electrospinning and subjected to brief annealing, at 80 ºC, during 30 min, to allow solvent evaporation.

6.2.3. Surface modification

Surface treatment was conducted in a Zepto plasma chamber Diener Electronics (Ø = 105 mm, L = 300 mm, V = 2.6 L) equipped with a 40 kHz radio frequency plasma

generator. The base pressure of system (obtained before plasma ignition) was 20 Pa. Plasma treatments were performed independently with Ar and O_2, used as working gases, for different times from 5 to 970 s and plasma powers from 10 to 100 W under a total pressure of 80 Pa.

6.2.4. Sample characterization

Fiber morphology was analyzed using scanning electron microscopy (SEM, Quanta 650, from FEI) with an accelerating voltage of 5 kV. The samples were previously coated with a thin gold layer using a sputter coating (Polaron, model SC502). Surface morphology and roughness of the PLLA films were studied by Atomic Force Microscopy (AFM) using a VEECO CP II AFM working in the tapping mode. A Si probe, RTES- PA-CP with a spring constant 20–80 $N.m^{-1}$ was used. The provided roughness value (Ra) represents the arithmetic average of the deviations from the center plane of the sample.

Wettability of the samples was determined by measuring the contact angle as described in experimental section of chapter 2. XPS and FTIR analysis were performed as described in experimental section of chapter 2.

DSC was performed in a Perkin–Elmer, model Pyris-1 acquiring data from 30-200 ºC, with a heating rate of 10 $ºC.min^{-1}$, under nitrogen purge. The samples were cut in small pieces and placed into 40 µL aluminum pans. The degree of crystallinity *(*ΔXc) was determined using Equation 6.1 [4]:

$$\Delta X_c = \frac{\Delta H}{\Delta H^o{}_m} \tag{6.1}$$

Where ΔH is the area under the thermogram between 65 and 160 ºC, and $\Delta H^o{}_m$ is the melting enthalpy (93.1 $J.g^{-1}$) [4].

6.2.5. Cytotoxicity assay

The indirect cytotoxicity evaluation of the samples was conducted adapting the ISO 10993-5 standard test method.

The extraction media was prepared by immersing the samples (6 $cm^2.mL^{-1}$) in a 24-well tissue culture polystyrene plate with DMEM, (*Gibco)* containing 1.0 $g.L^{-1}$ glucose supplemented with 10 % FBS, (*Biochrom*) and 1 % P/S, *(Biochrom)*, at 37 ºC in a 95 % humidified air containing 5 % CO_2 and incubated for 24 h. A 20 % of DMSO (*Sigma Aldrich*) was used as a positive control and the cell culture medium was employed as negative control.

Furthermore, MC3T3-E1 pre-osteoblast cells were seeded in the 96-well tissue culture polystyrene plate at the density of 2×10^4 $cells.mL^{-1}$ and incubated for 24 h to allow cell attachment on the plate. After 24 h, the culture medium from the 96-well tissue culture polystyrene plate was removed and the as-prepared extraction media were added to the wells (100 µL). Afterward, the cells were incubated for 72 h and the cell viability evaluation was quantified with MTT (*Sigma Aldrich*) assay.

The MTT assay measures the mitochondrial activity of the cells, which reflects the viable cell number. After 72 h, the medium of every well was removed and fresh medium containing 10 % MTT solution (stock solution of 5 mg $MTT.mL^{-1}$ in PBS solution was added. The viable cells with active metabolism convert MTT into a purple coloured formazan product. After 2 h of incubation, the MTT crystals were dissolved with DMSO and the optical density was measured at 570 nm.

All quantitative results were obtained from four replicate samples and controls and analyzed as the average of viability ± standard deviation (SD). The cell viability percentage was calculated according the Equation 3.1 [18].

6.3. Results and discussion

Plasma treatment was performed at different times (from 5 to 970 s) and powers (from 10 to 100 W for both Ar and O_2 gases). In the following, the results will be shown for those samples and conditions that better represent the observed variations.

6.3.1. Morphology

Morphology, topography and physico-chemical variations of the samples, if any, caused by the plasma treatment would be larger and more clearly quantified for the more aggressive plasma treatment conditions, achieving the desired hydrophilic membranes.

Thus, those analysis were performed in the electrospun membranes and films with the largest plasma treatment time (t = 970 s) and power (P = 100 W).

Thus, Figure 6.1 show SEM pictures of the untreated (Figure 6.1a) and treated membranes under Ar (Figure 6.1b) and O_2 (Figure 6.1c) at t = 970 s and P = 100 W as well as the histogram of the fiber diameters. The histograms of the fiber diameters were determined from the corresponding SEM images with the ImageJ software and taking into account 50 fibers.

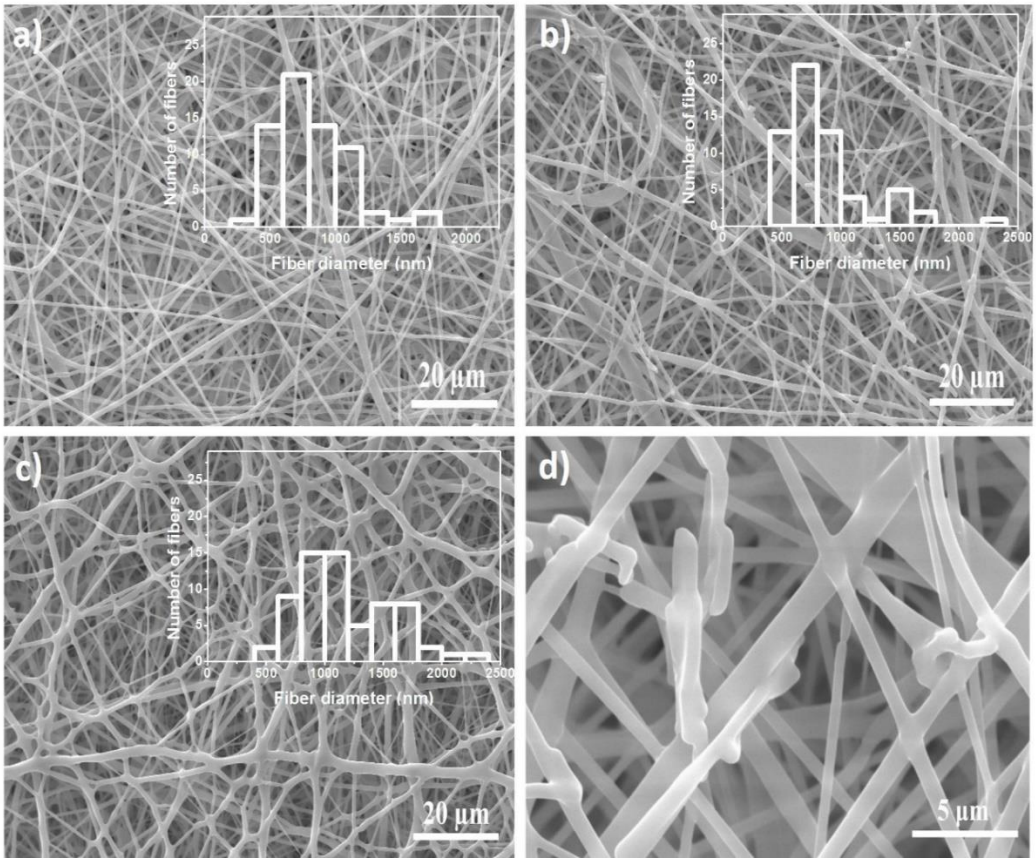

Figure 6.1. SEM images of electrospun PLLA membranes: a) untreated and plasma treated with b) argon and c) and d) oxygen at t = 970 s and P = 100 W.

As can be possible to observe PLLA fibers were successfully electrospun into a non-woven mesh with smooth fiber surface without the presence of beads (Figure 6.1a). After Ar plasma treatment (Figure 6.1b) the appearance of fiber mesh is similar to the pristine ones. Some fiber joining can be observed in Figure 6.1c and 6.1d (higher magnification) on the fibrils surface treated by O_2 probably related to surface polymer melting of the smaller fibers due to the high energy supplied by the plasma source [13].

Furthermore, fibers get a flat configuration after O_2 plasma. This important fiber modification, occurring at a larger scale, will superimpose any surface roughness variation, as it will be shown to occur in the film samples, and will determine the wettability observed. However, no complete fiber melting was detected showing the membrane still open space between fibers.

The influence of Ar and O_2 plasma treatments on fiber mean diameter was determined. Pristine PLLA mats present a mean average size of ~830 ± 282 nm (Figure 6.2a). After plasma treatments an average size of ~ 866 ± 361 nm and 1179 ± 397 nm were observed for Ar and O_2, (Figure 6.1c and 6.1d, respectively). Thus, Ar treatment does not induce significant variation of the fiber diameter, but O_2 plasma treatment, as leads to an increase of the average fiber diameter as a result of fiber joining.

The influence of the plasma treatment on the surface morphology and roughness of the polymer was studied by AFM in pristine and plasma treated PLLA films, due to the small size of the fibers. Figure 6.2 shows a 3D plot representation of PLLA surface (2 × 2 μm^2) obtained by AFM. It is shown that both Ar and O_2 plasma treatments induce changes in the surface morphology of PLLA that depends on the type of gas used in the plasma treatment. In general, ion etching during plasma treatment usually leads to a roughness increase in the polymer surface [16]. The surface of the untreated PLLA is characterized by a mean surface roughness (R_a) of 0.78±0.10 nm (Figure 6.2a). Ar plasma treatment does not induce significant changes in the Ra (0.85±0.63 nm) (Figure 6.2b). However, after O_2 plasma treatment, the surface roughness of PLLA increases to 3.4±2.1 nm. The increase in roughness is associated to ion etching during plasma treatment that can be followed by mass loss related to bond scission of PLLA and reactions of the radicals generated in the PLLA chains upon plasma exposure [16, 19]. When polymers are exposed to plasma, plasma cleaning and plasma etching occurs on the polymer surfaces [12]. As PLLA contains O_2 functionalities (ester groups), its surface presents high susceptibility to plasma etching [20]. Thus, it is concluded that a treatment time of 970 s, under O_2, promotes etching, which is not observed under Ar plasma.

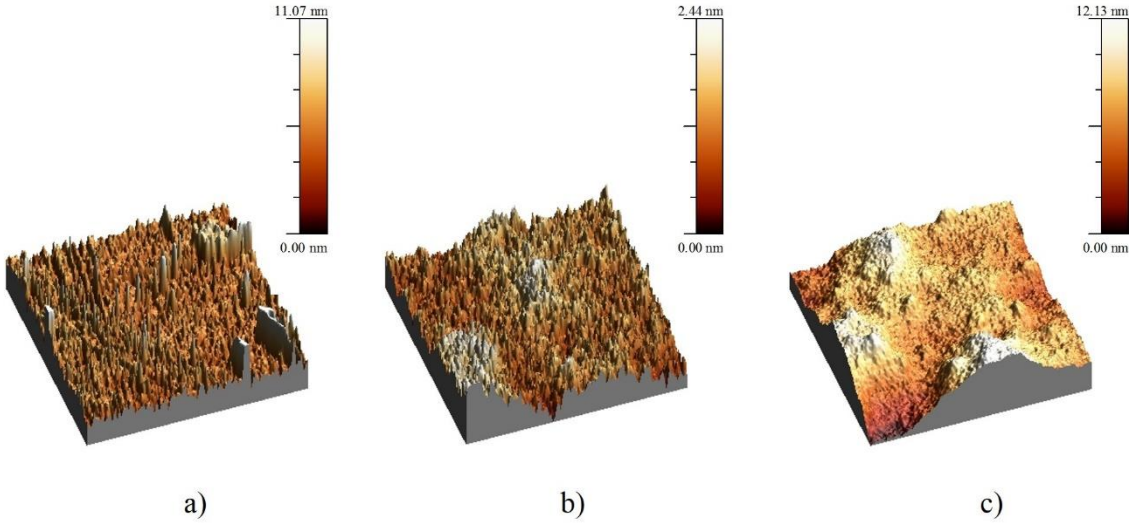

Figure 6.2. AFM images of the surface microstructure (2 × 2 μm scans) of PLLA films. a) Untreated PLLA films, b) PLLA plasma treated films (970 s and 100 W) with Ar and c) with O_2 gas plasma. The average R_a roughness of the samples are a) 0.78 nm, b) 0.85 nm and c) 3.4 nm, respectively.

6.3.2. Chemical surface variations

Plasma treatment generally leads to a surface modification process by the cleavage of the polymer molecular chains promoting the formation of free radicals that activates the surface [13]. To evaluate the quantitative elemental composition differences between the PLLA electrospun membranes and films before and after the plasma exposure time, a XPS analysis was performed. The results obtained for untreated membranes and films for the maximum plasma exposure time under Ar and O_2 are presented in Figure 6.4.

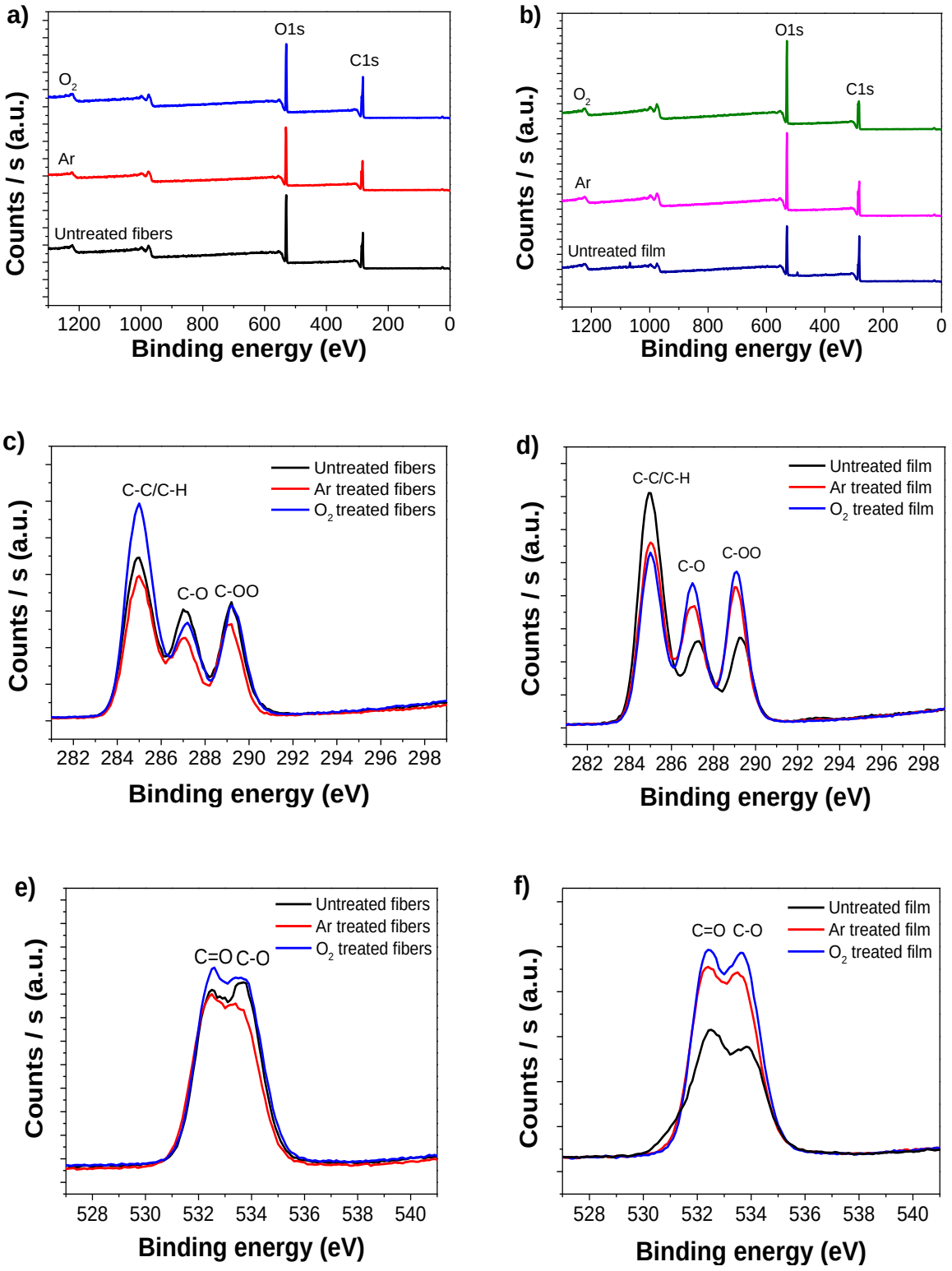

Figure 6.3. XPS results of untreated and treated PLLA electrospun membranes and films under O_2 and Ar plasma for a plasma treatment of 970 s with a power of 100 W: a, b) XPS survey scan c; d) C1s scan spectra and e, f) O1s spectra.

Figure 6.4a and 6.4b show that plasma exposure time does not induce relevant chemical changes in the composition of PLLA. In both pristine and plasma treated samples just carbon and oxygen were detected in the XPS spectra, due to the chemical structure of PLLA. Figure 6.4 shows the individual components of C1s (Figure 6.4c and 6.4d) and O1s (Figure 6.4e and 6.4f). From Figure 6.4c and d it is observed that PLLA fibers and films show three main C1s peaks at 284, 286 and 289 eV, characteristics of C-C/C-H, C-O and COO groups, respectively. The peaks at 532 and 533 eV in Figure 6.4e and 6.4f for O1s scanning spectra are assigned to C=O and C-O groups, respectively. It can be observed a low level oxidation process in the PLLA film surface, while for PLLA fibers treated with O_2 plasma the variations are within the experimental error.

Table 6.1 summarizes the XPS analysis for the % of elemental composition and the oxygen to carbon ratio (O/C) before and after the plasma exposition. The carbon and oxygen amounts present in PLLA untreated fibers are approximately 70 and 30 %, respectively.

Table 6.1. Surface chemical composition of untreated PLLA membranes and films modified by O_2 and Ar plasma at different treatment times.

Elemental composition (%)			
Surface	**C**	**O**	**O/C**
Untreated membranes	70.0±0.2	30.0±0.2	0.4
O_2 treatment time (s)			
10	68.0±0.2	32.0±0.2	0.5
970	69.0±1.1	31±1.1	0.4
Ar treatment time (s)			
25	64±0.6	36±0.6	0.6
970	66±0.6	34±0.6	0.5
Untreated Film	68±1.6	32±1.6	0.5
O_2 treatment time (s)			
10	65±1.7	35±1.8	0.5
970	65±1.2	35±1.2	0.5
Ar treatment time (s)			
25	68±1.2	32±1.2	0.5
970	66±0.3	34±0.3	0.5

Table 6.1 shows PLLA films values of approximately 68 % and 32 % of carbon and oxygen atoms, respectively. After O_2 and Ar plasma treatments, the amount of carbon atoms slightly decrease while the oxygen content increases being this increase more noticeable for treated PLLA films and for fibers exposure to Ar plasma. It was observed that the O/C ratio shows a small increase from 0.4 to approximately 0.5 in fibers and films, indicating that small chemical reactions occur in the fibers and films during plasma exposure under Ar and O_2. This slight increase can be explained by the scission of the C-H bond from the polymer chains due to the interaction of the O_2 and Ar plasma with the PLLA surface. During plasma treatments, the scission of carbon-hydrogen bond (C-H) due to the strength of the C-H (410 $kJ.mol^{-1}$) when compared to C=O (745 $kJ.mol^{-1}$) bonds induces radicals formation on the surface. After the activation of the surface, the free radicals can interact with the oxygen from air exposure leading to the formation of hydroperoxides groups enriched in oxygen, increasing the amount of O1s (Figure 6.4f). These compounds are highly unstable and can thermally decompose producing secondary radicals that subsequently are able to react with air exposure, originating newly formed C-O and C=O groups and therefore increasing oxygen concentration [13]. These considerations are in agreement with Table 6.1 where it is possible to observe that the carbon content slightly decreases when the plasma modification occurs. Figure 6.5 shows the possible chemical modifications that can lead to variations in the amount of carbon and oxygen contents in the PLLA surface of fibers and films. The formation of these polar groups on the PLLA surface leads to an increase in the hydrophilicity of the treated samples.

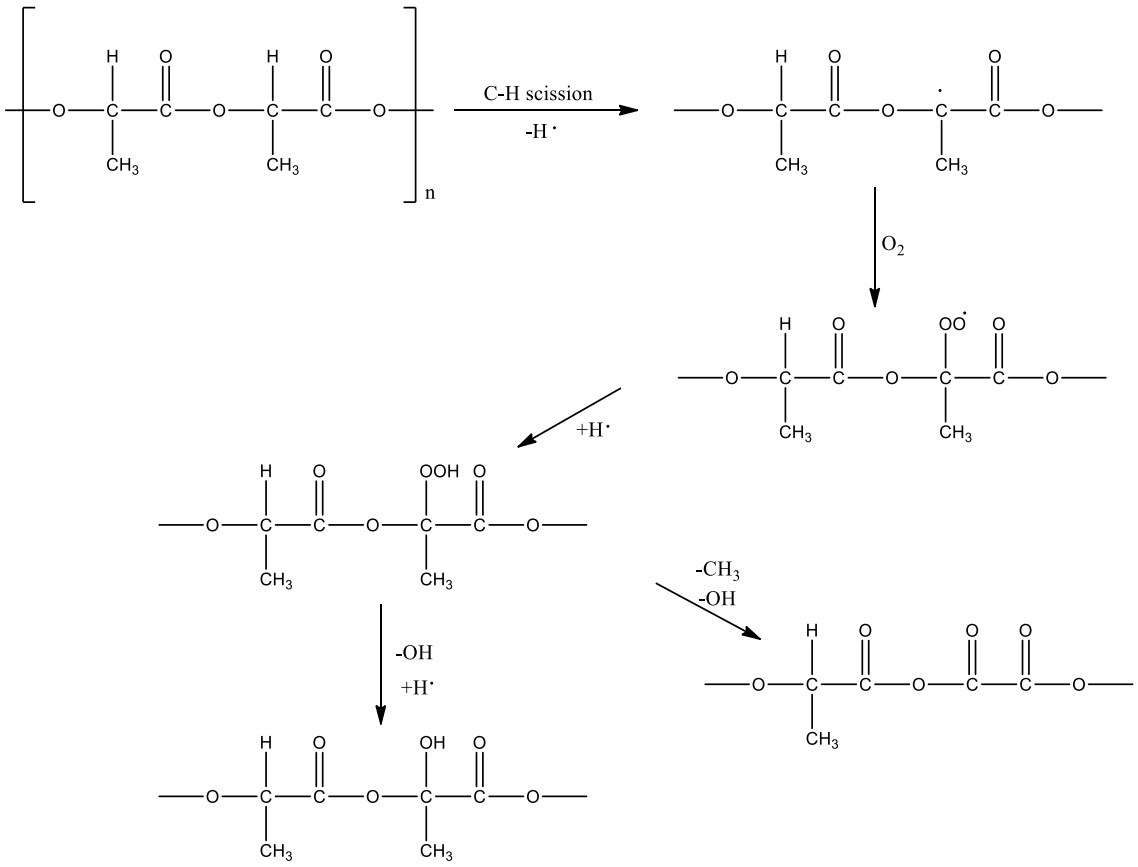

Figure 6.4. Schematic representation of Ar and O_2 plasma treatments on PLLA electrospun membranes and films. Plasma treatment introduces free radicals that can react with oxygen.

6.3.3. Physical - Chemical characterization

FTIR-ATR measurements were used to evaluate possible chemical changes in the PLLA polymer chain of electrospun membranes and films after a plasma exposure time of 970 s at 100 W. Figure 6.3a shows the infrared spectra for PLLA electrospun membranes and films before and after plasma exposure. The chemical structure of PLLA is formed by the repetition unit of -CH-C=O-O- [21]. As it is observed that no noticeable variations occurs between membranes and films or after plasma treatment under Ar and O_2 gas. All samples are characterized by the bands at 755 cm^{-1} and 870 cm^{-1}, both characteristics of CH_3 stretching and rocking, assigned to the crystalline and amorphous phase, respectively [22]. The absorption band at 1044 cm^{-1} is attributed to the stretching vibration of the C-CH_3 bond. The bands at 1130, 1357 and 1450 cm^{-1} are associated to r_s (CH_3), δ(CH) and δ_{as}(CH) stretch, respectively. The 1083, 1185, 1271 and 1747 cm^{-1} absorption bands, characteristics of the presence of oxygen compounds,

are ascribed to υ_s (C-O-C), ν_{as} (C–O–C) + r_{as} (CH_3), ν (CH) + ν (C-O-C) and ν (C=O), respectively [22]. As it has not been observed differences between the PLLA FTIR spectra before or after plasma treatments for both fiber mats and films, indicating that any chemical modification if present should have taken place at the surface and, therefore, can be analysed by XPS.

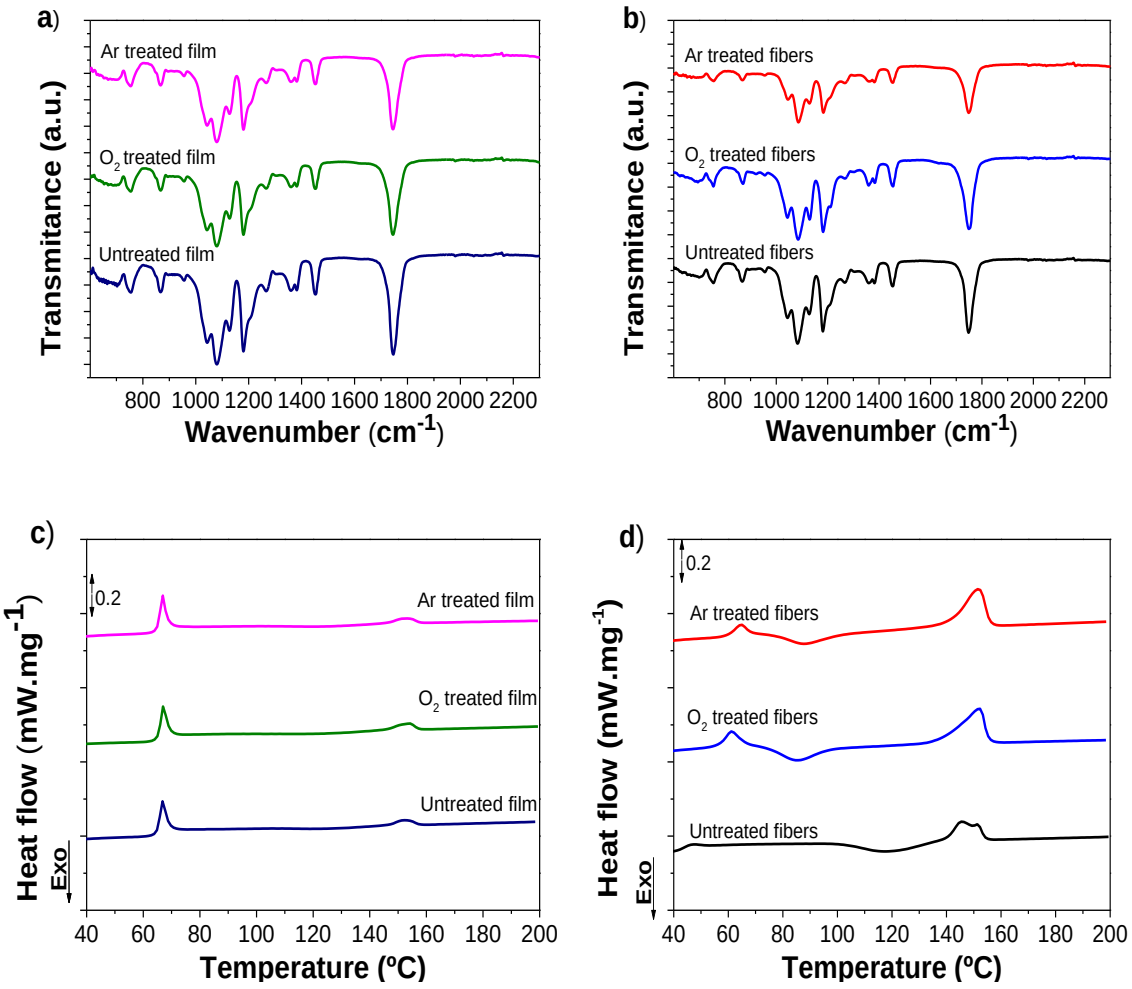

Figure 6.5. Physical-chemical characterization of electrospun PLLA membranes and films: a) and b) FTIR-ATR spectra and c) and d) DSC curves of untreated and treated PLLA electrospun membranes and films for a plasma treatment for 970 s at 100 W with Ar and O_2.

The thermal characterization of the PLLA samples was performed by DSC (Figure 6.3c and Figure 6.3d). All samples exhibit a strong endothermic peak at around 60 ºC corresponding to the glass transition and a single melting peak in the region between 140-160 ºC, in agreement to [4]. The melting peak in the PLLA films does not appear as

clearly as in the fibers indicating a lower degree of crystallinity. Further, no exothermic features are detected in the films, leading to conclude that there is no polymer crystallization during the DSC heating scans. On the other hand, untreated and treated PLLA electrospun membranes crystallizes during the DSC heating scan, showing a broad exotherm, immediately above the glass transition, in the range of 65-110 ºC, with a cold crystallization peak around 85 ºC. The cold crystallization behavior results from the ordering of PLLA molecular chains in a regular array above the glass transition, leading to the formation of a well-defined crystal structure. This fact shows that numerous crystal nuclei are present in the polymer as a result of the non-equilibrium chain conformations that result during the electrospinning process [4], which does not occur in the films. The degree of crystallinity of the samples was determined using Equation 6.1. It was observed that Ar and O_2 plasma treatments do not promote changes in the degree of crystallinity of films and membranes untreated PLLA ones. Both, electrospun mats and films are nearly amorphous, the degree of crystallinity of the films being ~ 4 % as evaluated by the area under the melting peak. The degree of crystallinity of the membranes is similar (as calculated by subtracting the cold crystallization from the total melting peak [4]) but reaches a maximum degree of crystallinity of ~32 % after cold crystallization. Again, this is similar for plasma treated membranes, indicating that the plasma effects are just confined to the surface of the membranes.

6.3.4. Samples wettability

Once the effect of the plasma treatment in the morphological and physico-chemical properties of the samples is understood, it is important to evaluate the effect in the wettability of the membranes. Plasma treatment of the samples generally causes a reduction of the contact angle and an increase in the surface energy. The contact angle measurements for PLLA samples before and after Ar and O_2 plasma treatment are presented in Figure 6.6. The water surface contact angle of the untreated fibers is 141 ± 4.3º being in agreement with the strong hydrophobicity associated to PLLA [3]. Figure 6.6 also show that the surface wettability of PLLA fibers and films depends on plasma treatment composition, time and power. Increasing argon plasma treatment time for a power of 100 W leads to a significant decrease in the contact angle of the PLLA fibers (Figure 6.6a), indicating a more hydrophilic surface. For argon treatment times higher

than 20 s, the PLLA electrospun fiber mats become superhydrophilic with a total water droplet absorption. Similar results are observed by varying plasma power for a given time (data not shown). Thus, for a treatment time of 20 s it was verified that 70 W is the minimum plasma power needed to achieve superhydrophilic membranes. The O_2 plasma treatment also enhances the PLLA surface hydrophilicity (Figure 6.6c), and a treatment time of 10 s leads the formation of superhydrophilic membranes. In fact, a minimum power plasma of 40 W is needed for obtaining superhydrophilic membranes for a treatment time of 10 s.

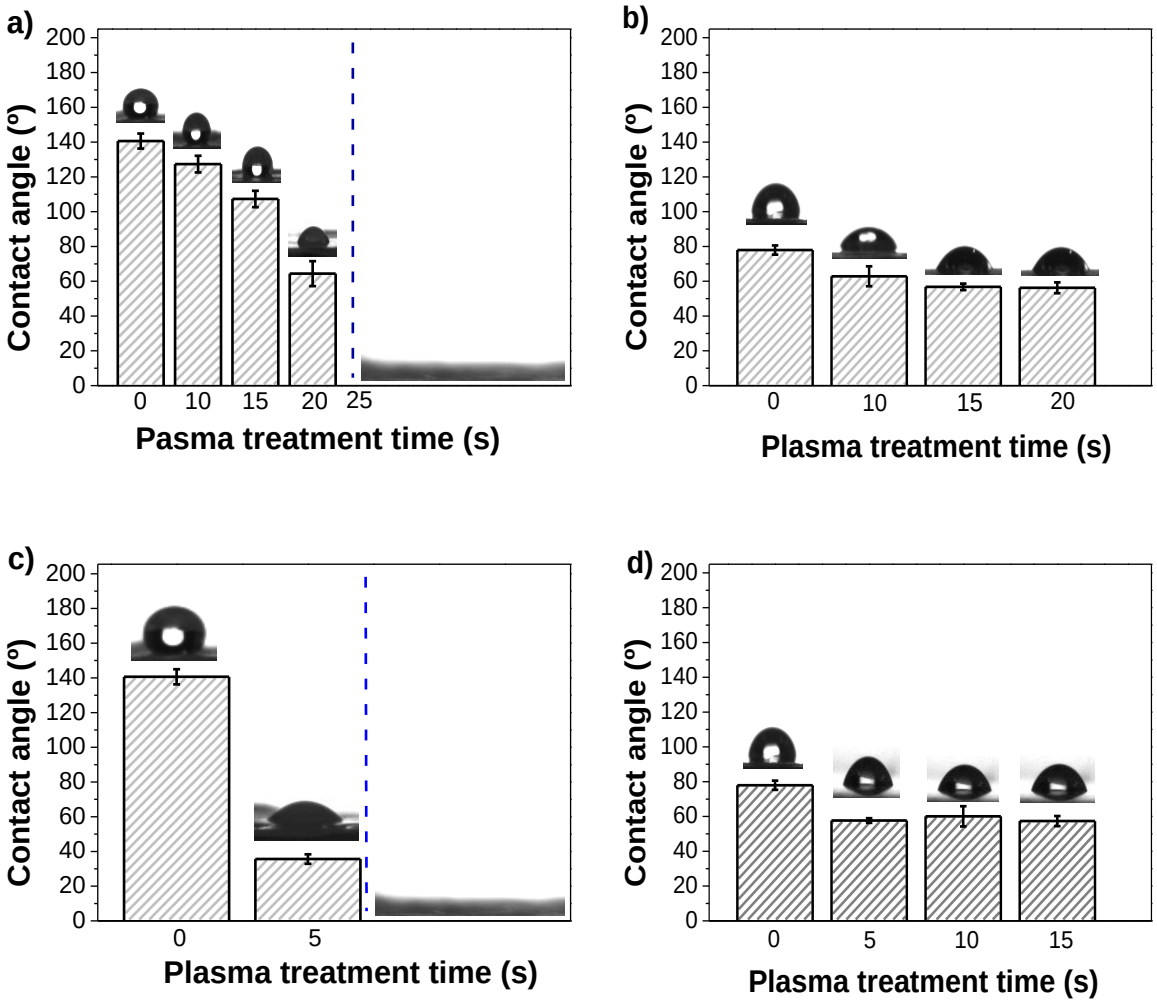

Figure 6.6. Influence of Ar plasma treatment time in the contact angle value for a) PLLA electrospun membranes and b) PLLA films and the influence of O_2 plasma treatment time for c) PLLA electrospun membranes and d) PLLA films at a power of 100 W. The bars in the graph are the standard deviations.

The decrease of the contact angle in the PLLA films after plasma treatment with both plasma treatment gases is not as pronounced as for the electrospun membranes. Figure 6.6b and 6.6d show a decrease from 78 ± 2.6º in untreated PLLA films to approximately 60º for both Ar and O_2 treatments. The fact that hydrophilic electrospun membranes are obtained is thus associated to the variation of the contact angle of the polymer itself, as shown by the variations in the films, and the capillarity of the electrospun membranes, which accounts for the major part of the effect. Variations in the polymer surface roughness and polymer mat morphology leads to an associated variation of the surface tension of the membrane, leading thus to a penetration of the water drop in the membrane and the consequent hydrophilic behavior [13].

6.3.5. Cell viability studies

For tissue engineering applications, it is important to evaluate whether plasma treatments lead to cytotoxicity of biocompatible PLLA films and electrospun membranes due to the induced surface modifications. The effects of polymer extract medium on the metabolic activity of MC3T3-E1 pre-osteoblast cells was performed using MTT assay after 72 h (Figure 6.7). According the ISO standard 10993-5, the samples are considered cytotoxic when the cell viability reduction is larger than 30 %. So it is possible observed that all the samples are not cytotoxic and thereby the treatment with argon or oxygen allow modifying the wettability of the PLLA samples with no influence on the toxicity of the material.

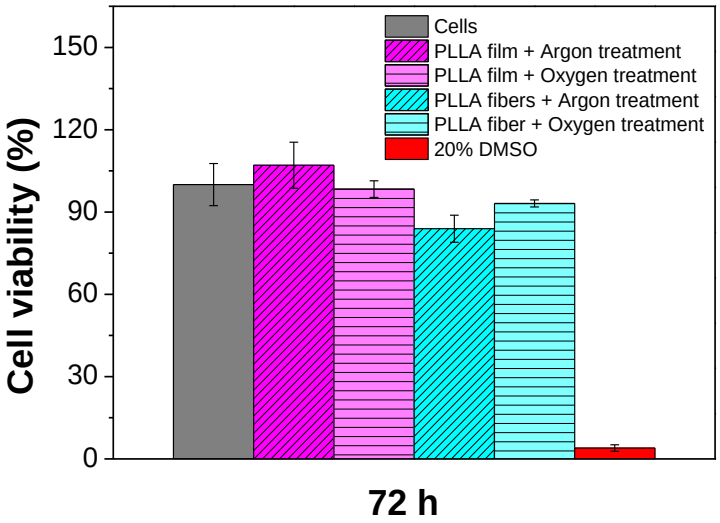

Figure 6.7. Cell viability of MC3T3-E1 pre-osteoblast cells in contact with as-prepared extraction media exposed with the different PLLA samples up to 72 h.

6.4. Conclusions

The influence of Ar and O_2 plasma treatments in PLLA films and electrospun membranes on their morphology, physical-chemical properties and wettability was determined.

A similar fiber mesh and average size was obtained for membranes treated under Ar plasma while an increase in average fiber diameter is observed after O_2 plasma treatment, mainly due to fiber joining. Associated to this effect, there is an increase in surface roughness, as observed in PLLA films surface after Ar and O_2 plasma treatments. On the other hand, no relevant variations are observed in the degree of crystallinity and polymer bond characteristics after the plasma treatments. Both electrospun membranes and films being nearly amorphous. The contact angle of the samples is dependent on the plasma treatment conditions (used gas, time and power)) and it is possible to modify hydrophobic electrospun fiber mats into superhydrophilic ones. This effect is obtained in the fibers mainly due to variations of the surface tension as plasma treatment in the films results in roughness variations. The formation of free radicals and to an increase of the polar groups in the PLLA surface, leading to lower variations of the surface water contact angle. Independently of the plasma treatment, the

obtained samples are not cytotoxic. Therefore, a way is shown to obtain superhydrophilic membranes suitable for biomedical applications.

6.5. References

1. Rana, D., et al., *Chapter 10 - Considerations on Designing Scaffold for Tissue Engineering*, in *Stem Cell Biology and Tissue Engineering in Dental Sciences*, A.V.S.S. Ramalingam, Editor. 2015, Academic Press: Boston. p. 133-148.
2. Ribeiro, C., et al., *Surface roughness dependent osteoblast and fibroblast response on poly(l-lactide) films and electrospun membranes.* Journal of Biomedical Materials Research Part A, 2015. **103**(7): p. 2260-2268.
3. Chen, J.-P. and C.-H. Su, *Surface modification of electrospun PLLA nanofibers by plasma treatment and cationized gelatin immobilization for cartilage tissue engineering.* Acta Biomaterialia, 2011. **7**(1): p. 234-243.
4. Ribeiro, C., et al., *Tailoring the morphology and crystallinity of poly(L-lactide acid) electrospun membranes.* Science and Technology of Advanced Materials, 2011. **12**(1): p. 015001.
5. Areias, A.C., et al., *Influence of crystallinity and fiber orientation on hydrophobicity and biological response of poly(l-lactide) electrospun mats.* Soft Matter, 2012. **8**(21): p. 5818-5825.
6. Fukada, E., *History and recent progress in piezoelectric polymers.* Ieee Transactions on Ultrasonics Ferroelectrics and Frequency Control, 2000. **47**(6): p. 1277-1290.
7. Ribeiro, C., et al., *Piezoelectric polymers as biomaterials for tissue engineering applications.* Colloids and Surfaces B: Biointerfaces, 2015. **136**: p. 46-55.
8. Ribeiro, C., et al., *Dynamic piezoelectric stimulation enhances osteogenic differentiation of human adipose stem cells.* Journal of Biomedical Materials Research Part A, 2015. **103**(6): p. 2172-2175.
9. Ribeiro, C., et al., *Surface roughness dependent osteoblast and fibroblast response on poly(L-lactide) films and electrospun membranes.* Journal of Biomedical Materials Research - Part A, 2015. **103**(7): p. 2260-2268.
10. Teo, W.E. and S. Ramakrishna, *A review on electrospinning design and nanofibre assemblies.* Nanotechnology, 2006. **17**(14): p. R89.
11. Yang, J., et al., *Enhancing the cell affinity of macroporous poly(L-lactide) cell scaffold by a convenient surface modification method.* Polymer International, 2003. **52**(12): p. 1892-1899.
12. Yoshida, S., et al., *Surface modification of polymers by plasma treatments for the enhancement of biocompatibility and controlled drug release.* Surface & Coatings Technology, 2013. **233**: p. 99-107.
13. Correia, D.M., et al., *Influence of oxygen plasma treatment parameters on poly(vinylidene fluoride) electrospun fiber mats wettability.* Progress in Organic Coatings, 2015. **85**: p. 151-158.
14. Khorasani, M.T., H. Mirzadeh, and S. Irani, *Plasma surface modification of poly (l-lactic acid) and poly (lactic-co-glycolic acid) films for improvement of nerve cells adhesion.* Radiation Physics and Chemistry, 2008. **77**(3): p. 280-287.

15. Slepičková Kasálková, N., et al., *Biocompatibility of plasma nanostructured biopolymers.* Nuclear Instruments and Methods in Physics Research Section B: Beam Interactions with Materials and Atoms, 2013. **307**: p. 642-646.

16. Cheng, Q., et al., *Plasma Surface Chemical Treatment of Electrospun Poly(l-Lactide) Microfibrous Scaffolds for Enhanced Cell Adhesion, Growth, and Infiltration.* Tissue Engineering. Part A, 2013. **19**(9-10): p. 1188-1198.

17. Ferreira, B.M.P., et al., *Plasma surface treatments of poly(l-lactic acid) (PLLA) and poly(hydroxybutyrate-co-hydroxyvalerate) (PHBV).* Materials Science and Engineering: C, 2009. **29**(3): p. 806-813.

18. Fischer, D., et al., *In vitro cytotoxicity testing of polycations: Influence of polymer structure on cell viability and hemolysis.* Biomaterials, 2003. **24**(7): p. 1121-1131.

19. Jordá-Vilaplana, A., et al., *Surface modification of polylactic acid (PLA) by air atmospheric plasma treatment.* European Polymer Journal, 2014. **58**: p. 23-33.

20. Chu, P.K., et al., *Plasma-surface modification of biomaterials.* Materials Science and Engineering: R: Reports, 2002. **36**(5–6): p. 143-206.

21. Avérous, L., *Chapter 21 - Polylactic Acid: Synthesis, Properties and Applications,* in *Monomers, Polymers and Composites from Renewable Resources,* M.N.B. Gandini, Editor. 2008, Elsevier: Amsterdam. p. 433-450.

22. Garlotta, D., *A Literature Review of Poly(Lactic Acid).* Journal of Polymers and the Environment, 2001. **9**(2): p. 63-84.

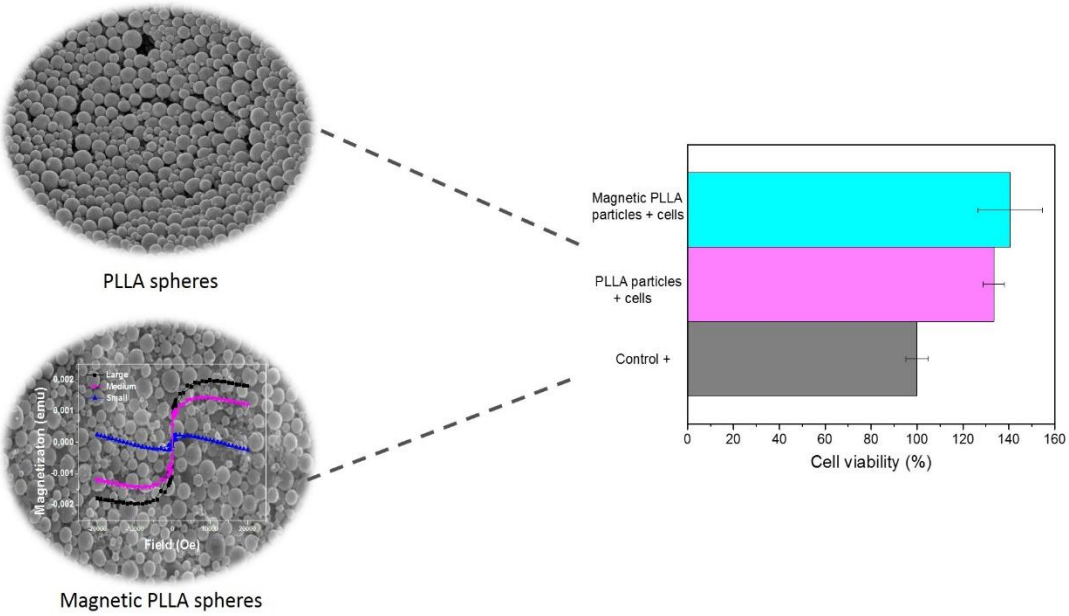

7. Poly(L-lactic acid) and - poly(L-lactic acid)/$CoFe_2O_4$ composite microspheres obtained by oil in water emulsion for biomedical applications

This chapter describes the production of biodegradable neat PLLA and magnetic PLLA microspheres by an oil in water emulsion method using PVA solution as emulsifier agent. The separation of the microspheres in different size ranges by centrifugation is presented and the stability of the neat and magnetic PLLA microspheres at different pH's evaluated. The study of the influence of production method in the physico-chemical properties of the PLLA microspheres was also performed, together with the evaluation of the suitability of the microspheres for tissue engineering applications.

D.M. Correia, V. Sencadas, C. Ribeiro, P.M. Martins, P. Martins, F. M. Gama, G. Botelho, S. Lanceros-Méndez. *Poly(L-lactic acid) and - poly(L-lactic acid)/COF_2O_4 composite microspheres obtained by oil in water emulsion for biomedical applications*. Submitted. 2015.

7.1. Introduction

As reported in chapter 3, piezoelectric polymers can be used as a bioactive electromechanically responsive materials for improving tissue engineering strategies [1]. Studies reveal that electrical stimulation influences cell proliferation, differentiation and regeneration [2] both under static [3, 4] and dynamic conditions [5]. These results show the potential of such materials for the development of a new generation of wireless electrically active scaffolds and structures for biomedical applications [2]. Magnetic nanoparticles and, in particular magnetostrictive ones, offer also strong application potential in the biomedical field, including drug delivery and biomolecular targeting, among others, triggered by external magnetic field. [6]. When combined with the piezoelectric effect it offers the possibility of developing magnetoelectric composites [7] that convert magnetic stimuli into electrical ones, leading to novel tissue engineering strategies [8, 9].

PLLA is a piezoelectric polymer and is electroactive properties were successfully explored for technological applications, being the β- form is the mainly responsible for the piezoelectric properties [10, 11].

PLLA microspheres can be produced by several methods based on different physicochemical methods, including solvent extraction/evaporation from an emulsion, aggregation by pH adjustment or heat, coacervation (phase separation), interfacial polymerization, ionic gelation, electrospray and spray drying, among other techniques [2, 12]. Emulsion-solvent evaporation method is among the most commonly used methods for the production of PLLA microspheres [13]. In this process, a solution containing the polymer is emulsified in a non-solvent phase (continuous phase), in the presence of an stabilizing agent, using a variety of physical methods such as homogenization and sonication [14]. PLLA microspheres of relatively small size and uniform size distribution can be obtained from an aqueous continuous phase containing PVA as stabilizer [14, 15].

PLLA neat microspheres or in the form of polymer blends or composites find applicability in the treatment of ocular pathologies, namely in regenerative medicine for retinal repair or other intraocular pathologies [12] and drug delivery [6, 16, 17].

Despite these interesting proofs of concept, there is a lack of systematic study reporting the effect of the processing parameters in the overall microparticles physico-chemical properties as well as on the encapsulation efficiency, magnetic properties and

biocompatibility of composite spheres with magnetic nanoparticles. In particular, the introduction of highly magnetostrictive nanoparticles, such as $CoFe_2O_4$, has not been reported. Thus, this work, reports on an effective method for the preparation of pristine and magnetic PLLA microspheres based on $CoFe_2O_4$ nanoparticles. Further, size and physico-chemical properties of the particles were evaluated as well as their suitability for biomedical applications.

7.2. Experimental

7.2.1. Materials

PLLA with an average molecular weight of 217.000 – 225.000 $g.mol^{-1}$, (Purasorb PL18) and poly(vinyl alcohol) (PVA) with an average molecular weight of 13.000 – 23.000, 98 % hydrolyzed were supplied by Purac and Sigma Aldrich. CF, from M*erck*, was used for the dissolution of the polymer. $CoFe_2O_4$ nanoparticles were purchased from Nanoamor with dimensions between 35 and 55 nm, and used as received.

7.2.2. Preparation of neat and magnetic PLLA microspheres

PLLA was dissolved in chloroform to achieve a polymer concentration of 3 % (w/v).
CF was used due to its ability to solubilize large amounts of polymer [18], and low miscibility with water, leading to a decrease of the amount of PVA adsorbed to the polymer-organic solvent–water interface [15].
The polymer solution was dissolved at 60 ºC under constant stirring until complete polymer dissolution. Then, the mixture was added into the emulsion of 0.5 % (w/v) PVA solution. Polymer and surfactant concentrations were selected based on previous works [19]. The emulsified suspension was mechanically stirred and the solvent was continuously evaporated overnight at room temperature. The resulting microspheres were washed with distillated water and isolated by different centrifugations at 1000, 2500 and 4000 rcf's during 5, 10 and 15 min, respectively. This procedure was repeated 5 times. Finally, polymer microspheres were freeze dried in a vacuum freeze-drying machine (Christ Alpha 2-4 LD Plus from BioBlock Scientific) for 48 h. Magnetic microspheres were also prepared by the aforementioned method. After completely

polymer dissolution 10 % (w/w) of $CoFe_2O_4$ nanoparticles were added to polymer solution. The next steps were the same used for neat microspheres preparation.

7.2.3. Characterization of the PLLA microspheres

The morphology of the microspheres was analyzed using SEM as described in experimental section of chapter 2. Spheres average diameter and distribution was calculated over approximately 60 micropheres using SEM images with 50000 X magnification and the ImageJ software.

FTIR-ATR and DSC analysis were performed as described in the experimental section of chapter 2. The degree of crystallinity of the PLLA microspheres was calculated by equation 7.1:

$$\Delta X_c = \frac{\Delta H_m - \Delta H_{cc}}{\Delta H^O{}_m} \quad (7.1)$$

where ΔH_m is the melting enthalpy, ΔH_{cc} the enthalpy of cold crystallization and $\Delta H^O{}_m$ represents the PLLA theoretical value of the melting enthalpy of a fully crystalline sample (93.1 $J.g^{-1}$) [20].

Dynamic light scattering (DLS) was used to obtain the average hydrodynamic size and size distribution of the microspheres. A Zetasizer NANO ZS-ZEN3600 (Malvern) was used and measurements were performed at 25 °C using the appropriated sample dilution in ultrapure water to prevent multi scattering events. The average and standard deviation value for each sample was obtained from 6 measurements.

Zeta potential was used to obtain the surface charge of the microspheres with a Zetasizer NANO ZS-ZEN3600. The zeta potential of the PLLA microparticles was evaluated at different pHs (2, 4, 7 and 9). Solutions of HCl (1 M) and NaOH (1M) were added to adjust the pH. The average value and standard deviation for each sample was obtained from 6 measurements.

According to Smoluchowski equation the zeta potential was determined from Equation 7.2 [21]:

$$\zeta = \frac{\Delta E}{\Delta P}\frac{\eta k}{\varepsilon\varepsilon_0} \quad (7.2)$$

where ζ is the zeta potential, ΔE and ΔP are the streaming potential and the applied pressure, respectively, η is the viscosity of the solution, k the conductivity of the solution, ε and ε_0 are the permittivity of the test solution and free space (8.85×10^{-12} $F.m^{-1}$), respectively.

The magnetic behavior of PLLA-$CoFe_2O_4$ microspheres was evaluated by a vibrating sample magnetometer (VSM) method the difference in the magnetic response obtained with and without the application of a 220 Oe DC magnetic field. The magnetic $CoFe_2O_4$ filler content within the microspheres was determined by Equation 7.3 [22]:

$$CoFe_2O_4\ wt.\%_{microspheres} = \frac{Saturation\ magnetization\ _{microspheres}}{60\ (\text{pure powder saturation magnetization})} \times 100 \quad (7.3)$$

7.2.4. Cell culture

MC3T3-E1 cells (Riken cell bank, Japan) were cultivated in DMEM (*Gibco*) 1 $g.L^{-1}$ glucose containing 10 % FBS (*Biochrom*) and 1 % P/S (*Biochrom*) at 37 ºC in a 5 % CO_2 incubator.

For cell culture assays, approximately 3 mg of dry PLLA microspheres (with and without magnetic nanoparticles) were placed in a 2 mL Eppendorf. For sterilization purposes, the microspheres were exposed to ultraviolet (UV) light for 1 h and washed 5 times with PBS solution for 5 min. After that, the microspheres were placed with DMEM without FBS overnight at 37 ºC in a 5 % CO_2 incubator.

For the cell viability assay, MC3T3-E1 pre-osteoblast cells were seeded at a density of 1.5×10^5 cells/Eppendorf with and without microspheres up to 72 h. In the Eppendorf with microspheres, the cells were mixed with the microspheres. Cell pellets without any microspheres were used as reference (control +) and only microspheres were used as negative control. To quantify the number of viable cell, 3-(4,5-dimethylthiazol-2-yl)-5-(3-carboxymethoxyphenyl)-2-(4-sulfophenyl)-2H-tetrazolium (MTS, CellTiter 96-

Aqueous one solution reagent, Promega) colorimetric method was used. In this assay, MTS is bioreduced by cells into a formazan product by dehydrogenase enzymes found in metabolically active cells. The absorbance of the formazan product measured at 490 nm is directly proportional to the viable cell number in cell culture. After 72 h, the supernatant of each Eppendorf was removed and fresh medium containing MTS solution in a 1:5 ratio was added and incubated at 37 ºC in a 5 % CO_2 incubator. After 2 h of incubation, 100 µL of each Eppendorf was transferred in triplicate to a 96-well plate and the optical density was measured at 490 nm. Four measurements were performed for each sample. The cell viability was determined by Equation 3.1.

7.3. Results and discussion

7.3.1. Polymer morphology and size distribution

Neat PLLA and magnetic microspheres were produced by water-in-oil emulsion (w/o) using a PVA solution as a stabilizer agent during the emulsification process in order to prevent the coalescence of the microspheres.

Pristine polymer microspheres show a smooth spherical surface, with a homogeneous shape, without concavities or distortions (Figure 7.1a), with a size distribution ranging between 0.050 and 0.40 nm with an average size of 0.16 ± 0.062 µm (Figure 7.1b), suggesting that the polymer solution was evenly dispersed in the aqueous phase, without precipitation of the solids [18, 19]. Higher solution viscosities than the ones use this work (see experimental section) creates difficulties in achieving small oil droplets homogeneously dispersed in the aqueous phase, leading to bigger microspheres [19, 23].

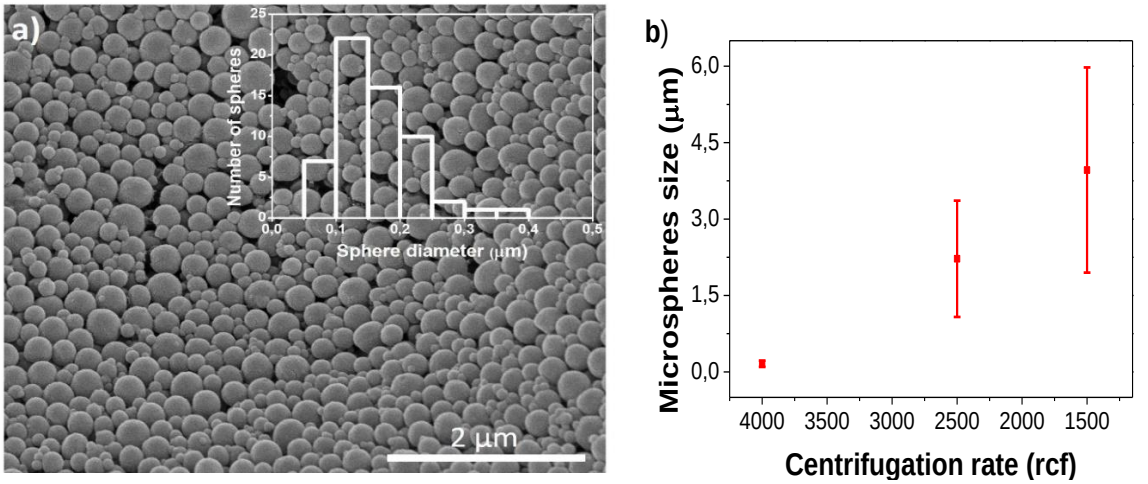

Figure 7.1. a) Morphology of PLLA microspheres centrifuged at 4000 rcf's and b) sphere size distribution after different centrifugation rates, obtained through measurement with ImageJ software.

Centrifugation of the microspheres at different centrifugation rates allows spheres separation by size (Figure 7.1b).Thus, microspheres with average size ranging from 0.16 ± 0.062 μm down to 3.9 ± 2.0 μm were obtained after centrifugation rates from 1500 to 4000 rcf.

Dynamic light scattering allows the measurement of microspheres hydrodynamic size and distribution. The behavior of PLLA in ultra-pure water was studied where the intensity of scattered light depends mainly on the number of particles and their dimensions. The values obtained by DSL where the microspheres size ranging from 1.9 ± 0.039 μm down to 0.46 ± 0.013 μm (Figure 7.2) are different from the ones measured after SEM imaging (Figure 7.1), which is ascribed to factors affecting the hydrodynamic measurements such as the agglomeration of the particles [24]. For agglomerated microspheres the diffusion rate is smaller than for isolated ones, leading to higher size values than the size assessed by SEM [24].

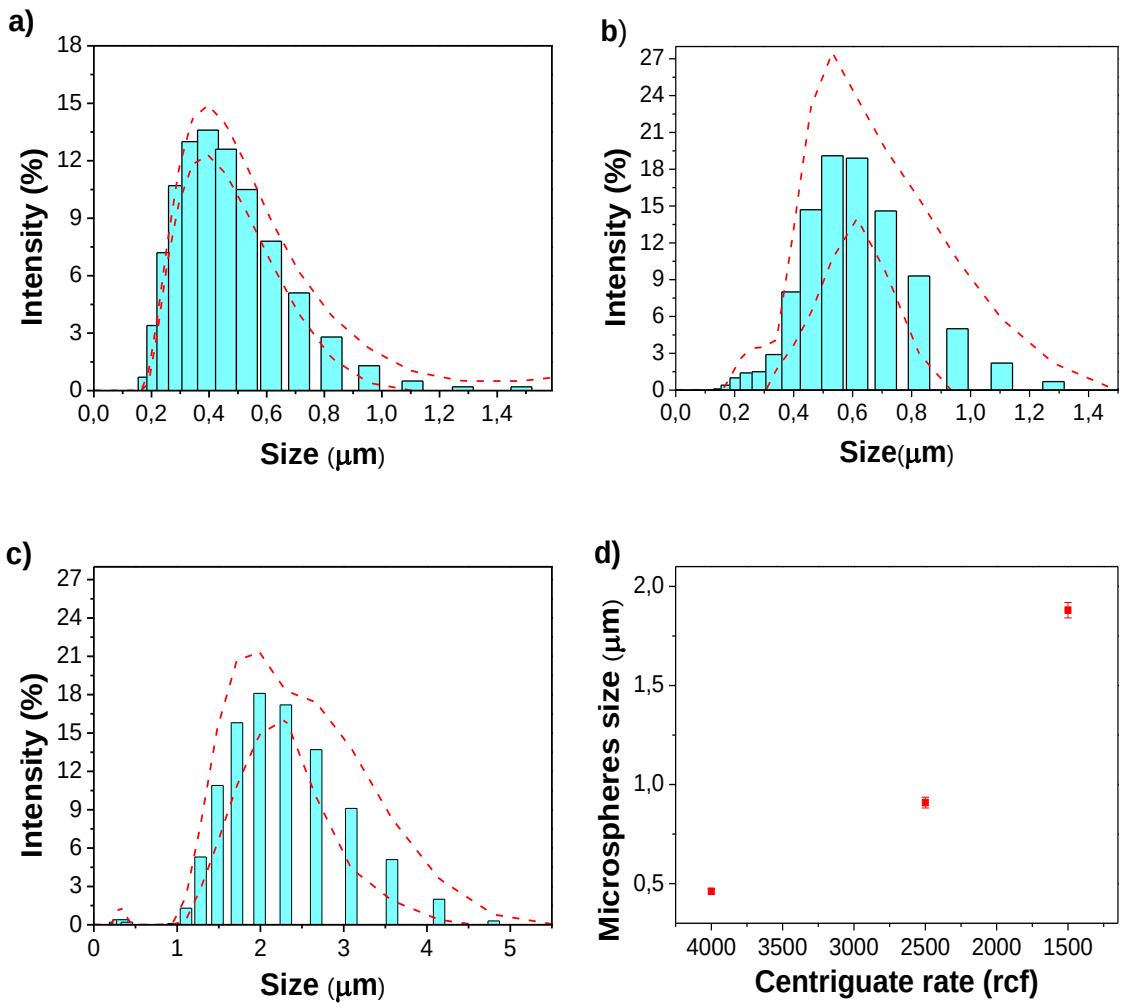

Figure 7.2. PLLA Particle size distribution obtained by DLS for different speed rotations: a) 4000 rcf's b) 2500 rcf´s, c) 1500 rcf's; and d) sphere size distribution at the different centrifugation rates.

With respect to the CoF_2O_4/PLLA microspheres (Figure 7.3), also smooth spherical microspheres were obtained, similar to the ones for pristine PLLA (Figure 7.1). Again, centrifugation allows to separate the particles by size, from 2.2 ± 0.60 μm for the lowest centrifugation rate to 0.87 ± 0.35 μm for the highest rate (Figure 7.3d). It is thus observed that the composite microspheres remain in the same size order as the pristine ones, being nevertheless the average size larger for each centrifugation rate. Finally, it was not possible to obtain the hydrodynamic size due to higher aggregation and sedimentation of the heavier particles during the measurements.

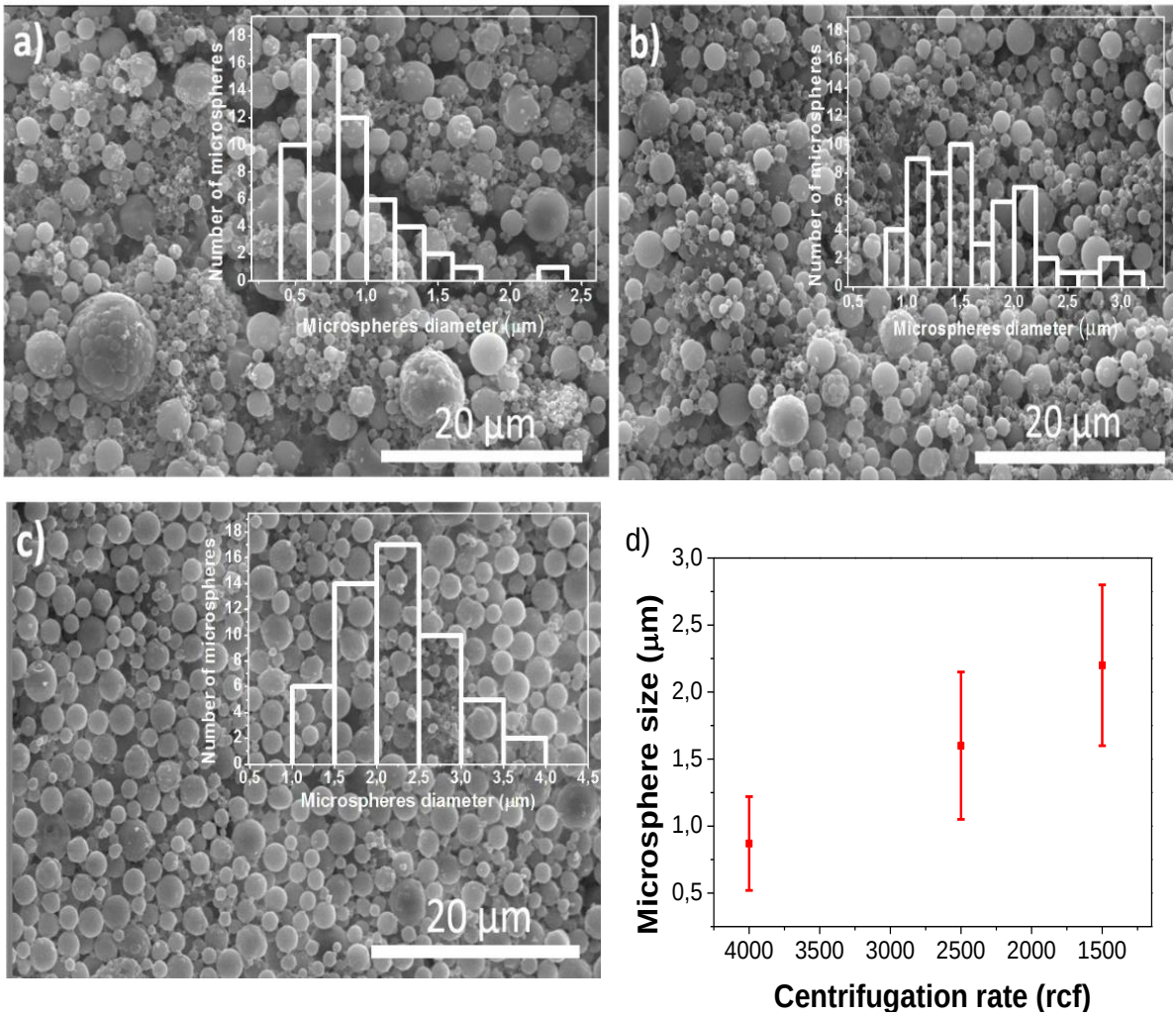

Figure 7.3. Morphology of the PLLA magnetic microspheres obtained under different centrifugation rates: a) 4000 rcf's, b) 2500 rcf´s and c) 1500 rcf's. The size distributions (insets) were obtained with the ImageJ software. d) Particle size distribution for the different centrifugation rates.

7.3.2. Physico-chemical and thermal properties

In order to evaluate possible chemical modifications of the PLLA structure due to the production method of the neat and magnetic PLLA microspheres a FTIR-ATR analysis was performed. Figure 7.4a shows the FTIR spectra of the neat and composite PLLA microspheres. Table 7.1 shows the main absorption bands present in the microspheres spectrum. The absorption bands in the region of 830-960 cm^{-1} for neat and magnetic microspheres are assigned to polymer backbone stretching and CH_3 rocking [25]. The

absorption band at 871 cm^{-1} is ascribed to CH_3 rocking of the amorphous crystalline α-phase. The presence of the absorption bands at 921 cm^{-1}, 955 and 1510 cm^{-1} assigned as the coupling of the C-C backbone stretching with the CH_3 rocking mode, indicating that neat PLLA microspheres crystallize into the α-form [20]. The absence of the absorption bands at 920 and 1510 cm^{-1} in magnetic PLLA microspheres indicate that the microspheres are probably in the amorphous state, as it will be confirmed later by DSC. The vibrational assignments in the region between 1000 and 1500 cm^{-1} are CH, CH_3 and C-O-C stretching bands characteristics of the α and α' forms [25]. The band at ~1451 cm^{-1} is assigned to the asymmetric deformation mode of CH_3. The region of 1300-1000 cm^{-1}, is mainly related to the C-O-C stretching vibrations and to C-O-C asymmetric vibrations linked with asymmetric CH_3 rocking vibrations [25].

Table 7.1. Characteristic FTIR absorption bands and assignments for neat and magnetic PLLA microspheres.

Wavenumber (cm^{-1})	**Absorption bands**
871	CH_3 rocking
921	Coupling of the C-C backbone stretching with the
955	CH_3 rocking mode
1080	stretching vibration of the methyl group (C-H)
1180	C-O-C asymmetric vibrations linked with
1200	asymmetric CH_3 rocking vibrations
1210	
1450	Stretching vibration of the methyl group (C-H)
1750	Stretching vibration of ester carbonyl (C=O).

Finally, the strong band at 1750 cm^{-1} identifies the stretching vibration of ester carbonyl (C=O). At 1080 cm^{-1} and the weak band at 1450 cm^{-1} corresponds to the stretching vibration of the methyl group (C-H) [26]. Neither modes are totally suppressed, nor do new modes seem to appear in neat and magnetic microspheres due to the emulsification process. Furthermore, no PVA residues were noticed in the microspheres FTIR spectra.

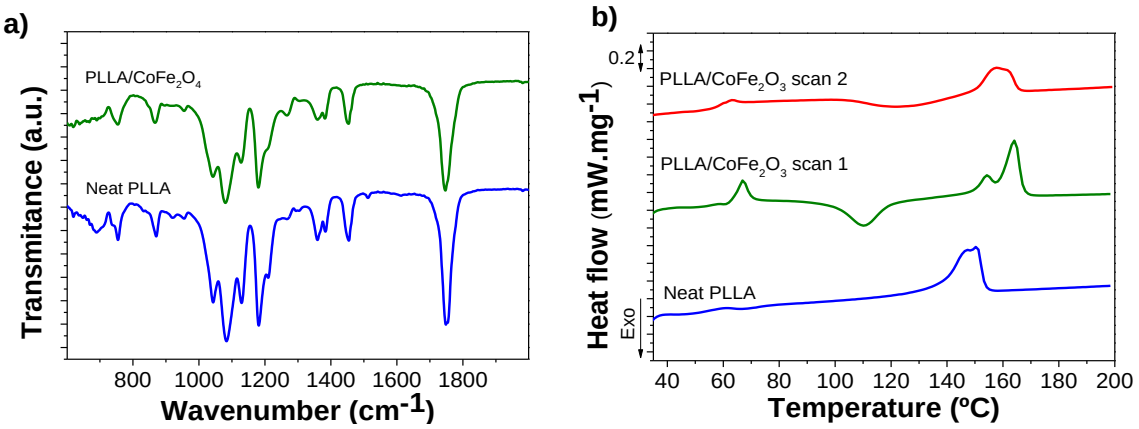

Figure 7.4. a) FTIR spectra b) DSC scans obtained for PLLA microspheres.

Solvent evaporation during the emulsification process of PLLA droplets can affect the degree of crystallinity of the polymer, together with other characteristics such as surface morphology and porosity [27]. Pristine PLLA microspheres showed a glass transition around 55 ºC and a melting transition that starts at ~120 ºC and ends at ~160 ºC with maximum at 152 ºC, with absence of a cold-crystallization process. With respect to the composite spheres, a shift towards higher temperatures was observed for the Tg and melting transition, suggesting that the presence of magnetic nanoparticles hinders polymer chains packing. Further, a cold crystallization process starting at ~80 ºC up to ~130 ºC, with maximum at ~110 ºC was observed after the glass transition process as the temperature increased. The presence of a shoulder during melting of the polymer for nanocomposite microspheres is also observed, which can be attributed to the different crystal sizes present in the samples: ones formed during the processing of the nanocomposite polymer particles, made from fragmented crystals, at lower temperature, and the higher temperature one due to the cold-recrystallization process that takes place during the heating scan itself. The fact that cold crystallization appears only 30 ºC above the glass transition indicates that a large number of crystal nuclei had already formed in the glass [28]. A second heating scan was recorded after cooling the sample from 200 ºC to room temperature. Interestingly, after this process, the sample showed a single broad endothermic peak melting temperature, suggesting that the double melting peak is due to the presence of small nuclei in the polymer that starts to reorganize and crystallize at temperatures above Tg during heating (Figure 7.4b).

The degree of crystallinity of neat and magnetic microspheres was calculated applying Equation 7.1 and a value of 40 % and 17 % was obtained for pristine and magnetic

nanocomposite particles: the difference in the degree of crystallinity is attributed to the interfacial electrostatic interaction between magnetic nanoparticles and the polymer chains [29] from the PLLA matrix which hindered the chains packing and consequently a decrease of polymer crystallinity.

Zeta (ζ) potential was used to characterize the surface of the PLLA microspheres at different pHs environments. This method is also an important factor for determining the stability of PLLA and nanocomposite microspheres against aggregation, when dispersed in a liquid such as the cell culture media [30]. Generally, the stability of the microspheres in suspension is improved with increasing of the absolute value of zeta potential [31]. Polymer surface microspheres are negatively charged and the surface charge increases with increasing pH (Figure 7.5). The negative charge of the microspheres is attributed to the presence of ionized carboxyl groups from lactic acid on particles surface [16], leading the particles to be quite stable in alkaline environments, while for more acidic environments ($pH \leq 4$) the spheres aggregate, forming clusters (Figure 7.5). It was observed that for a pH higher than 5 with a zeta potential of approximately -30 mV, the stability of the PLLA spheres increases and a stable colloidal dispersion is obtained. This fact can be explained due to the higher repulsion of the PLLA spheres hindering microspheres aggregation. At pH 7.4, the PLLA microspheres show a larger zeta potential and high negative values (-53 mV) are obtained. It is to notice that similar results were obtained for PLA and for PLGA nanospheres in neutral buffer [15], with zeta potential of -50 and -45 mV, respectively. The results also indicate that the PLLA microspheres produced by the oil in water method exhibit sensitivity to pH changes. This can be relevant for drug delivery applications with focus on the design and development of carriers for therapeutic and/or diagnostic purpose, in which is relevant that microspheres exhibit significant sensitivity to environmental variations including pH, among others [30]. For *in vivo* applications and drug attachment it is essential to monitor the colloidal stability of the microspheres as it leads to a better circulation time in blood stream and sustenance in biological fluids [30]. The high zeta potential values obtained also indicate that the oil in water method does not result in a high adsorption of PVA in the surface of the microspheres. With respect to the composite microspheres, they show lower zeta potential absolute values comparatively to neat PLLA microspheres, which can be in part attributed to the weight difference between nanocomposite particles and pristine polymer, that leads to the formation of clusters and consequently higher sedimentation rates, but also to the

strong surface interaction of the magnetic nanoparticles with the polymer layer which also leads to variations in the degree of crystallinity.

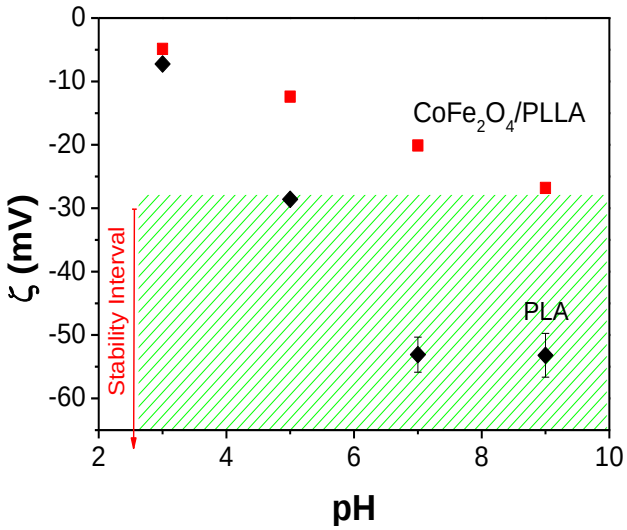

Figure 7.5. Zeta potential results at different pH for neat PLLA microspheres and magnetic PLLA microspheres.

7.3.3. Magnetic properties of the magnetic nanocomposite microspheres

Magnetic properties of the magnetic composite microspheres are critical for biomedical applications [32]. The magnetization curves of magnetic microspheres determined by VSM technique at room temperature are shown in Figure 7.6. Results show that the magnetization of the magnetic microspheres increase with increasing magnetic field until gradually reaches saturation. Large magnetic microspheres may have a bigger magnetic core compared to smaller particles and consequently, the saturated magnetization is higher (Figure 7.6). After the maximum magnetization value, the magnetization decreases due to diamagnetic PLLA [17]. The shape and magnetization maximum values of the measured hysteresis loops demonstrate that magnetic nanoparticles are randomly oriented within the polymer sphere matrix.

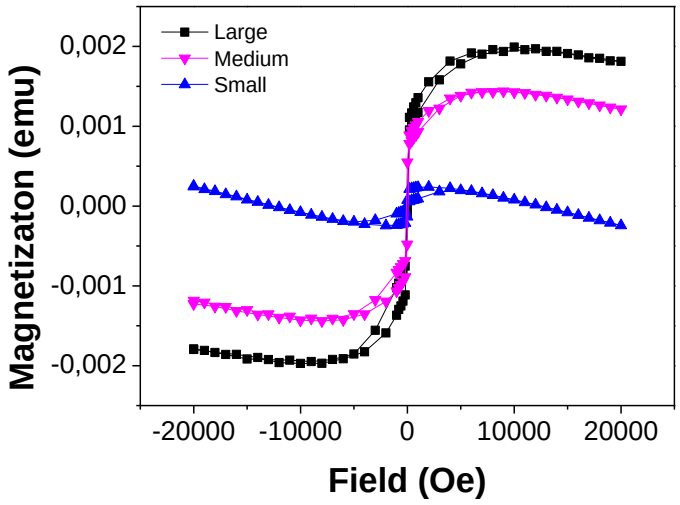

Figure 7.6. Magnetization curves of the magnetic PLLA microspheres.

Additionally from the hysteresis curves of Figure 7.5 and the saturation magnetization value of the pure $CoFe_2O_4$ nanoparticles [22] it is possible to estimate, trough Equation 7.3, the amount of $CoFe_2O_4$ nanoparticles within the microspheres (Table 7.2).

Table 7.2. Size, % (w/w) and magnetization of PLLA microspheres.

Microspheres size (µm)	**$CoFe_2O_4$ (% w/w) in the solution**	**$CoFe_2O_4$ + PLLA wt. (g)**	**Spheres saturation magnetization (measured) (emu)**	**$CoFe_2O_4$ weight in microspheres (g)**	**$CoFe_2O_4$ (% w/w) in microspheres**
Small (0.87±0.35)	10	1.0×10^{-4}	2.40×10^{-4}	4.0×10^{-6}	4.0
Medium (1.6 ±0.6)		6.0×10^{-4}	1.43×10^{-3}	2.38×10^{-5}	4.0
Large (2.2±0.6)		8.0×10^{-4}	1.99×10^{-3}	3.32×10^{-5}	4.1

In this way, the concentrations of $CoFe_2O_4$ nanoparticles in the spheres is lower than the ones on the composite solutions, in agreement to previous studies [22, 33], the loading efficiency being ~40 %. One possible explanation for this effect is the higher density of the $CoFe_2O_4$ nanoparticles when compared to the polymer matrix that might cause some sedimentation of nanoparticles in the solution during the microsphere formation. Further, it is to notice that the filler weight content within the microspheres is the same, independently of the sphere size, indicating a homogeneous distribution of the nanoparticles in the solution.

7.3.4. Cell culture

The viability of MC3T3-E1 pre-osteoblast cells seeded in an Eppendorf with and without PLLA microspheres was performed by MTS assay and the results are shown in Figure 7.7. It is observed observe that the cell agglomerates are viable for all the conditions. At 72 h, it was verified the formation of a cell/microspheres pellet in the bottom of the Eppendorf (data not shown) as verified in a previous study [2] with PVDF microparticles.

Comparing PLLA microspheres/cells pellet with the cell pellet it is verified a higher number of cells after 72 h of cell culture. These preliminary results show that PLLA microspheres with and without magnetic nanoparticles can provide a suitable environment for cell adhesion and growth.

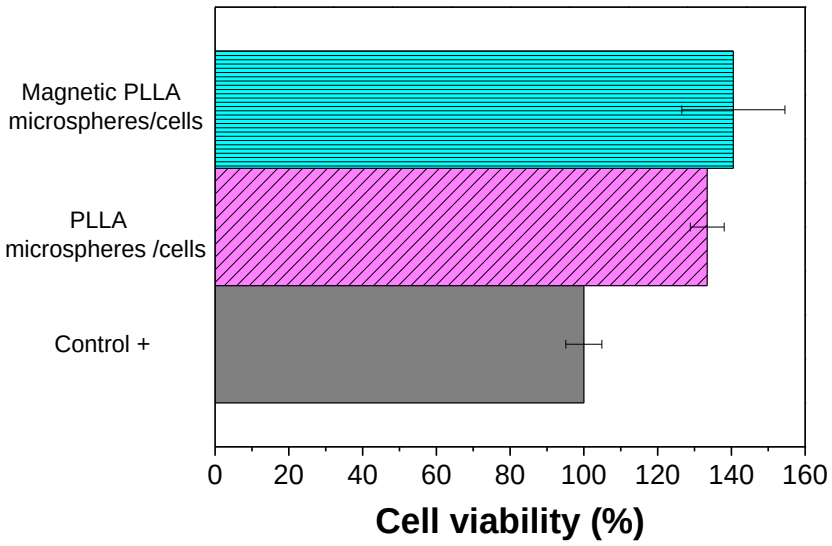

Figure 7.7. MTS results from proliferation assay of PLLA microspheres (with and without magnetic nanoparticles)/cells and cells pellets (control +). Results are expressed as mean ± standard deviation with n = 4.

7.4. Conclusions

Neat and magnetic $CoFe_2O_4$ composite PLLA microspheres were prepared by emulsion method using chloroform as solvent and a PVA solution as a stabilizer agent. The processing method allowed to obtain spherical PLLA microspheres with diameters

ranging between 0.16 to 3.9 μm for neat PLLA and between 0.8-2.2 μm for composite microspheres. The neat and magnetic microspheres are quite stable in alkaline environments. However, for more acidic environments (pH ≤ 4), the neat PLLA microspheres aggregate, forming clusters.

No changes occur in the chemical structure of PLLA during the microspheres formation and no PVA residues were observed. Both neat and magnetic PLLA present a glass transition temperature around 55 ºC, with double melting peaks. The degree of crystallinity of neat PLLA microspheres is 40 % after processing and the incorporation of the $CoFe_2O_4$ nanoparticles into the PLLA sample leads to obtain amorphous magnetic microspheres. The encapsulation efficiency of the magnetic nanoparticles is 40 %, independently of the particle size.

Cell viability studies performed with MC3T3-E1 pre-osteoblast cells showed good cell proliferation, which demonstrates the proper encapsulation of the cobalt ferrite nanoparticles and the suitability of the microspheres for biomedical applications.

7.5. References

1. Martins, P., A.C. Lopes, and S. Lanceros-Mendez, *Electroactive phases of poly(vinylidene fluoride): Determination, processing and applications.* Progress in Polymer Science, 2014. **39**(4): p. 683-706.

2. Correia, D.M., et al., *Electrosprayed poly(vinylidene fluoride) microparticles for tissue engineering applications.* Rsc Advances, 2014. **4**(62): p. 33013-33021.

3. Dias, J.C., et al., *Influence of fiber diameter and crystallinity on the stability of electrospun poly(l-lactic acid) membranes to hydrolytic degradation.* Polymer Testing, 2012. **31**(6): p. 770-776.

4. Pärssinen, J., et al., *Enhancement of adhesion and promotion of osteogenic differentiation of human adipose stem cells by poled electroactive poly(vinylidene fluoride).* Journal of Biomedical Materials Research Part A, 2015. **103**(3): p. 919-928.

5. Ribeiro, C., et al., *Dynamic piezoelectric stimulation enhances osteogenic differentiation of human adipose stem cells.* Journal of Biomedical Materials Research Part A, 2015. **103**(6): p. 2172-2175.

6. Zhang, X., et al., *Effects of surface modification on the properties of magnetic nanoparticles/PLA composite drug carriers and in vitro controlled release study.* Colloids and Surfaces A: Physicochemical and Engineering Aspects, 2013. **431**: p. 80-86.

7. Martins, P. and S. Lanceros-Méndez, *Polymer-based magnetoelectric materials.* Advanced Functional Materials, 2013. **23**(27): p. 3371-3385.

8. Ribeiro, C., et al., *Piezoelectric polymers as biomaterials for tissue engineering applications.* Colloids and Surfaces B: Biointerfaces, 2015. **136**: p. 46-55.

9. Závišová, V., et al., *Synthesis and characterization of polymeric nanospheres loaded with the anticancer drug paclitaxel and magnetic particles.* Journal of Magnetism and Magnetic Materials, 2009. **321**(10): p. 1613-1616.

10. Lee, S.J., A.P. Arun, and K.J. Kim, *Piezoelectric properties of electrospun poly(l-lactic acid) nanofiber web.* Materials Letters, 2015. **148**: p. 58-62.

11. Mitsunobu, Y., et al., *High piezoelectric performance of poly(lactic acid) film manufactured by solid-state extrusion.* Japanese Journal of Applied Physics, 2014. **53**(9S): p. 09PC02.

12. Herrero-Vanrell, R., et al., *The potential of using biodegradable microspheres in retinal diseases and other intraocular pathologies.* Progress in Retinal and Eye Research, 2014. **42**: p. 27-43.

13. Fernandes, J.G., et al., *PHB-PEO electrospun fiber membranes containing chlorhexidine for drug delivery applications.* Polymer Testing, 2014. **34**: p. 64-71.

14. Kim, K. and D. Pack, *Microspheres for Drug Delivery*, in *BioMEMS and Biomedical Nanotechnology*, M. Ferrari, A. Lee, and L.J. Lee, Editors. 2006, Springer US. p. 19-50.

15. Sahoo, S.K., et al., *Residual polyvinyl alcohol associated with poly (d,l-lactide-co-glycolide) nanoparticles affects their physical properties and cellular uptake.* Journal of Controlled Release, 2002. **82**(1): p. 105-114.

16. Ruan, G. and S.-S. Feng, *Preparation and characterization of poly(lactic acid)–poly(ethylene glycol)–poly(lactic acid) (PLA–PEG–PLA) microspheres for controlled release of paclitaxel.* Biomaterials, 2003. **24**(27): p. 5037-5044.

17. Li, F., X. Li, and B. Li, *Preparation of magnetic polylactic acid microspheres and investigation of its releasing property for loading curcumin.* Journal of Magnetism and Magnetic Materials, 2011. **323**(22): p. 2770-2775.

18. Freitas, M.N. and J.M. Marchetti, *Nimesulide PLA microspheres as a potential sustained release system for the treatment of inflammatory diseases.* International Journal of Pharmaceutics, 2005. **295**(1–2): p. 201-211.

19. Francis, L., et al., *Controlled Delivery of Gentamicin Using Poly(3-hydroxybutyrate) Microspheres.* International Journal of Molecular Sciences, 2011. **12**(7): p. 4294-4314.

20. Ribeiro, C., et al., *Tailoring the morphology and crystallinity of poly(L-lactide acid) electrospun membranes.* Science and Technology of Advanced Materials, 2011. **12**(1): p. 015001.

21. Lau, W.J., et al., *Characterization Methods of Thin Film Composite Nanofiltration Membranes.* Separation & Purification Reviews, 2014. **44**(2): p. 135-156.

22. Goncalves, R., et al., *Development of magnetoelectric $CoFe_2O_4$/poly(vinylidene fluoride) microspheres.* RSC Advances, 2015. **5**(45): p. 35852-35857.

23. Freiberg, S. and X.X. Zhu, *Polymer microspheres for controlled drug release.* International Journal of Pharmaceutics, 2004. **282**(1–2): p. 1-18.

24. Gonçalves, R., et al., *Nucleation of the electroactive β-phase, dielectric and magnetic response of poly(vinylidene fluoride) composites with Fe_2O_3 nanoparticles.* Journal of Non-Crystalline Solids, 2013. **361**: p. 93-99.

25. Krikorian, V. and D.J. Pochan, *Crystallization behavior of poly(L-lactic acid) nanocomposites: Nucleation and growth probed by infrared spectroscopy.* Macromolecules, 2005. **38**(15): p. 6520-6527.

26. Furukawa, T., et al., *Structure, Dispersibility, and Crystallinity of Poly(hydroxybutyrate)/Poly(l-lactic acid) Blends Studied by FT-IR Microspectroscopy and Differential Scanning Calorimetry.* Macromolecules, 2005. **38**(15): p. 6445-6454.

27. Chung, T.-W., Y.-Y. Huang, and Y.-Z. Liu, *Effects of the rate of solvent evaporation on the characteristics of drug loaded PLLA and PDLLA microspheres.* International Journal of Pharmaceutics, 2001. **212**(2): p. 161-169.

28. Sencadas, V., et al., *Thermal Properties of Electrospun Poly(Lactic Acid) Membranes.* Journal of Macromolecular Science, Part B, 2011. **51**(3): p. 411-424.

29. Martins, P., et al., *On the origin of the electroactive poly(vinylidene fluoride) β-phase nucleation by ferrite nanoparticles via surface electrostatic interactions.* CrystEngComm, 2012. **14**(8): p. 2807-2811.

30. Moorkoth, D. and K. Nampoothiri, *Synthesis, Colloidal Properties and Cytotoxicity of Biopolymer Nanoparticles.* Applied Biochemistry and Biotechnology, 2014. **174**(6): p. 2181-2194.

31. Wang, W., et al., *Poly(lactic acid)/chitosan hybrid nanoparticles for controlled release of anticancer drug.* Materials Science and Engineering: C, 2015. **46**: p. 514-520.

32. Tran, N. and T.J. Webster, *Magnetic nanoparticles: biomedical applications and challenges.* Journal of Materials Chemistry, 2010. **20**(40): p. 8760-8767.

33. Goncalves, R., et al., *Magnetoelectric $CoFe_2O_4$/polyvinylidene fluoride electrospun nanofibres.* Nanoscale, 2015. **7**(17): p. 8058-8061.

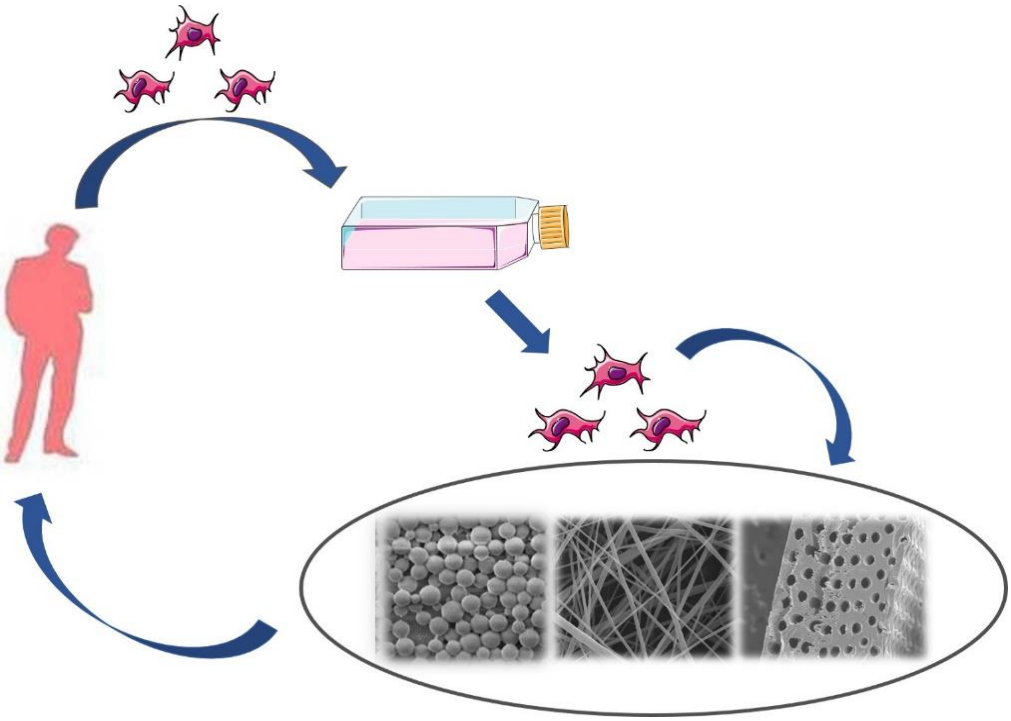

8. Conclusions and future works

This chapter presents the main conclusions of the present work, devoted to the processing of piezoelectric materials with different morphologies with potential for tissue engineering applications and their surface wettability modification. Further, some suggestions for future works are also provided.

8.1. Conclusion

The development of new scaffolds with different morphologies has been demonstrated as a good approach for improved tissue engineering strategies. The ability to tailor morphology, physico-chemical properties, surface wettability and in some cases the mechanical properties are crucial to understand the potential of the developed biomaterials for a specific tissue application. In particular for some tissues such as nervous system and bone, in which electrical and/or electromechanical signals are relevant for cell-functions, the use of electroactive materials, in particular piezoelectric polymers, for the scaffolds production emerges as a high potential and growing field, due to their ability to mimic specific body responses.

In the present work, scaffolds based on piezoelectric poly(vinylidene fluoride) (PVDF), poly(hydroxybutyrate) (PHB) and poly(L-lactic acid) (PLLA) with different morphologies, from microspheres, to three-dimensional (3D) scaffolds were obtained, in particular for PVDF. Also the modification of the wettability of the PVDF and PLLA electrospun membranes was evaluated.

It was demonstrated that PVDF can be processed into three distinct morphologies: microspheres, electrospun membranes and three dimensional scaffolds. Further, due to the difficult incorporation of the cell culture medium into the PVDF electrospun membranes, plasma treatments under oxygen atmosphere were performed in order to promote an increase of cell adhesion. Results showed that surface treatments lead to superhydrophilic membranes due to significant surface chemical modifications (introduction of oxygen and release of fluorine atoms). The surface treatment allows to maintaining the fiber average size (~400 ± 200 nm), electroactive β-phase (42 %) and cell viability. PVDF microspheres produced by electrospray with average diameters ranging between 0.81 ± 0.34 and 5.55 ± 2.34 μm in the β-phase (63-74 %) also promote cell adhesion, demonstrating its potential for tissue engineering applications. Three dimensional PVDF scaffolds were produced by three distinct methods: solvent casting with particulate and nylon fibers leaching and freeze extraction with poly(vinyl alcohol) (PVA) templates. These methods allow the production of structures with different pore architectures and porosities. Solvent casting with particulate leaching leads to porous formation with sizes between 300-400 μm while using nylon fibers as porogen and freeze extraction with PVA templates the pore size of the scaffolds depends to the diameter of the sacrificial nylon (60-130 μm) and PVA filaments (316-413 μm). The

porosity of the scaffolds influences the Young modulus of the constructs. All scaffolds are obtained in the β-phase (~45 %) and present a degree of crystallinity in the range ~33 to 55 %.

As PVDF is biocompatible but not biodegradable, hindering some specific applications, the processing of biodegradable polymers, such as PHB and PLLA, into different morphologies (fibers and spheres) has been achieved. Electrospun PHB membranes can be produced by electrospinning, the processing parameters influencing fiber average size. The polymer crystalline phase (X_c = 53 %) seems to be independent to the processing conditions and a single degradation step was observed during the thermal degradation. Cell viability studies demonstrated its potential for tissue engineering. PLLA can be also produced by electrospinning into electrospun membranes and in films by solvent casting. Plasma treatments under Ar and O_2 promoted the modification of the membrane surface wettability. A decrease in the contact angle and a roughness increase in PLLA films were observed and in the case of membranes, superhydrophilic membranes were obtained under Ar and O_2 plasma treatments. No influence of plasma treatment was detected in the physico–chemical characteristics of PLLA. Cell viability studies indicated that Ar and O_2 plasma treatments does not influence the metabolic activity of the cells.

Neat and magnetic $CoFe_2O_4$ filled composite PLLA microspheres with size diameters ranging between 0.16 to 3.9 μm for neat PLLA and between 0.8-2.2 μm for the composite microspheres were prepared by emulsion method using a poly(vinyl alcohol) (PVA) solution as a stabilizer agent. The microspheres are stable in alkaline environments. The processing method does not induce chemical changes in the chemical polymer structure. Neat PLLA microspheres with a degree of crystallinity of 40 % were obtained, whereas the incorporation of the $CoFe_2O_4$ nanoparticles into the PLLA sample leads to obtain amorphous magnetic microspheres. Cell viability studies showed good cell proliferation, which demonstrates the proper encapsulation of the ferrite nanoparticles and the suitability of the microspheres for biomedical applications.

Thus, this work demonstrates that the main polymers with suitable piezoelectric properties for tissue engineering applications can be processed in a variety of morphologies (microspheres, fiber mats, films and three-dimensional scaffolds) that allow the implementation of novel tissue engineering strategies. Further, it was shown that the wettability of the membranes can be suitably modified by plasma treatment.

8.2. Future work

In the present work, it was proved that it is possible to produce electroactive scaffolds with different morphologies. In this sense three main research areas arise as interesting studies:

- Influence of the electroactive response and the different morphologies in the cell behavior (proliferation and differentiation) of different cell types.

- Development of composites and blends in order to further tune scaffolds response, such as the incorporation of magnetic particles and conductive polymers to improve the magnetic and electrical stimulation.

- Biofunctionalization of the different scaffolds with biomolecules such as specific proteins to enhance cell adhesion and proliferation to the scaffolds that will further provide the electromechanical stimuli.